TISSUE NONLINEARITY AS A NOVEL MECHANISM FOR THE FREQUENCY DEPENDENCE OF RESPIRATORY RESISTANCE TO AIRFLOW IN DISEASE

by

Anas Tahir

Submitted in partial fulfilment of the requirements
for the degree of Master of Applied Science

at

Dalhousie University
Halifax, Nova Scotia
December 2021

To Mom, Dad, Omar, and Osama

TABLE OF CONTENTS

LIST OF TABLES

LIST OF FIGURES

ABSTRACT

RATIONALE: The frequency dependence of resistance, $R(f)$, is currently being used as a clinical measure, thought to assess small airway heterogeneity of the respiratory system. However, it also can arise from tissue viscoelasticity, upper airway shunt, and recently a novel mechanism due to time-variation in mechanical properties, but potential sources of this time variation such as from the nonlinear mechanical properties have not been investigated. ***METHODS***: Here using measurements from lung tissue and analytical modeling using constant phase models amended with nonlinear tissue or pressure-volume mechanics, we investigated if the time-varying mechanics that can arise from tissue nonlinearities during stretch lead to increases in $R(f)$. We explored these models at different operating stretches or volumes with different stretch amplitudes and different degrees of nonlinearities. We also modeled the normal pressure volume relationship as well as curves representative of fibrosis and emphysema. We also investigated if time-varying properties from ventilation or oscillometry due to the nonlinear pressure-volume relationship can also predict $R(f)$ and if it is increased in patients with lung transplants including patients with chronic lung allograft dysfunction. ***RESULTS AND DISCUSSION***: We found that nonlinearity in tissue and the respiratory system could increase low-frequency resistance above the static model resistance and thus lead to $R(f)$ greater than predicted from the constant phase model. $R(f)$ increased more strongly with increases in mean stretch volume, amplitude, or the exponent of the nonlinearity. The increase in $R(f)$ was mechanistically related to the time variation of stiffness during oscillatory stretch or ventilation of the models. $R(f)$ was increased as much as 200% during modeled mechanical ventilation in the ventilation frequency range ($0.2 - 5\ Hz$), however, this effect was nearly absent during modeled oscillometry ($5 - 37\ Hz$). This can be largely attributed to the much smaller oscillation amplitude, and lack of any effects from the breathing motion in the oscillometry frequency range in our model. ***CONCLUSIONS***: Nonlinearity in lung tissue or the pressure-volume curve during stretch or ventilation respectively, leads to time variations in mechanical properties that cause increases in low-frequency resistance and thus $R(f)$ larger than observed from tissue viscoelastic properties alone. Increases in nonlinearity can be a source of $R(f)$ not previously identified that may be important to the interpretation of the effects of lung disease on lung tissue mechanics and provides a novel mechanism for the origin of the $R(f)$ and its changes. While pressure-volume nonlinearity can strongly affect $R(f)$ determined during mechanical ventilation, measurements by oscillometry are likely not susceptible, although we did not model other sources of time variation such as flow limitation.

LIST OF ABBREVIATIONS USED

α	nonlinear model exponent
β	constant phase model exponent
ε	strain
η	hysteresivity
λ	stretch ratio
ω	angular frequency
Ψ	window in the Welch periodogram
BOS	bronchiolitis obliterans syndrome
$CLAD$	chronic lung allograft dysfunction
$COPD$	chronic obstructive pulmonary disease
$COVID-19$	coronavirus disease 2019
CPM	constant phase model
CoV	coefficient of variation
cmH_2O	centimeter of water
E	model elastance
E_m	mean elastance
E_{rs}	elastance of the respiratory system
E_v	variable elastance
ECM	extra-cellular matrix
$FEV1$	forced expiratory volume in one second
FFT	fast Fourier transform
FRC	functional residual capacity
FVC	forced vital capacity
f	frequency
f_{os}	oscillatory frequency
G	constant phase model tissue damping

H	constant phase model tissue elastance
I	inertance of the respiratory system
LT	lung transplant
MRI	magnetic resonant imaging
OS or OV	operating strain or operating volume
OVW	optimal ventilator waveform
P	pressure
$PreBD$	pre-bronchodilator
PV	pressure volume
$QLCPM$	quasi linear constant phase model
QLM	quasi linear model
R_{rs}	resistance of the respiratory system
R	model resistance
R_m	mean resistance
R_v	variable resistance
$R(f)$	frequency dependance of respiratory resistance
R_{5-19}	R_{rs} at 5 Hz minus R_{rs} at 19 Hz
S	instantaneous stiffness
SA	strain amplitude
T	stress
TLC	total lung capacity
T-VSPECT/CT	Technegas™ ventilation single-photon emission computed tomography / computed tomography
t	time
V	volume
$\dot{V}$	flow
$\ddot{V}$	volume acceleration
VDP	ventilation defect percentage

X_{rs}	reactance of the respiratory system
Z_{rs}	the impedance of the respiratory system
Z	impedance

ACKNOWLEDGEMENTS

First, I would like to express my sincere gratitude to my thesis supervisor, Prof. Geoffrey N. Maksym, for his guidance and patience in teaching me a huge amount of knowledge that I was not familiar with before starting the MASc program. Indeed, your generous style of teaching, which is to explain concepts in a very sophisticated but at the same time the simple level has inspired me to be a better researcher in the future. I would like to thank very warmly Dr. Robert Adamson, and Dr. Kamal El Sankary, as well as Dr. Andrew French for their support and insightful feedback on my work. I would also like to thank Dr. Jeremy Brown for his assistance throughout the program and checking in during COVID tough times.

I would like to thank all the summer students Chloe Potter, Alex Brezovan, Melanie Renn, and Julie Chen for helping me collect the data and analyze the images. I especially like to thank Daren Cole for his constant help and support in developing the tissue bath setup in the lab. I also would like to thank Scott Fulton, Dr. Paul Hernandez, Dr. Andrew Ross and their team for helping and guiding me in the CLAD study.

Lastly, I would like to mention that without the unconditional love and support from my family, this would have been impossible. Mom, for your motherly and scientific advice, dad, for your strength and positivity that I could always rely on, and Omar for constantly reminding me that life has more important aspects than science or financial success.

CHAPTER 1: LITERATURE REVIEW

This chapter presents a literature review focused on what is known, concerning the frequency dependence of respiratory mechanical resistance and its origins/sources. It begins with a brief review of the lung structure and function, followed by the mechanics of the respiratory system and the different mechanisms for the frequency dependence of resistance. Then I provide a brief introduction to the measurement of nonlinear lung tissue properties and analytical modeling that led directly to the investigation of how tissue and pressure-volume nonlinearities may contribute to the frequency dependence of resistance in mechanical impedance measurements, finishing with a brief review of how heterogeneity in ventilation is assessed using imaging.

1.1 ANATOMY AND PHYSIOLOGY OF THE LUNG

The conducting pathways to the gas exchanging region of the respiratory system begin at the nose and end at the alveoli. The pathway consists of the nasal cavity, posterior pharynx, glottis, vocal cords, trachea, tracheobronchial tree, and lung interstitium consisting of connective tissue, including the smooth muscle, as well as lymphatics amongst other structures. Outside the lungs is the chest wall which moves with inflation and deflation of the lungs and is defined to include the muscles of the chest and rib cage, heart, and diaphragm. Below the diaphragm is the abdominal contents that also move during breathing. The airways, the lung tissue, and the chest wall tissue all contribute to the mechanical properties of the respiratory system.

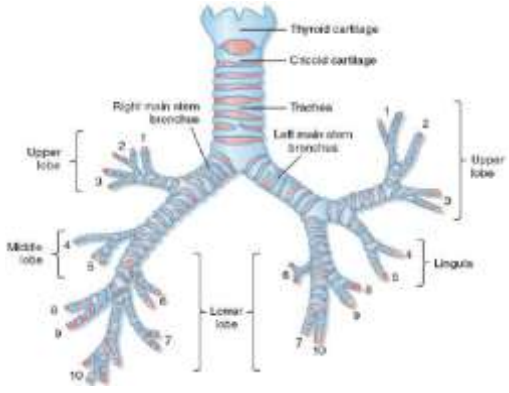

Figure 1.1: Airway tree (reproduced with permission from [1]*)*

Structurally, airways (in the lung) run from the trachea to bronchi to bronchioles to terminal bronchioles, which are the conducting zone where air enters and leave. Air is delivered to alveoli through a branching airway tree structure, which is further divided into respiratory bronchioles extending to alveolar ducts and sacs where gas exchange takes place (Figure 1.1). Therefore, the lung is a heterogeneous branching tree which in disease results in heterogeneous ventilation due to airway narrowing (especially in the small airways – defined to be less than 2 mm), mucous plugging, or changes to lung tissue such as fibrotic lesions.

The lung tissue structure is composed of many different extracellular fibers and intercellular soft tissue that make up the extracellular matrix. The major constituent includes the collagen fibers which limit distensibility and elastin which is a major contributor to elastic recoil. Collagen and elastin, together with the surface tension from the alveolar surface, and the gas compressibility within the available lung volume largely determine lung elastance or stiffness. Together with the chest wall stiffness, these provide the elastic properties of the respiratory system and to a lesser extent, the viscoelastic deformation of these tissues contributes to the mechanical resistance of the respiratory system.

1.2 RESPIRATORY SYSTEM MECHANICS

The mechanics of the respiratory system determine the forces and work required during breathing by the deformation of the respiratory tissues and the movement of air. Essentially the mechanics are defined by the pressures required to move the volume of air as it flows through the airway tree and as the associated tissues deform. When we inhale, negative pressure is created by the diaphragm and supporting muscles contraction resulting in lung expansion. Similarly, when we exhale, positive pressure is created by the passive elastic recoil of the lung pulling the chest inward and driving the flow out, and it can be aided by accessory muscles of expiration in the chest wall including the abdominal cavity. In obstructive diseases, the primary pathology is that the flow of air is impeded or obstructed, while in restrictive disease flow can also be reduced, but it's largely because of the loss in lung volumes and stiffening of the lung tissue. Several of the mechanical features of the respiratory system can be measured using several different methods. Spirometry is the measurement of flow during learned maneuvers using a spirometer. Key measurements include the Forced Expired Volume in 1 second (FEV1) and the Forced Vital Capacity (FVC) which is the

total volume obtained by integrating the flow between total lung capacity at maximum lung inflation to residual volume, at the end of a forced expiratory maneuver. In plethysmography, a subject is seated in a closed box which usually also includes spirometry for the measurement of respiratory flows. By panting on the mouthpiece after the end of a normal expiration while the valve to the outside of the box is closed, the Functional Residual Capacity (FRC) can be determined. This is by the simultaneous measurement of the pressure changes in the box (outside of the chest wall) and the pressure changes of the lungs at the airway opening and using Boyle's Law. The FRC is the lung volume at the end of a normal exhalation and is the equilibrium volume between the forces of expansion from the chest wall and contraction from the elastic recoil of the lung pulling inwards. Other lung volumes such as residual volume or Total Lung Capacity (TLC) can be determined referencing the FRC measurement. Often spirometry is combined with plethysmography on the same equipment. Similarly using slow maneuvers over the whole volume range of the lung the pressure-volume curve can be obtained, and the lung compliance can be determined (i.e., the slope of the curve), which is an inverse of the measure of lung stiffness.

A key parameter of the respiratory system mechanics is the resistance to airflow. The resistance in any tube is defined as the pressure difference measured between two points along the tube divided by the flow in liters/s. Lung resistance can be inferred using plethysmography using a sophisticated algorithm. However, the total respiratory system resistance from the mouth across the lung and chest wall can also be measured using oscillometry which is an approach gaining in popularity. The increased interest in this method is in part because spirometry is more challenging to perform for some subjects such as elderly individuals and young children, and plethysmography is expensive and bulky requiring a large sealable box

Standard oscillometry applies small oscillations at frequencies in the range between 5 and 40 Hz via a mouthpiece during breathing usually for several breaths within 20 $seconds$ or more. Figure 1.2 (left) shows a subject on a mouthpiece breathing normally while the oscillations are delivered by the oscillometer through a detachable disposable antibacterial/antiviral filter mouthpiece, (right) shows representative data collected by the device that is displayed in real-time. By measuring how much pressure is required for a given flow at each frequency one can compute the respiratory system impedance to that flow (Figure 1.2). The respiratory system impedance, Z_{rs}, is determined at each frequency of oscillation from the ratio of the pressure to flow in the frequency domain. in equation 1.1:

$$Z_{rs}(f) = \frac{P(f)}{\dot{V}(f)} = R_{rs}(f) + iX_{rs}(f) \quad (1.1)$$

where P is pressure and $\dot{V}$ is flow and f is the frequency of oscillation. R_{rs} is the resistance, which is that part of the impedance in phase with the flow, while the reactance Xrs is that part of the impedance that describes the pressure-volume relationship and is out of phase with the flow. It is composed of the

1) elastic properties arising from the stretch of the tissues and surface tension which dominates X_{rs} at low frequencies and
2) the inertive properties largely form the acceleration of air which dominates X_{rs} at high frequencies.

Signal processing is used to reduce the effects of breathing noise and reject any artifacts that might occur due to coughing, holding the breath, etc., and multiple measurements are done with acceptable measurements from at least 3 with the coefficient of variance of the resistance less than 10% for adults or less than 15% in children [2]–[5]. In a healthy subject, R_{rs} is nearly constant over the frequency range of oscillometry, but in obstructive disease, resistance typically becomes frequency dependent in an almost inverse hyperbolic fashion. The source of this frequency dependence is a matter of controversy that is explored in this thesis.

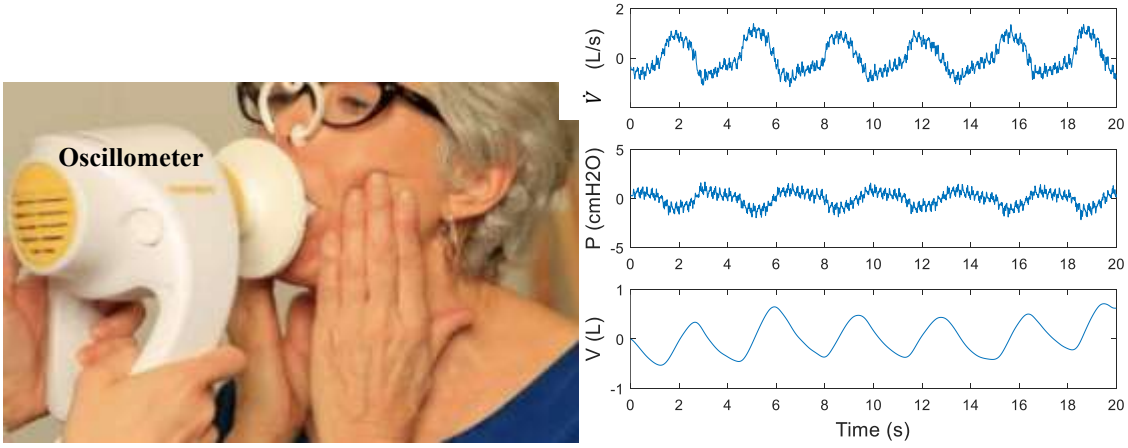

Figure 1.2. Oscillometry system and measured flow, pressure, and volume curves with time. (used with permission from Thorasys)

1.3 FREQUENCY DEPENDENCE OF RESPIRATORY RESISTANCE $R(f)$

Frequency dependence of R_{rs}, which will be denoted as $R(f)$ has been observed to increase in asthma and COPD. For example, Figure 1.3 shows frequency dependence increasing with the

severity of asthma with similar behavior observable in COPD [6]. However, $R(f)$ is also known to occur in very young healthy children and infants [7]–[9]. Similarly, it is observed in healthy small animals such as mice or rodents [10]–[13].

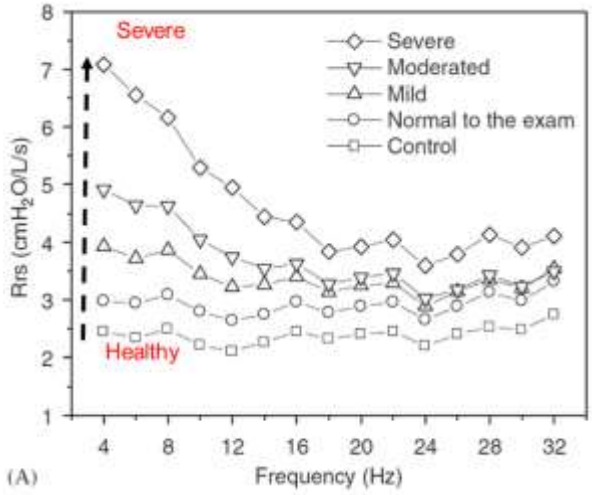

Figure 1.3: $R(f)$ *from healthy control subject to groups clinically diagnosed with increasing level of severity of asthma (reproduced with permission from* [6]*)*

Looking at Figure 1.3, R is fairly flat in healthy subjects, and it increases with the severity of asthma. $R(f)$ begins to occur in mild asthma reaching as much as 3 $cmH_20.s/l$ subtracting the resistance at 20 Hz from the resistance at 5 Hz which is the standard measure of $R(f)$.

1.4 MECHANISM FOR $R(f)$

There are three established mechanisms for $R(f)$ and one novel mechanism recently discovered in our lab. The established mechanisms include **1)** tissue viscoelasticity [14]–[16], **2)** airway resistance heterogeneity [17], [18], and **3)** upper airway shunt [19]–[21]. The most recent mechanism is from time-varying mechanics, whereby Alamdari et al. [22], [23] showed using modeling that $R(f)$ occurs when the stiffness of the respiratory system as can be estimated from low frequency X_{rs} is non-stationary and varies in phase with the with the imposed oscillations of flow. Alamdari et al. modelled mechanical ventilation of subjects while measuring pressure and flow in response to a temporally varying single compartment resistance and elastance model where elastance varied sinusoidally with time. Such variations in elastance can occur during mechanical ventilation or during periodic flow limitation during exhalation that can occur in disease [22]. This

mechanism is now recognized as potential source of $R(f)$ [24], [25]. These mechanisms for $R(f)$ are described in more detail in the next sections.

1.4.1 Lung tissue viscoelasticity:

One of the four identified sources of $R(f)$ is lung tissue viscoelasticity. Viscoelasticity is a macroscopic property of matter used to collectively describe both the liquid-like and solid-like characteristics of a material. In contrast to perfect elasticity, viscoelastic substances do not maintain constant stress under constant deformation, but the stress in the material slowly relaxes, a phenomenon called stress relaxation [15]. In the frequency domain, in response to oscillations, stress-strain behavior is rate-dependent. This is observed when the mechanical properties are expressed as a mechanical impedance (stress or pressure response to imposed flow), the impedance displays an approximately inverse hyperbolic frequency dependence. However, airway resistance is Newtonian and is frequency independent. At low frequencies, the resistance of the respiratory system is frequency-dependent from the lowest frequencies measured near $0.05\,Hz$ to about $0.6\,Hz$ in adults and this is thought to arise from the viscoelastic tissue mechanics [14] rather than airway pressure losses which are constant for higher frequencies in the oscillometry range. This behavior is often modeled using lumped element models composed of ideal elastic springs and ideal viscous dashpots [15]. Multiple pairs of these viscoelastic elements can be used to describe the observed inverse frequency dependence thought to arise from tissue viscoelasticity. The number of elements required to effectively describe the frequency dependence depends on the observed frequency range for the inverse frequency dependence with an inverse distribution of viscoelastic time constants describing the behavior fairly well [26]. No mechanism has been identified to account for this potential distribution, but it is thought to arise from the complexity of the interactions of the structural elements mainly the collagen and elastin network within a soft glycosaminoglycan matrix [5].

Figure 1.4 (left), shows a schematic of the elastin and collagen-based mesh structure of lung tissue in the alveolar structure within an acinus at a larger scale, which may provide a structural mechanism for scaling of viscoelastic time constants as larger fibers weave and interconnect at greater distances, as do the alveolar walls and septal boundaries between lung structures. The data pointe of Figure 1.4 (right) shows the frequency dependence of resistance from

healthy dog lung tissue before and after and histamine challenge, showing that airway smooth muscle contraction increases the frequency dependence of resistance, similar to how the dependence is observed to be greater in asthma [15].

Also shown in Figure 1.4 (right) are curves that well-describe the frequency dependence and represent a common model for tissue viscoelasticity known as the **constant phase model** (CPM) (equation1.2):

$$Z(\omega) = \frac{G+jH}{\omega^{1-\beta}} = R(\omega) + jX(\omega) \qquad (1.2)$$

where G is called the tissue damping and H is the tissue elastance and o is an exponent with a value typically between 0.9 and 0.95, giving inverse hyperbolic frequency dependence in both the dissipative (G) and elastic (H) portion of the mechanical impedance, very close to $\frac{1}{\omega}$.

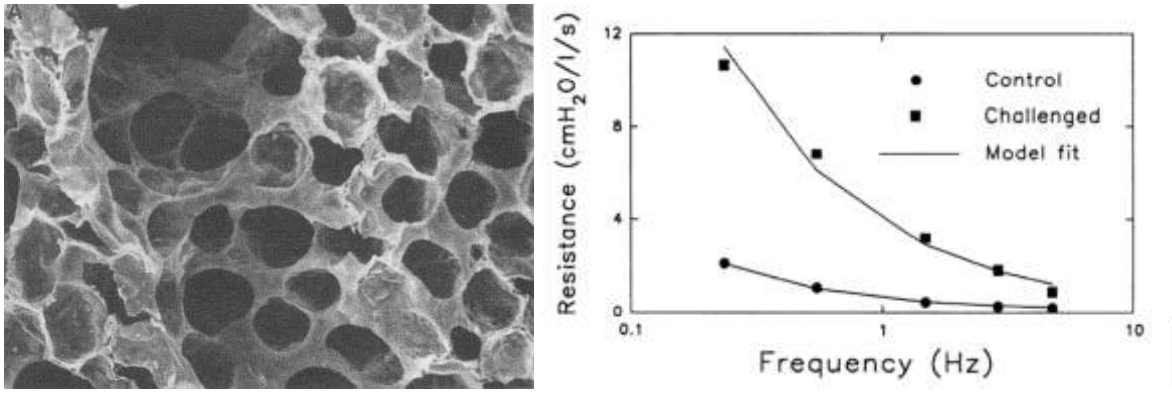

Figure 1.4: (left) Alveolar walls within which are networks of collagen and elastance fibers which with surface tension forces deform viscoelastically governing tissue stress-strain relationship (right) Resistance is frequency dependent and increases after contractile agonist challenge measured in dog lungs (reproduced with permission from [15]*)*

1.4.2 Ventilation Heterogeneity of the lung:

A second identified source of $R(f)$ is from airway impedance heterogeneity which is often termed ventilation heterogeneity. Inverse hyperbolic $R(f)$ can also arise from a multibranch network of airways, but only if the tree is not symmetric. Homogenous ventilation in a symmetric tree means the behavior can be defined by a single resistance. However, if the airways have heterogeneity in their diameters, this causes heterogeneity in impedance and thus ventilation. Indeed the simplest parallel two-compartment model demonstrates $R(f)$ over almost a decade in oscillation frequency, when the two branch resistances are unequal [17]. More branches are needed

to extend the frequency range, and of course, there are many thousands of branches in the lung. Normally in non-diseased human lungs, there is negligible frequency dependence in the ranges $4-40\ Hz$, but in diseases with increasing airway diameter heterogeneity, leading to different time constants, the impedance becomes increasingly frequency-dependent [18]. Since the Newtonian resistance of an airway is highly dependent on its diameter particularly at small diameters, this could account for the observed frequency dependence in vivo in obstructive disease. However, heterogeneity in tissue properties that may occur in disease could also contribute to the observed frequency dependence in disease. Interestingly normal differences in airway diameters, and the difference that arises from gravity-dependent effects, narrowing airways more in the dependent regions (more compressed regions) at the base of the lung does not appear to be substantial enough to produce frequency dependence in healthy adults at least in the oscillometry range of 4 to 40 Hz. This may be a factor contributing to $R(f)$ in pre-school children. Some heterogeneity in tissue and airway properties might arise with changes in disease that affect the stress-strain nonlinearity of lung tissue, which may be relevant in the 4^{th} mechanism for $R(f)$ discussed further below.

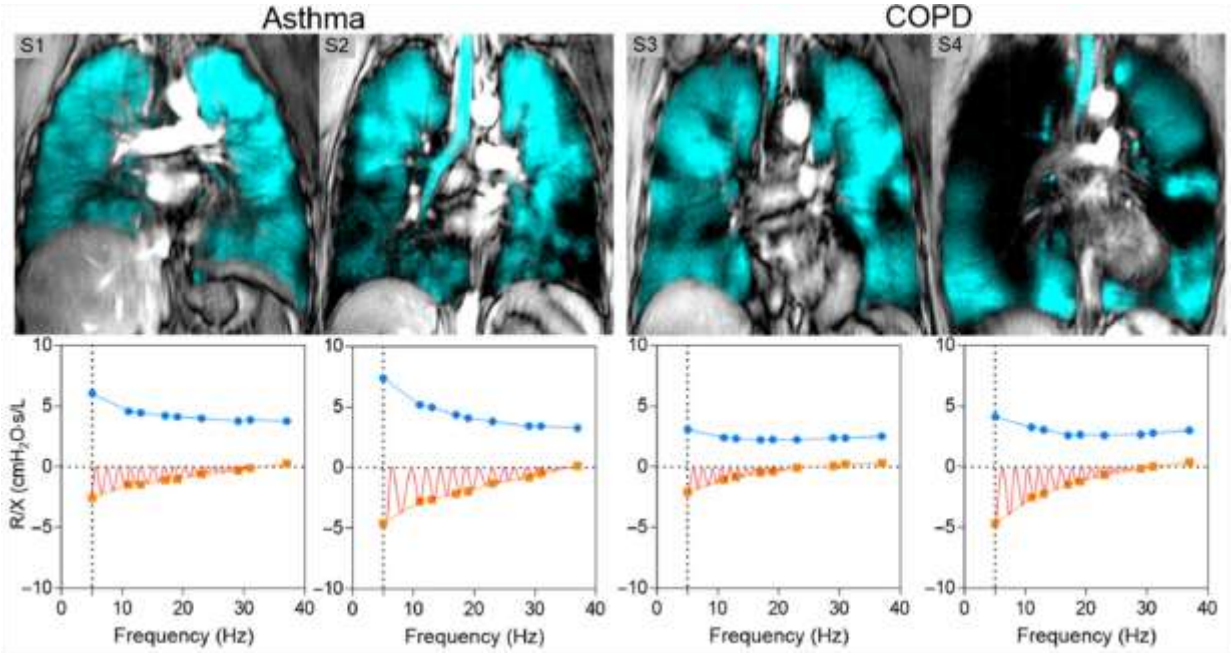

Figure 1.5: Qualitative analysis of Heterogeneity. S1 & S2 hyperpolarized He MRI imaging of two Asthmatic subjects with less and higher heterogeneity reflected in the ventilation in turquoise with the thoracic cavity in gray scale. Respectively oscillometry images of the patients showing resistance in blue and reactance in orange with respect to frequencies. The hatched area in orange is Ax which is not studied in this thesis. S3 & S4 shows respective COPD patients MRI images and oscillometry plots. (reproduced with permission from[27]*)*

Heterogeneity in ventilation can be observed by several imaging methods, including MRI. Imaging in [27] is done using hyperpolarized gas either Helium (^{3}He) or Xenon ^{129}Xe typically, in MRI Ventilation Imaging, which uses a nonradioactive, gaseous contrast agent that, when inhaled, allows images of lung ventilation to be taken with good spatial and temporal resolution. Figure 1.5 shows two examples of diseased cases, asthma, and chronic obstructive pulmonary disease (COPD). COPD is characterized by long-term breathing problems and poor airflow. It is common in older subjects or smokers. Two representative patients per disease are chosen to show the $R(f)$ due to heterogeneity in [27]. It is evident that in the case of asthma, subject one has more homogenous ventilation characterized by the blue color imagining in the boundaries of the lung in black. We can also see the oscillometry results for each subject in Figure 1.5. Due to homogenous ventilation in subject 1, we can see there is $R(f)$ (which is defined as resistance at $5\,Hz$ minus resistance at $19\,Hz$. The $5\,Hz$ component is the lowest frequency of oscillation delivered by the oscillometry device, and $19\,Hz$ is the closest oscillation frequency to $20\,Hz$ which is conventionally used to represent the plateau resistance, such that R_{5-19} is the difference in resistance quantifying $R(f)$. However, it is significantly increased in subject 2 where ventilation is more heterogenous. Similarly for the case of patients with COPD, subject 3 shows more homogenous ventilation compared to subject 4 – resulting in the significant increase in $R(f)$ in subject 4 compared to subject 3. Therefore, heterogeneity is highly attributed to $R(f)$ especially in obstructive diseases like asthma and COPD

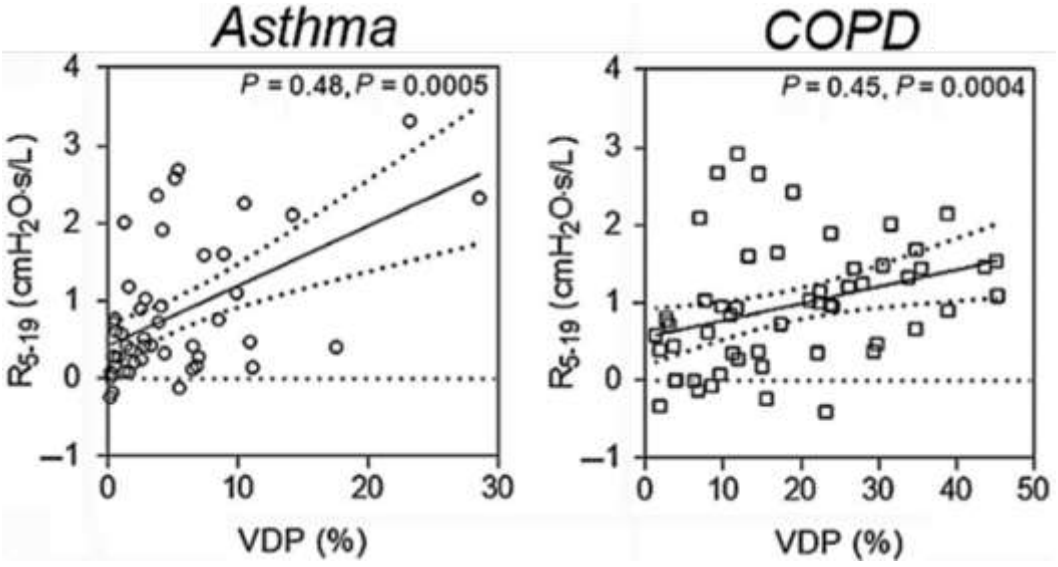

Figure 1.6: (left) $R(f)$ *vs %VDP plot for Asthma and (right) COPD respectively (reproduced with permission from* [27]*)*

It has been shown previously that ventilation heterogeneity is associated with $R(f)$. One way to quantify ventilation heterogeneity is via the ventilation defect percentage (VDP), which is the total ventilation defect volume normalized to the thoracic cavity volume. VDP is correlated with $R(f)$ using R_{5-19} but it can be seen there is a substantial variation amongst subjects (Figure 1.6). VDP is a single index, that may only partly capture the distribution of airway diameter narrowing that could cause $R(f)$, if these are indeed mechanistically linked.

1.4.3 Upper Airway Shunt:

A third possible source of $R(f)$ is upper airway shunt. This is the oscillatory flow that bypasses the path through the lung and chest wall tissues and goes instead into oscillating the cheeks and soft tissues in the upper airway above the glottis. This can be modeled as a parallel shunt impedance pathway from the source of the oscillations to 'ground' which is atmospheric pressure outside the body. The shunt has a strong effect when the respiratory impedance is high. The dominant effect is lowering the measured impedance from what it would have been without the available shunt, but it can also alter the measured frequency dependence of resistance [9-11], although this varies amongst reported studies.

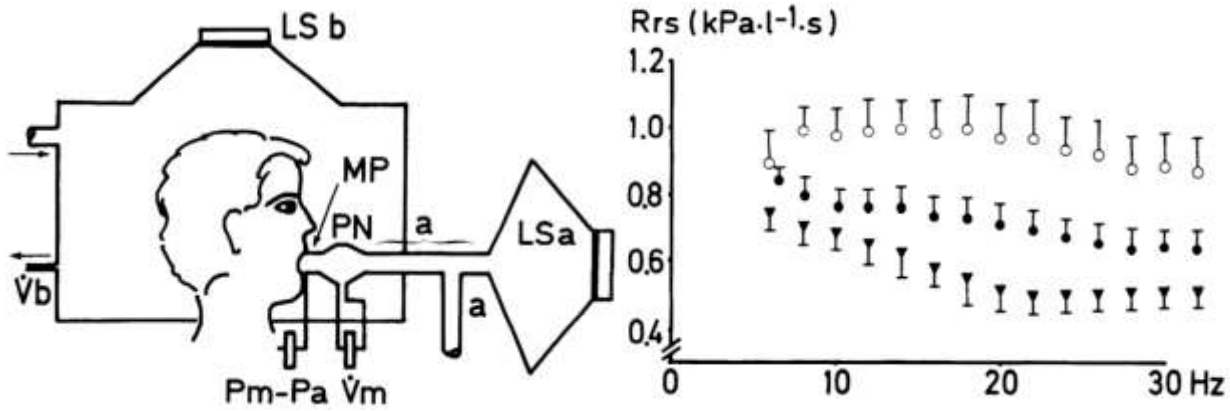

Figure 1.7 (left) Head generator; (right) Effect of Upper Airway Shunt (reproduced with permission from [28]*)*

The upper airway shunt can be measured by using a head generator which attempts to present an identical oscillation to the outside of the cheeks negating the shunt (Figure 1.7, left). In Figure 1.7 (right) are the recorded impedance of a person with a fairly high impedance of about $9\ cmH20.s/l$ $(0.9\ kPa.s/l)$. The hollow dots indicate when loudspeaker $LS\ b$ is in motion approximately matching the pressure at MP from loudspeaker $LS\ a$ also in motion, gives a higher

impedance across frequency and little $R(f)$. The solid dots are the conventional technique with $LS\ a$ alone including using a nose clip and cheek hold, and there is a some $R(f)$ evident. Larger $R(f)$ is apparent without a nose-clip or cheek-hold and impedance is more strongly affected. In individuals with lower typical R_{rs} ($2.0\ cmH20.\ s/l$) the effect of shunt is much smaller. Figure 1.8 (left & right) shows the effects of modeling shunt using experimentally determined measurements of the shunt impedance with typical respiratory impedance in moderate asthma < $5\ cmH20.\ s/l$ at $5\ Hz$, inferring that the effects of shunt may be quite modest [21].

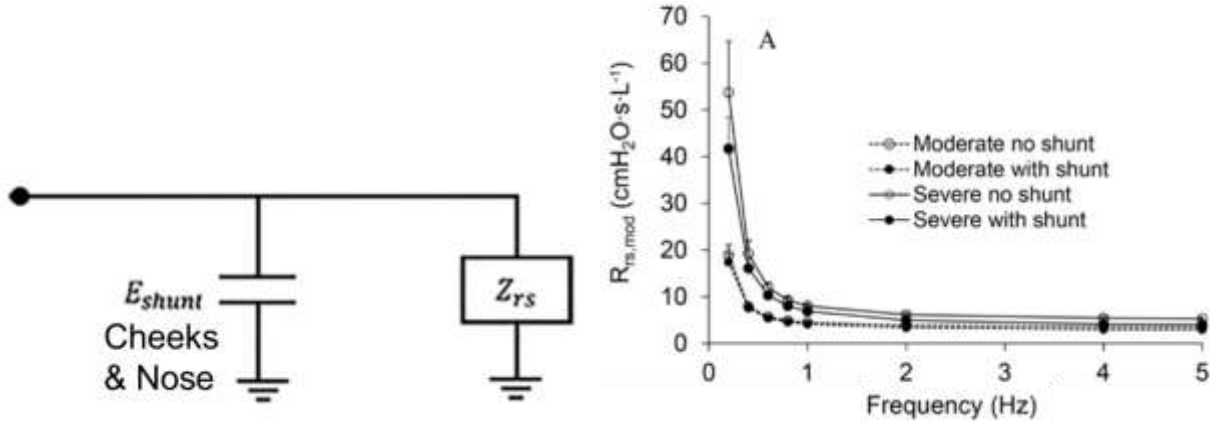

Figure 1.8 (left) Upper Airway Shunt as model parameter; (right) Effect of Upper Airway Shunt over $R(f)$ *(reproduced with permission from* [20], [21]*)*

1.4.4 Time-varying lung (tissue) mechanics:

A fourth possible source of $R(f)$ is time-varying lung (tissue) mechanics, which was only recently identified [22], [23]. Time-variation in lung mechanics can come from multiple sources. They can arise from variations in airway diameters during breathing with changes in lung volume with inspiration and expiration. This can also include the opening of collapsed or partially collapsed airways at very low lung volumes or due to disease termed recruitment and their collapse termed derecruitment, which is observed most commonly as expiratory flow limitation in COPD where airways are very compliant and partially collapse. Even partial collapse can mean oscillatory flow no longer travels past the sites of flow limitation, which increases impedance, but this is relieved during inspiration and impedance falls. While these variations were known, it was generally assumed that this variation was normally small and regardless would be averaged out over many breaths when estimating the mean impedance. However, the changing impedance with

time means the system is non-stationary, which is one of the assumptions in the estimation method of impedance ($Z_{rs}(f) = \frac{P(f)}{\dot{V}(f)} = R_{rs}(f) + iX_{rs}(f)$ (1.1 1.1).

However, to correct this equation 1.2, we can represent a time-varying impedance as follows in equation 1.3:

$$Z(f,t) = \frac{P(f,t)}{\dot{V}(f,t)} = R(f,t) + jX(f,t) \quad (1.3)$$

It's often thought the effects of time variation can be minimized by reducing the window during which the variation occurs, or including a very wide window, assuming the non-stationarity within the window averages away. However, a signal analysis approach has been developed to consider this behavior, developed by Zadeh in 1950 which we will refer to here as the Zadeh transform [29].

$$\Gamma(j\omega;t) = \int_{-\infty}^{\infty} S(t,\xi)e^{-j\omega(t-\xi)}d\xi \quad (1.4)$$

where rather than a normal transfer function $\Gamma(j\omega)$, $\Gamma(j\omega;t)$ is the function of $j\omega$ involving t as a parameter, ξ is the time delay, $S(t,\xi)$ analogous to the impulse response function that is not fixed, which Zadeh solved using Heaviside expansion in variable networks. Further details and examples of its solution are found in [29] and Alamdari et al [22], [23].

This transform, while being used occasionally in circuit theory is seldom used in network modelling, and in biological systems has only had limited use in despite potential many potential applications [30]–[33]. It was first applied to respiratory mechanics by our lab in 2019 [22], [23]. Alamdari et al. [22], [23] showed that time variation in mechanics could produce $R(f)$, using two modelling approaches, using both the Zadeh transform as well as direct time domain modelling, finding the same results. We did not employ the Zadeh transform in this thesis instead we used direct time modeling that Alamdari et al. did here. Alamdari et al. thus provided a new mechanism for $R(f)$, mathematically connecting temporal variation in mechanical properties to $R(f)$, which had been assumed to be a static mechanical behavior attributed previously to either tissue viscoelasticity, small airway heterogeneity or occasionally upper airway shunt. Notably, they showed that if temporal variation in elastance varied at the oscillation frequency and in phase or partially in phase with the flow, this led to $R(f)$. If completely in phase with the flow this had no effect on $X(f)$. Also, temporal variation in resistance had only a negligible effect on $X(f)$ and no

effect on $R(f)$. The effect of temporal variation in elastance was amplitude-dependent, the greater the variation, the greater the $R(f)$. This was important since although both $R(f)$ and temporal variation of mechanics are both known to be increased in disease, they were not thought to be potentially mechanistically associated [19].

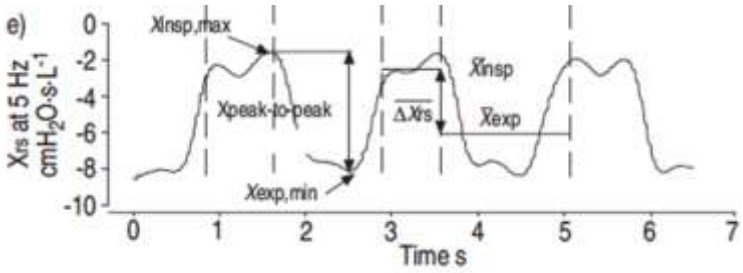

Figure 1.9: Experimental tracing from a representative flow-limited patient and definition of the indices used to characterize the respiratory system reactance (X_{rs}) time course during a single breath. (reproduced with permission from [34]*)*

Figure 1.9, shows the time-varying reactance X_{rs} at $5\ Hz$ attributed to varying elastance, largely due to expiratory flow limitation [34]. The variation is quite large, at about $6\ cmH20.\ s/l$. This may have led to $R(f)$ observed typically in COPD [34].

In summary, there are 4 potential mechanisms for $R(f)$. Currently the most commonly attributed source in disease for $R(f)$ is heterogeneity attributed to the small airways, while viscoelasticity of the tissues is felt to be dominant at lower frequencies below and near breathing frequency in health, with shunt potentially a factor at high impedance. The most poorly understood and recently contributed source is from time-varying lung mechanics.

However, the potential mechanisms for time-varying mechanics sufficient to produce $R(f)$ and in which frequency range have not been explored, and how these mechanisms might change their influence on $R(f)$ is unknown. One important factor characteristic of the mechanical properties of the lung and the lung tissue is its highly nonlinear stress-strain or pressure-volume relationship, which is known to be altered in disease. The nonlinearity would naturally lead to time variation in an apparent stiffness during any oscillatory stretching such as done by mechanical ventilation or during oscillometry. That is, because of the nonlinearity there is a change in slope of the stress-strain (or pressure-volume) curve and the instantaneous apparent stiffness (or elasticity) varies. This is similar to the case when a parameter of the underlying system changes with time, changing its mechanical stiffness in a time varying manner. Since the nonlinearity can

change in disease [35]–[37], understanding it's potential contribution to $R(f)$ is important as $R(f)$ is also increased in disease [6], [27], [38],as was mentioned previously on page 8 .

Thus, the principal aim of this thesis is to quantify this potential source to better understand the mechanisms underlying this contribution to the frequency dependence of resistance. A secondary aim will be to briefly compare this source to heterogeneity, as heterogeneity is most commonly considered to be the dominant mechanism to produce $R(f)$. These aims together with hypotheses are provided in more detail later in the next chapter.

1.5 INVESTIGATING $R(f)$ DUE TO TIME-VARYING MECHANICS ARISING FROM NON-LINEAR LUNG TISSUE PROPERTIES

$R(f)$ as previously described, has become/used as one of the clinical measures to diagnose or monitor respiratory disease especially obstructive disease. The research questions we are probing in this thesis are – **Does the $R(f)$ comes from respiratory system nonlinearity, and if so, what is the potential magnitude of this contribution? And how does this mechanism occur from tissue properties or from the combined nonlinearity characteristic in the pressure-volume relationship of the respiratory system?** We initially began our investigation experimentally using ex-vivo lung tissue but due to COVID-19, we had to shift to mathematical modeling of nonlinear lung characteristics and its effect over $R(f)$.

1.5.1 Experimental: Lung Measurements

In-vitro tissue measurements can give a good understanding of the underlying mechanics of the organ. Hence, the first proposed thesis plan was to measure tissue mechanics in vitro directly measuring the nonlinear tissue properties, the development of time-varying stiffness, and use that to predict $R(f)$ and compare that to measured $R(f)$. Altering the tissue mechanics using enzymes such as collagenase and elastase as a model of disease was also to be explored. Since some of this work was completed, I briefly report it in this thesis for potential future development. To do this I began developing a tissue bath where pig lung tissue strips would be used to study the stress-strain relationship which would give the underlying lung mechanics through material properties. Different approaches exist for tissue baths of lung tissue, including from alveolar walls and

parenchymal slices to contractile function airway smooth muscle strips or airway rings, and the medium can be easily changed to degrade tissue structure using collagenase and elastase [39]–[41]. It is also possible to measure the mechanics of the whole lung ex-vivo, including human lungs delivering air via the trachea and sometimes media via the vasculature [41]. However, it was not possible to achieve this aim even though most of the apparatus used for the tissue measurement had been prepared due to lab restrictions in COVID-19. The thesis since pivoted to using published tissue data and focus on modeling the tissue mechanics analytically and computationally producing the time variation of mechanics, simulating its measurement, and comparing the $R(f)$ under different conditions and altered mechanics.

1.5.2 Analytical: Lung Modeling

In the early 1970s – 1980s, several models of lung tissue or respiratory mechanics were developed using lumped mechanical elements, which followed one of the early seminal papers in 1955 [42]–[60]. The simplest lumped element model of respiratory mechanics comprises a single spring as the elastic element, with a dashpot to account for tissue viscosity and/or Newtonian airflow resistance. If higher frequencies were being modeled as an inertial element is added to account for the acceleration of the mass. This is known as the equation of motion of the respiratory system and has been applied to parts of the system as well such as the lung excluding the chest wall and upper airway $P = EV + R\dot{V} + I\ddot{V}$, where P is the airway opening pressure, E is respiratory system elastance, $V$is the respiratory volume, R is the respiratory system resistance, $\dot{V}$is airflow to the airway opening, I is inertia and $\ddot{V}$ is acceleration of the volume. Considering lung tissue on its own, the stress-strain nonlinearity was modeled empirically, as in Navajas et al [39], as well as more complex approaches using springs of different stiffnesses for elastin and collagen using distributed properties [39], [61], [62]. Most models attempted to describe the nonlinear stress-strain curve as a static elastic nonlinearity without including the tissue viscoelastic or time-dependent behavior, but a few included sources of resistive losses such as spring and dashpot elements, or the conceptual fractional dimensional spring pot [61][62]. It was hypothesized and also shown that models with a distribution of time constants arising from multiple spring and dashpot pairs could produce the frequency dependence of impedance known to be characteristic of lung tissue [26].

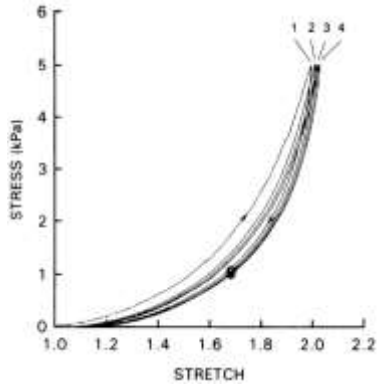

Figure 1.10: Stress-Strain relationship of dog lung tissue (reproduced with permission from [39]*)*

Figure 1.10 shows the nonlinearity of lung tissue [39], [63], taken from canine lung tissue undergoing a very slow cyclic stretch over a wide range. This is known as preconditioning when tissue is initially stretched experimentally in an apparatus and shows the gradual shift to larger stretch values with the cycles becoming more reproducible. A loss of hysteresis is also observed. Navajas et al [39] used analytical modeling to explore how the nonlinearity affected small-amplitude linear behavior, probing changes in strain amplitude and changes operating point (mean strain), and indeed also measured frequency dependence of impedance. However, they did not assess if the time-varying behavior in tissue stiffness that would have been present was linked with any frequency dependence of Rrs, which is one of my hypotheses.

The stress-strain curves shown can be fit to a nonlinear curve i.e., exponential in equation 1.5.

$$T = T_r e^{\alpha(\lambda - \lambda_r)} \tag{1.5}$$

Where T_r is the stress when the stretch ratio is equal to a reference stretch λ_r and α is a nonlinearity exponential constant.

Alamdari et al. [22], [23], [64], as mentioned earlier, explored how time-varying respiratory mechanics could lead to the frequency dependence of Rrs, both in a single compartment model and in a parallel compartment model. He did not utilize any mechanisms such as tissue properties for the imposed time variation. Figure 1.11 shows a reproduction of this modeling that I developed in preliminary work of the single-compartment model (Figure 1.11, right) with time-varying in $E(t)$ as shown in the equations, with sinusoidally varying E_v, and the frequency dependence that reproduced Alamdari's findings in Figure 1.11 (left).

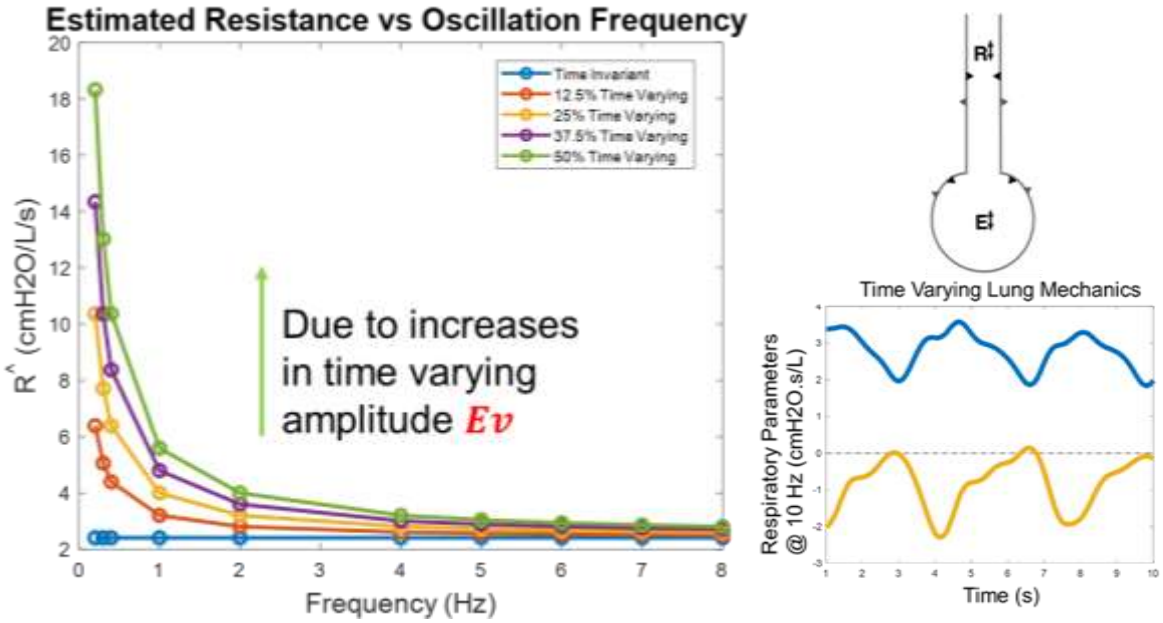

Figure 1.11: (left) Time-varying mechanics behind the $R(f)$ (right) Single compartment model with time varying mechanics of lung.

Briefly the resistance, $R(t)$ and elastance $E(t)$ are modeled as time-varying parameters as follows in equations 1.6 & 1.7:

$$R(t) = R_m + R_v \sin(2\pi f_{os} t) \tag{1.6}$$

$$E(t) = E_m + E_v \sin(2\pi f_{os} t) \tag{1.7}$$

Where R_m is the mean resistance and R_v is the amplitude of the variation at the oscillation frequency f_{os}, and E_m is the mean elastance and E_v is the amplitude of the variation. Using the single-compartment model (equation 1.2) and the Zadeh transform (equations 1.3 and 1.4), Alamdari showed that the time-varying impedance was as follows:

$$P(t) = R_m A 2\pi f_{os} \sin(2\pi f_{os} t) - E_m A \cos(2\pi f_{os} t) + V_m \boldsymbol{E_v} \sin(2\pi f_{os} t) \tag{1.8}$$

where Z is the impedance of the lung determined by the ratio of P (pressure) to $\dot{V}$ (flow) at specific f_{os} (oscillation frequency). A are the amplitude of sinusoidal varying volume, and the red colored terms are highlighted for their relationship in the next equation. Alamdari showed that resistance at the oscillation frequency, and only considering the component of pressure in phase with flow, will be dependent on the following variables given in equation 1.9:

$$R_{f=f_{os}} = \frac{P(t)}{\dot{V}(t)} = R_{mean} + \frac{V_m E_v}{A 2\pi f_{os}} \quad (1.9)$$

However in practice resistance is determined by estimating the real part of impedance Z where Z is estimated by performing the Welch periodogram technique to compute $Z(f)$ as follows in equation 1.10:

$$Z(f) = \frac{1}{N} * \sum_{k=1}^{n} \left(\frac{FFT(\Psi(P(t)_k))}{FFT(\Psi(\dot{V}(t)_k))} \right) \quad (1.10)$$

which is commonly used to estimate impedance in oscillometry. This equation described how the time domain P and $\dot{V}$ are divided into k windows of finite duration, a windowing function Ψ is applied typically using a hamming window, then each is Fourier Transformed using the FFT, the ratio is taken, to compute impedances for each window, and the average of the k impedances computed as the final impedance as a function of frequency, at the frequencies of oscillation. Usually, the windows are overlapped anywhere from 50% to 95%.

It can be seen from equation 1.9 that resistance R_f where the subscript f is used to denote the frequency of oscillation, arises from the $\frac{1}{f_{os}}$ term in Equation 1.9, and it depends on the mean volume at which the lung oscillates (that is where on the pressure-volume static relation the oscillation occurs) and depends inversely on the amplitude of the volume input signal, and depends on the magnitude of the time-varying elastance, E_v (indicated in the box legend of Figure 1.11 (left)). If in the case of no time variation (E_v = 0) there will be no frequency dependence of resistance, which is the blue flat line in Figure 1.11 (left). An increase in E_v increases the frequency dependence of resistance. However, Alamdari et al had no mechanism for why E_v would be altered, it was simply varied arbitrarily. They also showed that the $R(f)$ depended on the phase of the oscillation of elastance, with maximal $R(f)$ when the phase of oscillation was in phase with the flow signal, and no effect when the phase within phase with the volume. Alamdari also demonstrated this behavior using the Zadeh transform [29] showing with two separate modeling approaches that $R(f)$ can arise from time variation of elastic behavior. It can potentially be a substantial source of $R(f)$ given the large variation evident in X_{rs} at 5 Hz in COPD as shown in Figure 1.9.

As indicated above, one mechanism for inducing an apparent variation in elastance is the nonlinearity in lung tissue to potentially contribute to the frequency dependence of R_{rs}. This is

observed when we are tracking Z_{rs} with larger amplitude oscillations or at different operating points exploring changes in the slope of the stress-strain or the PV curves. However, this variation would be in phase with volume, and as Alamdari predicted is not expected to produce $R(f)$ which he showed arose from variations in-phase with flow or strain rate. When stretching soft tissues such as lung tissue, it is established that the output stress is a fixed phase shift behind the input strain. This is well described by a model known as the constant phase model or CPM as described in more details below. This means a portion of the output stress is in phase with the input strain, but a smaller portion of the stress (typically 10 to 20%) is 90 degrees out of phase with the strain and is thus is in phase with strain rate.

At any point in the stress-strain curve the elastic stiffness can be approximated to the slope of the stress-strain curve, and with a change in the mean stretch, or increase in the oscillatory stretch, the slope changes, can be thought of as an apparent stiffness changing with time, although it is driven by the input strain. Previously the effect of this apparent time variation on impedance and $R(f)$ has not been modeled but is similar to the time variation arbitrarily considered by Alamdari et al (cite his thesis and his paper). In this thesis I assess if the nonlinearity similarly can provide a potential source of sufficient temporal or nonlinear variation to contribute significantly to the frequency dependence of the resistance as observed in vivo. Also, since lung tissue elastic properties are known to change with disease, this may also contribute to the increased $R(f)$ observed with the disease as previously mentioned. Of course, lung tissue nonlinearity is only one source of potential temporal variation and is the focus of Aim 1.

1.6 INVESTIGATING $R(f)$ DUE TO HETEROGENEITY OF VENTILATION IN THE LUNG

Since heterogeneity in airway diameters is thought to be the predominant source of frequency dependence of resistance in whole lungs, I felt I could also take advantage of some work being done in my lab measuring heterogeneity of ventilation in patient's post-lung transplant that develop lung dysfunction known as chronic lung allograft dysfunction (CLAD). These patients also have measurements of respiratory impedance including time variation of impedance potentially useful to my thesis objectives. Thus, the following provides a brief review of CLAD

and how imaging methods can demonstrate the heterogeneity of ventilation attributable to airway diameter variation.

1.6.1 Chronic Lung Allograft Dysfunction Study

Patients that receive lung transplants are at risk of developing CLAD which leads to breathing dysfunction and altered lung mechanics. Within 5 years of lung transplant (LT), $40-50\%$ of recipients will develop (CLAD), which most often results in the fatal disease bronchiolitis obliterans (BOS) [65]. BOS is a disease that initiates in the small airways, obstructing airflow. Unfortunately, the current assessment of lung health using spirometry in post-lung transplant patients is inadequate to detect CLAD [66], as it is insensitive to the small airway obstruction.

Here in our lab group, we are investigating Technegas single-photon emission tomography ventilation SPECT/CT (T-VSPECT/CT) to assess ventilation heterogeneity. T-VSPECT/CT using Technegas is an imaging technique where patients are asked to inhale Technegas-TM, which is air containing Tc04 labeled carbon nanoparticles that travel through the airways during inhalation and deposits in the alveoli and are later detected by their gamma particle emission [67]. Uneven deposition and regions with no ventilation indicate changes that may be due to CLAD. These patients are known to develop heterogeneous disease, but this has not been previously measured by SPECT/CT. Ventilation images were compared with standard lung function using spirometry as well as oscillometry which measures impedance to airflow and can be sensitive to heterogeneity in small airway obstruction [68] which will be shown in detail in the next chapters.

CHAPTER 2: OBJECTIVES AND HYPOTHESES

This chapter presents the hypotheses and corresponding objectives of this thesis, which are as follows:

Hypothesis 1: The $R(f)$ in lung tissue is dependent on the **time-varying mechanics** arising from **nonlinear** tissue as well as whole lung properties and may be a source of $R(f)$ in respiratory system mechanics.

Objective 1: This will be investigated by introducing the nonlinearity into the most common tissue and whole lung impedance model, known as the constant phase model. Using the combined model, we will use oscillatory input over a range of frequencies, oscillation amplitudes, and operating points, assess the time-varying mechanical properties and assess the $R(f)$, in two frequencies ranges, 0.03 to $5\ Hz$ and the standard oscillometry range $5\ Hz$ to $37\ Hz$,

Hypothesis 2: The $R(f)$ in respiratory mechanics is more greatly dependent on the **heterogeneity** of impedance.

Objective 2a: This will be explored through VSPECT/CT imaging in post-LT subjects who develop heterogeneous lung dysfunction. Using quantitative measures of from imaging and oscillometry measurements of $R(f)$, we will see if heterogeneity in post-LT patients is correlated with $R(f)$.

Objective 2b: The effect of time-varying lung mechanics will also be studied in post-LT patients using the time variation in reactance at $10\ Hz$ as an estimate of the time variation in elastance and tested by correlation with measured $R(f)$ over 5 to $37\ Hz$.

In chapter 3, I describe the approaches to measure time-varying mechanics of lung tissue in a tissue bath. In chapter 4, I investigated the lung tissue nonlinearity model and studied where time-varying lung characteristics are expected to arise resulting in $R(f)$. I simulated different amplitude and operating point effects over stress-strain curves as well as increases in nonlinearity to study diseased cases which might give us insight that diseases will have a higher effect over $R(f)$, due to time-variation coming from nonlinearity, making it clinically significant parameter for diagnosis.

In chapter 5, I investigate the whole lung nonlinearity pressure-volume models in a similar approach to chapter 4, exploring the behavior including changes in the Pressure-volume relationship appropriate for diseases that are known to alter the PV nonlinearity – Fibrosis and emphysema, and explore these over two frequency ranges near breathing, and the oscillometry frequency range.

In chapter 6, I describe our Chronic Lung Allograft Disease Study, from which I used some of the data to correlate the ventilation heterogeneity, and the time-varying characteristics of lung impedance collected by oscillometry with $R(f)$. In our lab group performed by other students, we analyzed the SPECT/CT images to obtain quantitative results using published approaches. Then I used a measure known as the coefficient of variation (CoV) as a measure of heterogeneity to test its correlation to $R(f)$. I also correlated time-varying reactance obtained from the lung transplant patients to $R(f)$. In chapter 7, I present concluding thoughts on the thesis and suggestions for future work.

CHAPTER 3: INVESTIGATING $R(f)$ DUE TO TIME-VARYING MECHANICS ARISING FROM NON-LINEAR LUNG TISSUE PROPERTIES (IN-VITRO TISSUE APPROACH)

This chapter presents methods and results of the in-vitro tissue approach that was used to establish the time-varying mechanics arising from the nonlinear tissue properties of the lung resulting in $R(f)$. It starts with the in-vitro tissue approach where all the steps taken to develop the tissue bath and tissue preparation are presented. The chapter follows with results and a discussion of some of the obtained outcomes.

3.1 METHODS

We designed the tissue bath from requirements both to maintain the flow of nutrients to living tissue and maintain it at close to normal body temperature. Important requirements of the tissue bath are **maintaining tissue viability,** the **force,** and length **ranges**, as well as the frequency bandwidth for exploring frequency dependence of tissue mechanics as can be seen in appendix A.

3.1.1 Tissue Preparation

We chose pig lung tissue as it is similar to human lung tissue and is readily available from local abattoirs and our sourcing of the tissue and use was approved by animal care at Dalhousie University. Pig lung tissue is taken from the left inferior lobe of the lung. First, the left pig lung is obtained from the abattoir and then kept in Krebs Solution and kept within a cooler packed with ice for transportation. Once the lung arrives at the lab, it is flushed with 1 liter of new Krebs Solution to make sure that blood is removed. The pleura is removed manually and then using a scalpel a couple of tissue strips of $3 \times 1 \times 1\ cm$ are obtained, selecting tissue without large bronchial segments. The strips are then placed in Krebs in a beaker where they float and then are briefly degassed by placing the beaker in a vacuum pump chamber which takes less than $30\ sec$, and the tissue sinks. The strips are then ready to be removed and using cyanoacrylate glue can be affixed to plastic attachments. These plastic attachments were designed by a summer student (C. Potter) and are used to fit the tissue within the tissue bath as described below.

3.1.2 Setup

The preparation of the tissue bath was adapted from Maksym [69] (Figure 3.1). It included 3 baths and tubing to allow fresh media circulation, including a heater and a pump. The upper bath contains a $100W$ cup heater and Omron Heater controller which is intended to keep the tissue bath at a constant temperature for constant flow at a design temperature above 32^oC and less than 37^oC. The lower bath collects overflow from the tissue bath and the pump returns fluid to the upper bath. The noise of the pump is separated from the tissue bath and the flow to the tissue bath is regulated by a pinch valve using this design. The main bath includes the actuator attachment on one side and the selected force transducer (Honeywell – Low Range Precision Miniature Load Cell, Model 31 Low) embedded into the tissue bath wall on the other side. For tissue attachment the fluid can be drained using the lower exit tube valve and tissue is put in place using attachments that slide into the actuator arm connector and the force transducer connector tightened with set screws.

We chose a force transducer that could operate under fluid and with a maximum force range that exceeded a maximum expected force by a safety factor of 1.5, which was $50g$. The length actuator must provide a range of at least 30 mm for full strain, but to provide the flexibility the design requirement was a length range of double this of 60 mm. The speed requirement was 3 Hz at an amplitude of 10% strain which is $3\ cycles/sec\ \times 2 \times \pi \times 0.1 \times 30\ mm\ =\ 56\ mm/s$.

The bath included two outlets: the higher outlet was for a tissue while submerged in media, and the lower was for tissue suspended in air if waves in the media contaminated the force measurements. This was done with the assistance of our technician D. Cole, who designed the thumbscrew regulators to help regulate fluid flow. The attachments for the tissue were developed by C. Potter and were 3D printed to allow low fluid disruption during motion. To keep the tissue alive, and help maintain the appropriate pH, it is necessary to oxygenate the Krebs solution using carbogen ($95\%\ O_2, 5\%\ CO_2$) provided via a fish tank diffuser in the lower bath.

We sourced a stepper motor-based length actuator from a colleague that appeared to meet these requirements from its specifications. We built a simple stand that was clamped to the bench and began testing it against the requirements. It was controlled by ST-5S Applied Motion Driver using Serial Communication from the computer. A test controller software and user interface were planned to control the actuator, record the actuator position, and force output and save the data on a PC with Windows 10 and LabView 2019. A prototype version was developed enabling testing

of the actuator control to see if it met our requirements. The design requirements and some design calculations to test the actuator are in appendix A.

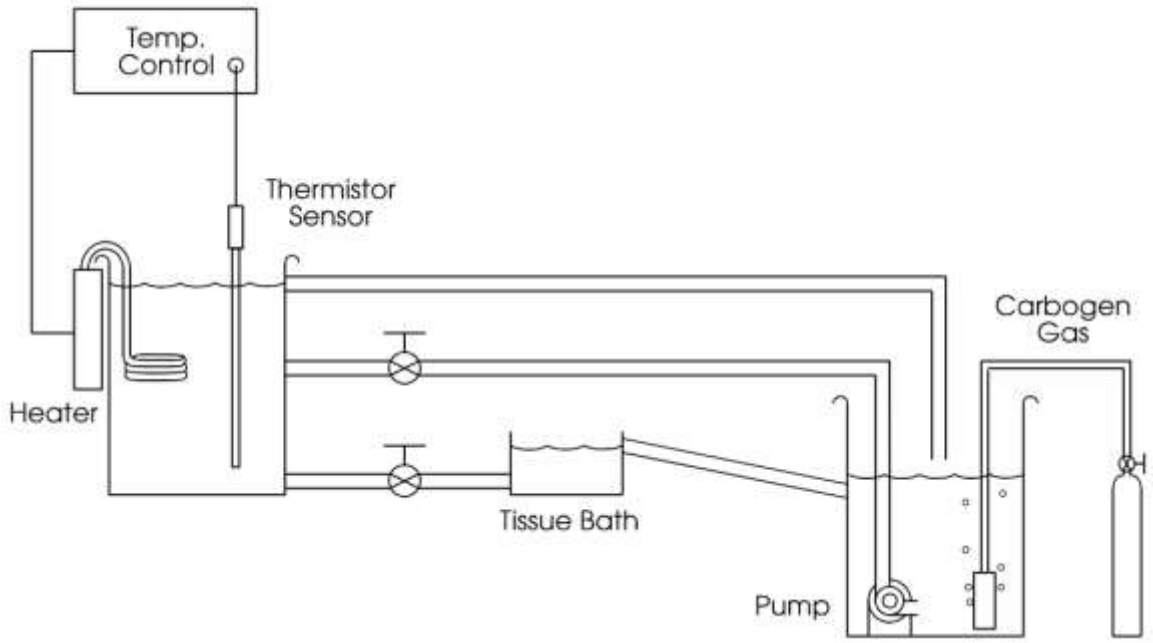

Figure 3.1: Tissue Bath from Maksym's Thesis [70]

The software was to do the following: **1)** preconditioning to adapt the tissue over the strain range to be tested which helps make subsequent experiments reproducible and **2)** fixed oscillations mimicking oscillatory measurements of mechanics varying amplitude, operating points (mean stretch), and frequencies of oscillation chosen to explore the physiological ranges of stretch and stress. Preconditioning cycles are fixed slow rate stretching from zero to a maximum stretch or stress (e.g., $5\ kPa$) and return to $zero$ for n cycles (typically 5), which would be done prior to experimental measures.

After some software development and several attempts to achieve the manufacturer's stated performance characteristics, we concluded that the existing actuator would unfortunately not fulfill the desired requirements. While the actuator exceeded the velocity requirements as per their specifications for single instructions and single direction motion, in practice the communication delays were too high to achieve stable oscillatory motion. This is also shown in appendix A. We thus switched to a design using servomotor-controlled linear actuators, and we explored and chose a solution from different manufacturers that would meet our requirements. The best options are

presented in appendix A. However due to COVID-19, which prevented us from proceeding with tissue-based lab work for an uncertain time, we decided to instead use published lung tissue data and extend the modeling and analyses. We could potentially return to experimental measurements of lung tissue mechanics after my MASc as part of a potential Ph.D. if determined to be still useful.

3.2 RESULTS AND DISCUSSIONS

Here I described the tissue bath construction which was completed before COVID-19 and some of the actuator testing. Figure 3.2 on the left shows the main bath indicating the actuator and force transducer where the pig lung tissue would be attached 3D printed attachments via cyanoacrylate glue. On the right is the 3D printed assembly drawing created by A. Brezovan a co-op student in our lab. Also shown are the upper bath where the heater would be installed, the main bath with actuator and force transducer tissue attachments circled in red, and the lower bath 3D assembly drawing.

We were able to develop software in LabVIEW to test the actuator. As described above the actuator failed to meet our requirements for oscillatory motion. This was because the time required between commands inherent in the actuator controller was too long to maintain smooth oscillatory motion with direction reversals at the desired frequencies, achieving stable motion only at lower than 0.03 Hz.

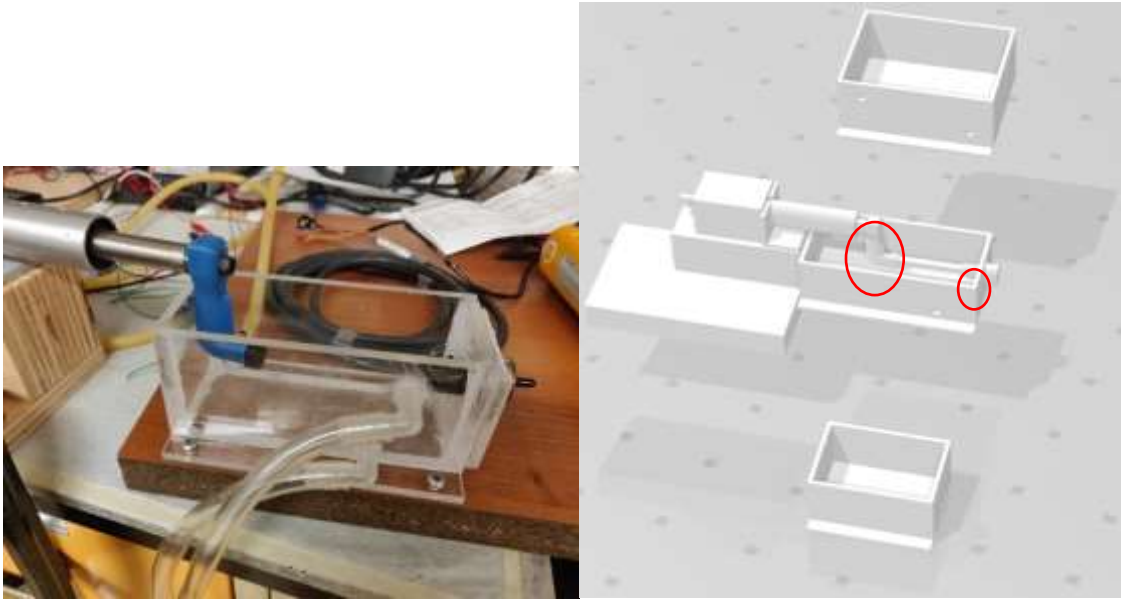

Figure 3.2: Tissue Main Bath setup and 3D design of whole tissue bath

Figure 3.3 shows the basic tissue preparation steps. The tissue is sliced to approximately $30\,mm \times 3\,mm \times 3mm$ (Figure 3.3 (left)) while on the right is the tissue floating in Krebs solution prior to degassing.

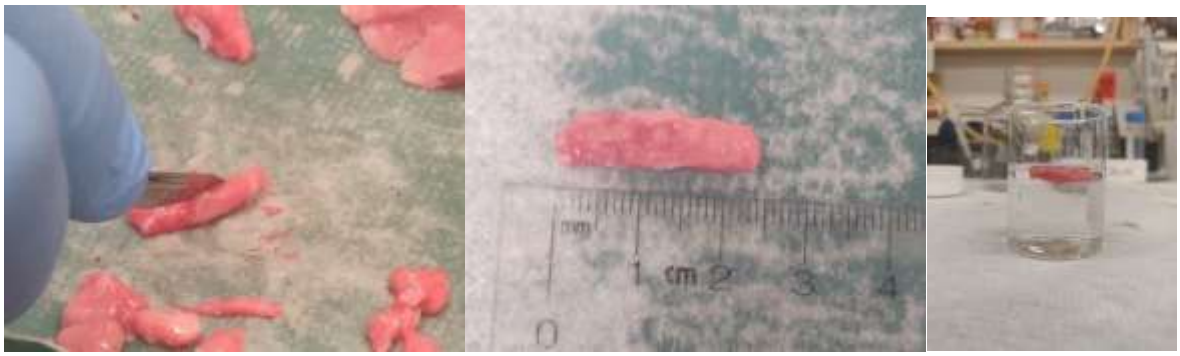

Figure 3.3: Steps to obtain pig lung tissue strip: (left) slicing of pig lung tissue using scapple to the desired length, (right) floating lung tissue in Krebs solution.

The tissue bath was developed, and the tissue preparation looked promising, but the actuator needed improvement. However, I was not able to conduct any experiments due to COVID-19, there is sufficient published data that we can proceed without collecting instead we modified the project to focus on the modeling as can be seen in Chapters 4 & 5.

CHAPTER 4: LUNG TISSUE MODELING

In this chapter lung tissue, nonlinear viscoelastic models are investigated and studied where time-varying lung characteristics are expected to arise resulting in $R(f)$.

4.1 METHODS

In this section, I describe the development of different analytical tissue models for modeling the stress-strain characteristics of lung tissue, since this is more directly relevant to the measurement of respiratory mechanics in-vivo. I consider models based on mechanics parameters from healthy cases, as well as mimicking states of the disease known to alter the lung tissue properties. The models are developed to specifically explore the impact of time-varying lung properties on the mechanical impedance and in particular, the mechanical tissue or lung resistance that arises from the normal nonlinear properties of the lung tissue as well as abnormal properties that can occur in disease.

4.1.1 Nonlinearity in a lung tissue model

To be able to calculate impedance vs time, and to reproduce the results of Alamdari as a starting point, we first tested the approach using a linear single-compartment (equation of motion-based) model, where we made sure that the time-varying elastance is in phase with the flow and we also chose the amplitude of the sine wave to be inversely proportional to the amplitude of the wave $\frac{A}{\omega_{os}}$ which means the velocity amplitude is constant with frequency, useful for actual actuators, but not a limitation for simulation. I found as expected that this model provided simple linear behavior using the single-compartment model with independent $R(t)$ and $E(t)$ matching the modeling of Alamdari et al.

To explore time variation leading to $R(f)$ that we hypothesize that it can arise from tissue stress-strain nonlinearity; we used the model of Navajas et al who obtained stress-strain relationships from seven dog-lung tissue strips, and who also demonstrated that this relationship well described the quasi-static nonlinear behavior given in equation 1.5.

$$T = T_r e^{\alpha(\lambda - \lambda_r)} \tag{1.5}$$

Where T is stress, and T_r is relative stress at stretch ratio λ equal to the reference stretch ration λ_r and α is a constant. The instantaneous stiffness of this is the slope at any stretch and will vary with varying $\lambda(t)$.

We then combined the nonlinearity of equation 1.5 with the constant phase model shown later in the next section, where we also explored the effects of changing operating points, i.e., operating stresses in the exponential nonlinearity, resulting in the time variation which we expect might result in $R(f)$.

4.1.2 Tissue nonlinearity time-varying characteristics model

MODEL DEVELOPMENT: We developed a model of the lung tissue mechanics based on a more commonly used linear model known as the constant phase model (CPM). This model links the in-phase elastic response and out of phase dissipative response to stretch via a constant phase difference, β, and has been established to well describe tissue behavior, as well as lung mechanics at low frequencies [11], [14], [37], [62], [71]. As implemented by Kaczka et al. [37], [72] who applied it to the stress-strain behavior of lung tissue, it is as follows:

$$CPM: \frac{\sigma(\omega)}{\varepsilon(\omega)} = jG\omega^{\beta} + H\omega^{\beta}; \tag{4.1}$$

$$\beta = 1 - \left(\frac{2}{\pi}\right)\tan^{-1}\left(\frac{G}{H}\right) = 1 - \left(\frac{2}{\pi}\right)\tan^{-1}(\eta) = 1 - \left(\frac{2}{\pi}\right)\phi \tag{4.2}$$

where σ is the stress on the lung tissue and ε is the strain, G is the viscous property, i.e., loss modulus of the tissue and H is the stiffness i.e., storage modulus, and β beta is the phase angle between the loss and storage modulus respectively.

This is a linear model, and here I develop a quasilinear constant phase model (QLCPM) including the exponential nonlinear relationship from Navajas et al. (equation 2.5 [39]) in a very similar approach to quasi-linear viscoelastic tissue modeling (QLM) known as the quasi-linear theory of viscoelasticity found in Fung et al [26], but here using the CPM linear model above as the linear component. I first re-express the stretch ratio λ by the more common strain ε, and explicitly including it as an oscillatory variable dependent on radial frequency ω:

$$\varepsilon(\omega) = \lambda(\omega) - 1; \tag{4.3}$$

and instead of β, I instead use the more commonly used constant hysteresivity η which is defined as the ratio between G and H.

$$\eta = \frac{G}{H} = \frac{\omega R}{E}; \qquad \phi = \tan^{-1}\eta \tag{4.4}$$

Note that the values from the CPM can be related to the parameters of the standard single compartment viscoelastic model $G = \omega R$ and $E = H$, although in the CPM they are related via the hysteresivity constant. The constant phase model is often also known as the structural damping model since energy dissipation (in G) is related to energy storage (via H) by a constant, and the dissipation is thought to come from a fixed fraction of the elastic motion of the structure [73]. ϕ is then the angle between resistive or out of phase stress and elastic or in phase stress from deformation in equation **Error! Reference source not found.**4.4.

Now in order to calculate mechanical impedance, which will ultimately be used to estimate the $R(f)$, we start with the standard relation, assuming linearity and stationarity are. linear and time-invariant behavior,

$$Z(\omega) = \frac{\sigma(\omega)}{\dot{\varepsilon}(\omega)} = \frac{\sigma(\omega)}{j\omega\varepsilon(\omega)} \tag{4.5}$$

where $Z(\omega)$ is the impedance of the lung tissue and the dot denotes the time derivative of strain and j is the imaginary number $\sqrt{-1}$. Now using this in the CPM model we have,

$$Z(\omega) = \frac{\sigma(\omega)}{j\omega\varepsilon(\omega)} = \frac{jG\omega^{\beta} + H\omega^{\beta}}{j\omega} = \frac{G + jH}{\omega^{1-\beta}} \tag{4.6}$$

Note also that impedance can be defined with respect to strain rate or the rate of change of the stretch ratio:

$$Z(\omega) = \frac{\sigma(\omega)}{\dot{\varepsilon}(\omega)} = \frac{\sigma(\omega)}{(\dot{\lambda(\omega)} - 1)} = \frac{\sigma(\omega)}{\dot{\lambda}(\omega)} \tag{4.7}$$

Also, the viscous component can be written in terms of stiffness which depends on the value of eta. Therefore, the final stress-strain relationship is as follows:

$$\frac{\sigma(\omega)}{\varepsilon(\omega)} = jG\omega^{\beta} + H\omega^{\beta} = j\eta H\omega^{\beta} + H\omega^{\beta} \tag{4.8}$$

Therefore, the resulting relationship of stress stretch will be:

$$\sigma(t) = \left(j\eta H\omega^{\beta} + H\omega^{\beta}\right)\lambda(t); \tag{4.9}$$

Where stretch is sinusoidally changing with time:

$$\lambda(t) = \lambda_{amp}\, sin(\omega_{os}t) + \lambda_r; \tag{4.10}$$

$\lambda(t)$ is a time-varying stretch as mentioned in the last experiment where the slope is resulting in exponential i.e., lung tissue stiffness, λ_{amp} is stretch amplitude and λ_r is the operating point. Therefore, the resulting stress stretch model of QLM is

$$QLM: \sigma(t) = \sigma_o e^{\alpha\lambda(t)} \tag{4.11}$$

This equation 4.11 represents the QLM model for computing the resultant stress for any input strain. And QLCPM is

$$QLCPM: \sigma(t) = \left(j\eta H\omega^{\beta} + H\omega^{\beta}\right)\left(e^{\alpha\lambda(t)}\right) \tag{4.12}$$

Here we are using a shorthand notation where j is used to invoke a portion of the stress to be out of phase with the strain and in phase with the strain rate. This is because a fundamental feature of the constant phase model is that a portion of the stress varies with constant phase delay defined by η to the portion of the stress that is in phase with strain. For example, if $\lambda(t)$ is $\sin(\omega t)$ then

$$\sigma(t) = \eta H\omega^{\beta} e^{\alpha\cos(\omega t)} + H\omega^{\beta} e^{\alpha\sin(\omega t)} \tag{4.13}$$

This equation 4.13 represents the QLCPM model for computing the resultant stress for any input strain and represents an implementation of the quasi-linear theory of viscoelasticity found in Fung et al [26]. It should be noted that no parameter in this model is varying in time, yet the apparent stiffness of the model can be shown to vary. This is different from the approach of Alamdari, but I show below that the nonlinearity through introducing a variation in the apparent arising from the oscillatory input can lead to $R(f)$.

EXPERIMENTAL PROTOCOL: We simulated the CPM and QLCPM models for different stretch/strain amplitudes of $0.05, 0.1, 0.2,$ and 0.4. It is expected that higher stretch amplitudes will induce higher nonlinearity resulting in higher $R(f)$ which is done in the next section. Zadeh showed that impedance can depend on the effects of time variation in system parameters. More recently this was applied to the single-compartment model of respiratory mechanics, where Alamdari et al. used two separate modeling approaches, both the Zadeh transform and direct

temporal modeling, and demonstrated using an arbitrary time-varying elastance that this could produce effects on the real part of impedance, specifically $R(f)$. Here in equation 4.12 is also a model that naturally leads to time-varying of stiffness, which is produced by the nonlinearity in the QLCPM in this work, contributing to $R(f)$. To help show this we quantified how much stiffness varied by defining a simple proxy of the time-varying stiffness, termed here the Delta Stiffness, which is defined as the difference between the peak and valley from a calculating of the change in stress over the change in strain within one sample. This closely approximates changes in stiffness when η is small.

Then we looked at the effect of operating strains of $0.4, 0.6, 0.8,$ and 1 at the stretch amplitude of 0.05. We expect at higher levels of strains the lung stiffness increases as well as nonlinearity making it more exponential. Higher strain results in higher $R(f)$ as well. Therefore, both effects of stretch/strain amplitude and operating points are studied, and the results of the formulation are given in the next section.

We then looked at the effects of the exponent alpha. The first small stretch amplitude of 0.05 was used to study the behavior at the operating strain of 0.68. It is expected that for higher values of alpha, that this will amplify $R(f)$. Each of these is important to establish since increases in $R(f)$ have been sometimes attributed to alternative mechanisms when observed in obstructive diseases. For investigating this dependence, we used the stretch amplitude of 0.4 and the operating strain of 0.683 with alpha changed to half and twice the representative value of 4.65 for dog lung tissue from Navajas et al [39]. We also examined the effect of the different alphas at different operating strains at the lowest stretch amplitude of 0.05 to examine if the effects persisted even at the small amplitude approximation which is used often as a justification enabling one to ignore the effects of nonlinearities.

We also obtained the instantaneous stiffness as a measure to quantify the study time-varying stiffness response due to nonlinearity. It is calculated as stress difference between samples divided by strain difference between samples as follows:

$$S = \frac{\sigma(t_2)-\sigma(t_1)}{\varepsilon(t_2)-\varepsilon(t_1)} = \frac{\Delta\sigma(t)}{\Delta\varepsilon(t)} \quad (4.13)$$

In the case of CPM, it is expected that instantaneous stiffness will be constant over time as the slope is linear, whereas for QLCPM it is likely to vary. We looked at the respective resistance and reactance at the low-frequency range (in log scale) due to lung tissue size.

It is important to note that the CPM and thus the QLCPM produce $R(f)$ without any time variation of stiffness when η is non-zero. This can be seen from the signal compartment linear model (equation 1.1) that $R = \frac{\eta E}{\omega}$, without time variation of stiffness. Thus, what we are hypothesizing here is that $R(f)$ may be amplified in the QLCPM models due to the presence of the nonlinearity leading to time-varying stiffness. We further expect this to be larger with higher stretch amplitudes at lower frequencies, and larger at larger operating strains, where the nonlinearity is steeper.

4.2 RESULTS:

4.2.1 Nonlinearity in a lung tissue model

The effect of exponential static nonlinearity arising from the material properties of lung tissue (i.e., stress-strain relationship) was first investigated with two different operating stretch ranges on the Navajas et al stress-strain behavior curve (equation 1.5). Here it can be shown using the QLM model equation 4.11, examining the temporal changes of stress and the instantaneous stiffness (Figure 4.1).

Figure 4.1 shows the effect of the stress and the stiffness calculated as the instantaneous slope at two different operating points of stress (mean stretch of 1.4 and 1.8) but the same stretch amplitude. At a higher stretch, the stress range during an oscillatory stretch is larger due to the higher stiffness, and the mean stiffness has increased ~7-fold.

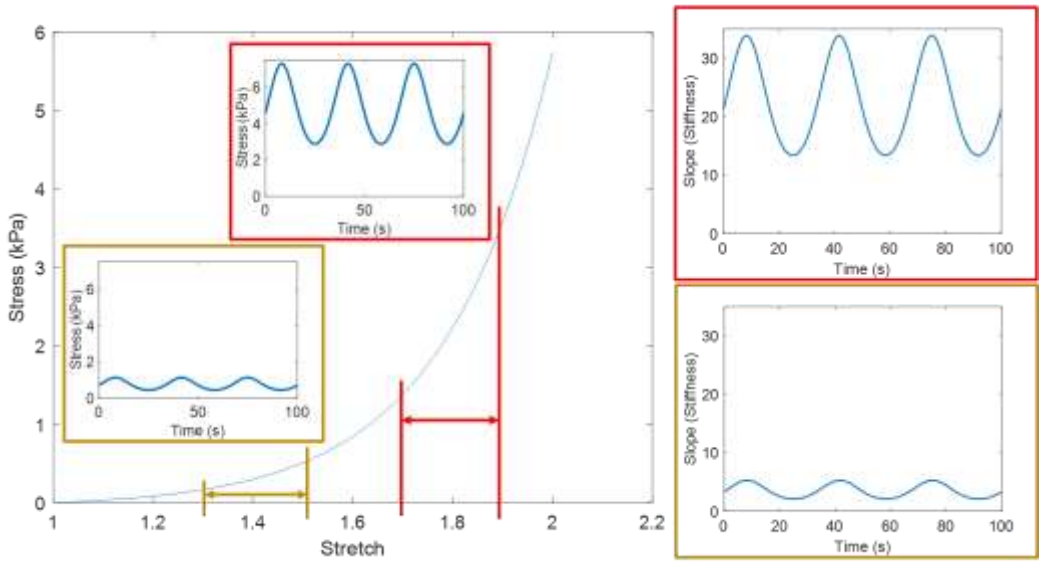

Figure 4.1: Nonlinear cyclic stretch strain curve, yellow outlined figures show stretch range between 1.3 and 1.5 with resulting time-varying stress and stiffness, similarly blue outlined figure indicates for a stretch range of 1.7 and 1.9.

4.2.2 Tissue nonlinearity time-varying characteristics model

The effect of exponential static nonlinearity arising from the material properties of lung tissue (i.e., stress-strain relationship) combined with constant phase model is as follows:

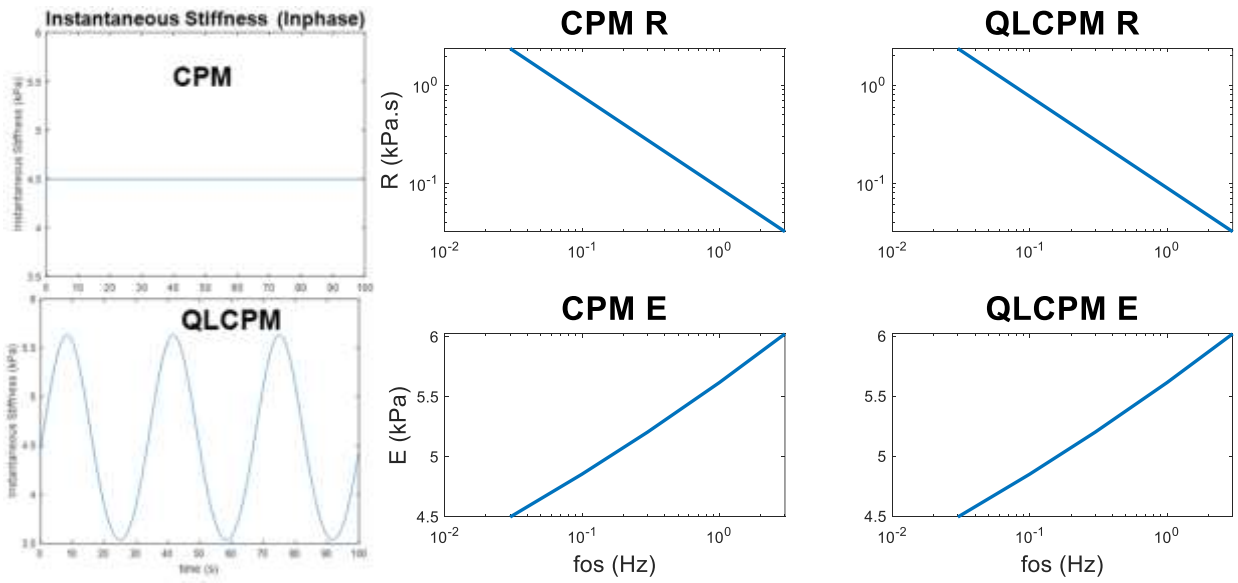

Figure 4.2: (a) Resulting instantaneous stiffness vs time for CPM (top) and QLCPM (bottom) (b)Resistance and Elastance vs frequency for CPM & QLCPM models

Figure 4.2 (a top) shows the flat line at 4.5 kPa showing that stiffness of the CPM is not changing with time, Figure 4.2 (a bottom) shows the instantaneous stiffness is sinusoidal changing with time for QLCPM equation 4.13, showing the effect of nonlinearity imparting. In Figure 4.2 (b), we matched the linear constant phase model by adjusting the H (Elastance) to have the same stiffness matching the slopes at 0.65 operating strain. At small amplitudes, the linear resistance and linear elastance calculated as per equations 4.1 & 4.13 are thus identical shown across frequency comparing CPM to QLCPM. This can also be seen in Figure 4.4 which shows R vs frequency at 0.05 amplitude the curves are superimposed. Recall there is frequency dependence explicit in the CPM model through the term eta (equation 4.2). However, when the amplitude is increased while this frequency dependence is unaltered in the CPM model, it increases nearly 50% more due to the nonlinearity present in the QLCPM model (right). This means that the nonlinearity of the stress-strain curve, through time variation led to an increase in the $R(f)$.

Figure 4.3 shows the stress-strain relationship for different strain amplitudes (SA). It is evident that for CPM the behavior is linear (i.e., each loop is larger proportionately to the amplitude and with the same slope). Whereas the loops are curved in QLCPM and the increase in size is not proportionate to the amplitude.

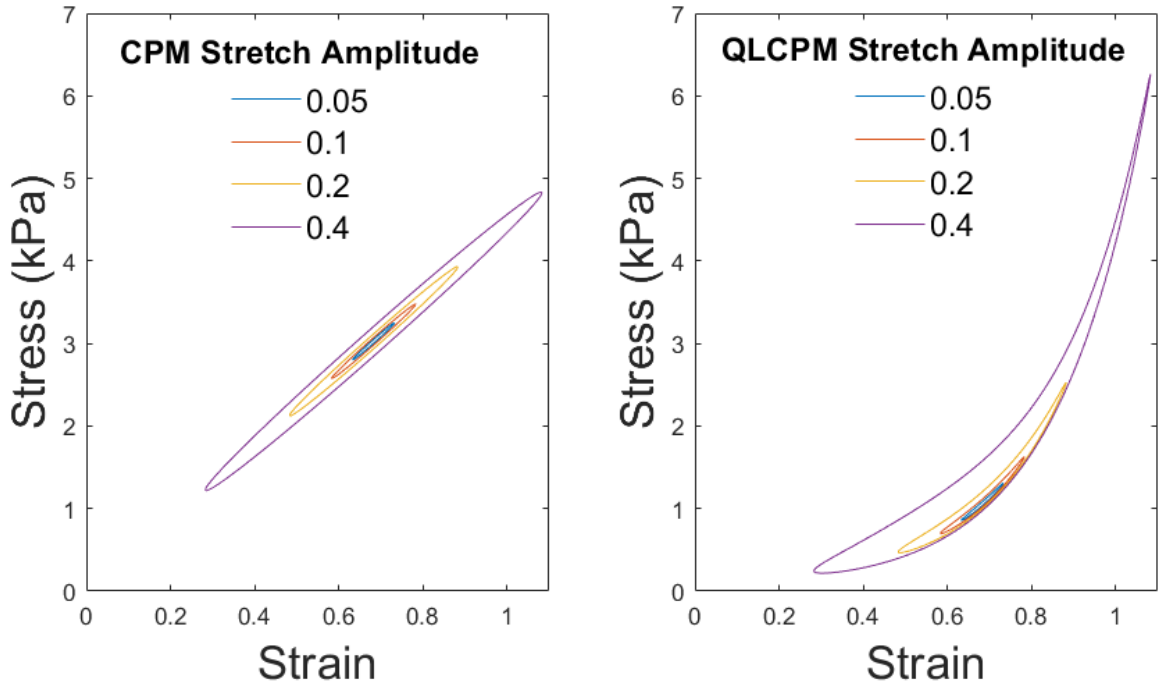

Figure 4.3: CPM & QLCPM models for a range of strain amplitudes

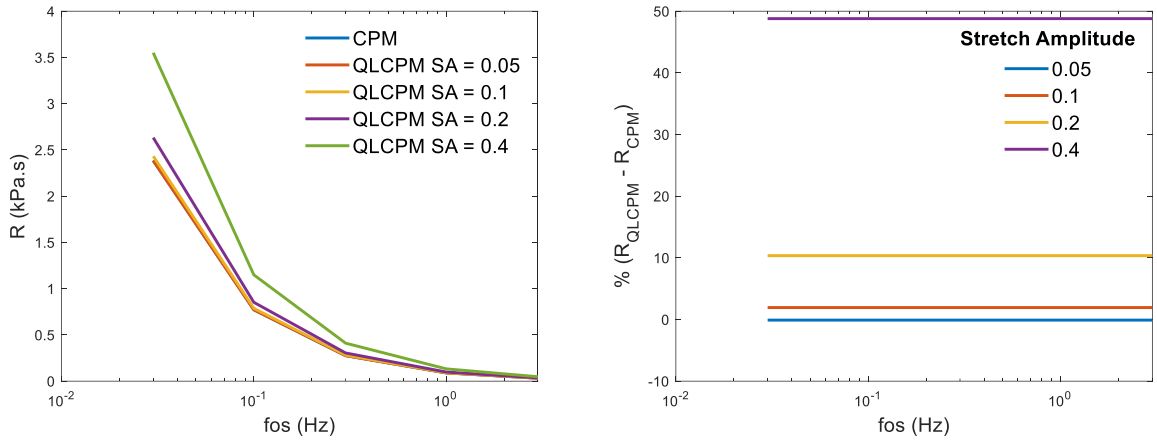

Figure 4.4 (left) R(f) for CPM & QLCPM for different SA and (right) percentage difference between CPM & QLCPM

Figure 4.4 (left) shows the same frequency dependence that can be observed in Figure 4.2 for CPM for each SA amplitude (denoted just CPM), underneath the curve for QLCPM at SA of 0.05. However, as SA increases the $R(f)$ curves move to higher R. The percent increases are plotted in Figure 4.4 (right)

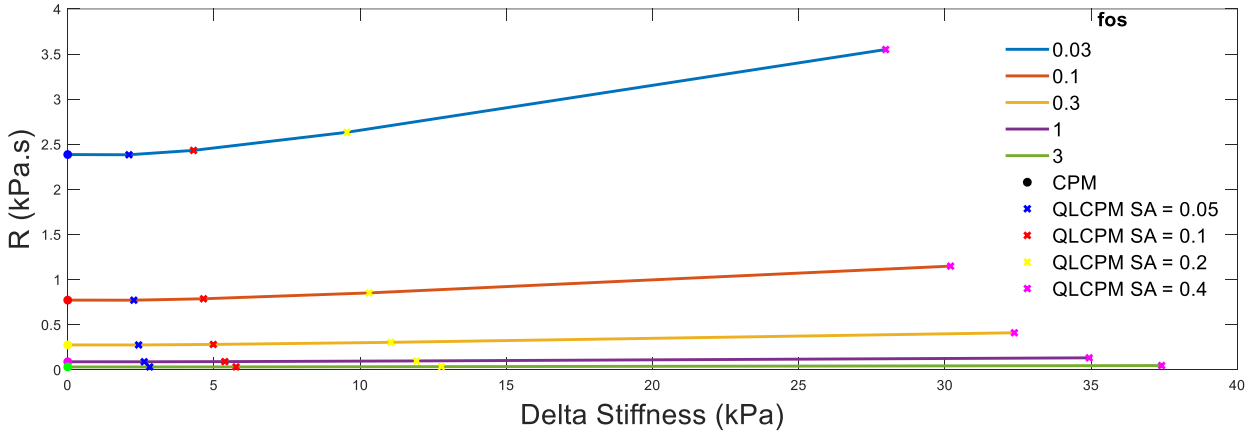

Figure 4.5: Time-varying stiffness effect on R(f) dependent on SA at different frequencies

The frequency dependence in the QLCPM is depicted vs delta stiffness showing the dependence on R on SA observed using delta stiffness is greatest at low frequencies (see the $f_{os} = 0.03\ Hz$ curve) that at low amplitude. This dependence is absent in CPM (solid circles).

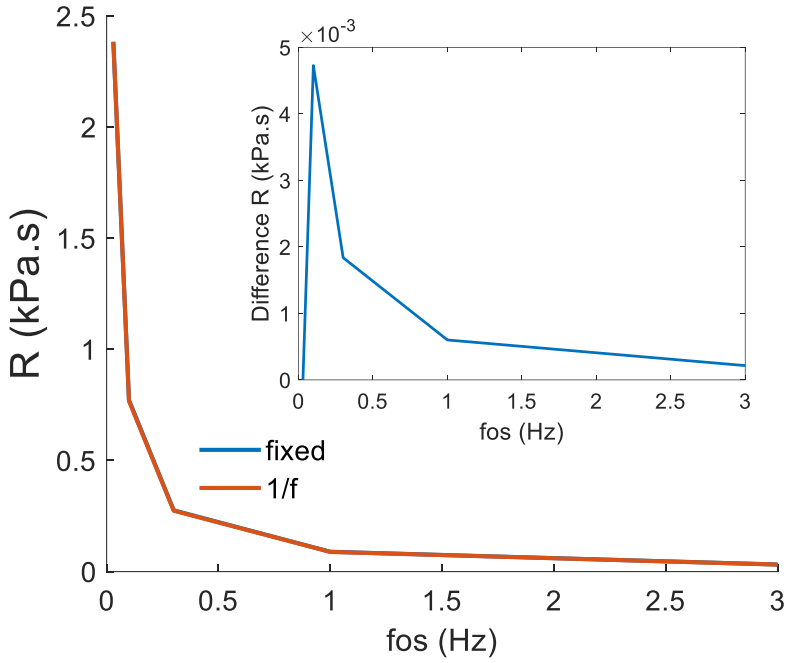

Figure 4.6: $R(f)$ for fixed and $\frac{1}{f}$ stretch amplitude. Inset shows small difference between fixed and $\frac{1}{f}$ stretch amplitude responses.

When testing lung tissue response, it is often measured over the whole frequency range making the strain amplitude $\frac{1}{f}$ dependent; that is at high oscillation frequencies, the SA is reduced inversely with frequency largely limited due to actuator speed limitations. Choosing inversely frequency-dependent SA did not much change $R(f)$ compared with constant amplitude oscillation; the inset shows very small differences in response (Figure 4.6)

When SA was fixed at 0.05 but operating strain changed (Figure 4.7) the $R(f)$ in QPLCM was highest at the highest operating point of $OS = 1$ (Figure 4.8). The highest $R(f)$ at the OS of 1 leads to an increase in $R(f)$ by 346% compared to the $R(f)$ for CPM (Figure 4.8).

Figure 4.9 similar to Figure 4.5 shows that the increase in $R(f)$ is directly related to the time-varying stiffness from the nonlinearity in QLCPM. The circles in the plot show the $R(f)$ in the CPM model and adding time variation from the nonlinearity leads to a dramatic increase in $R(f)$.

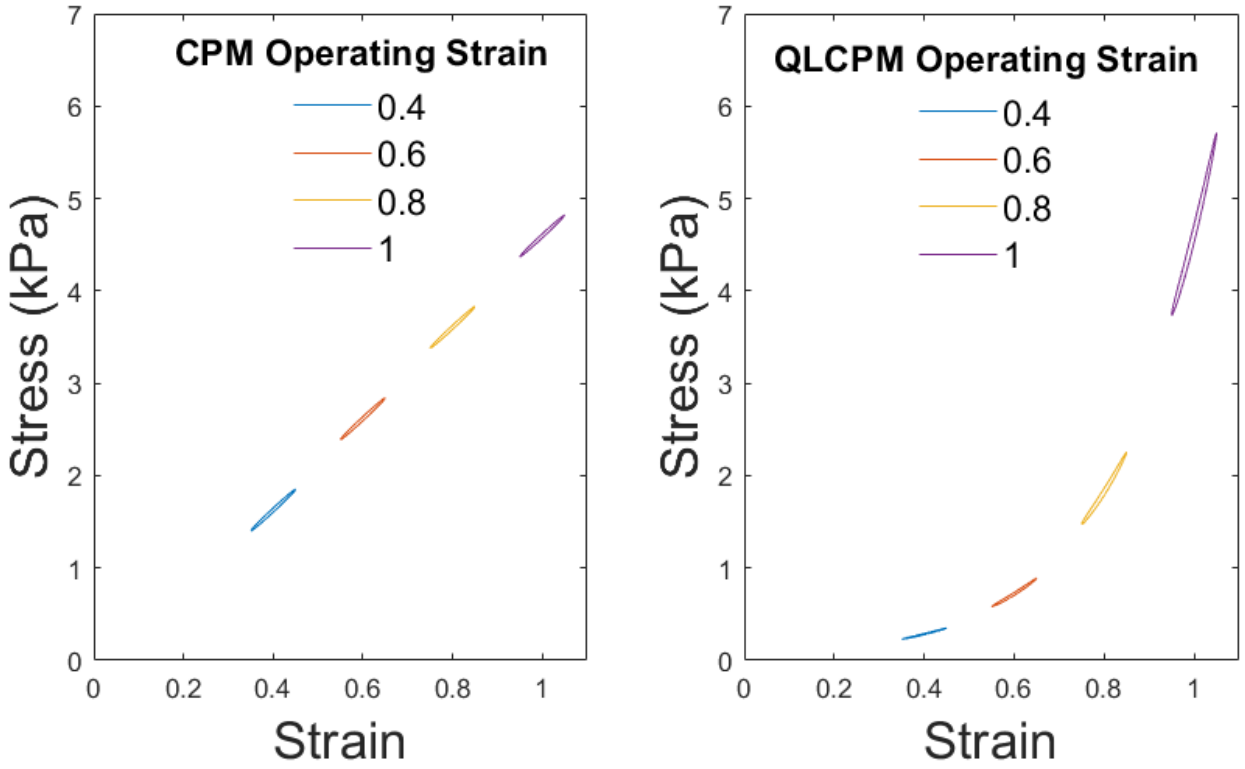

Figure 4.7: CPM & QLCPM models for a range of operating strains

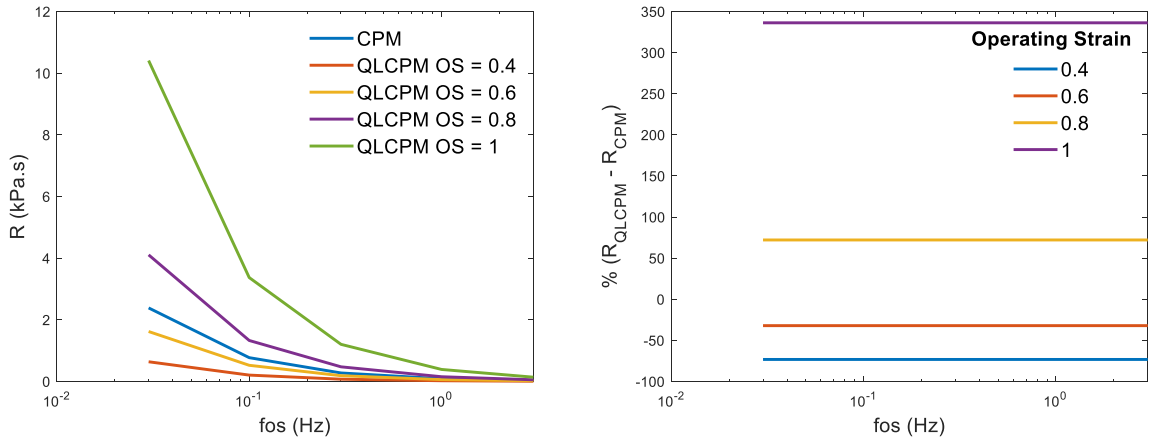

Figure 4.8: (left) R(f) for CPM & QLCPM for different operating strains and (right) percentage difference between CPM & QLCPM

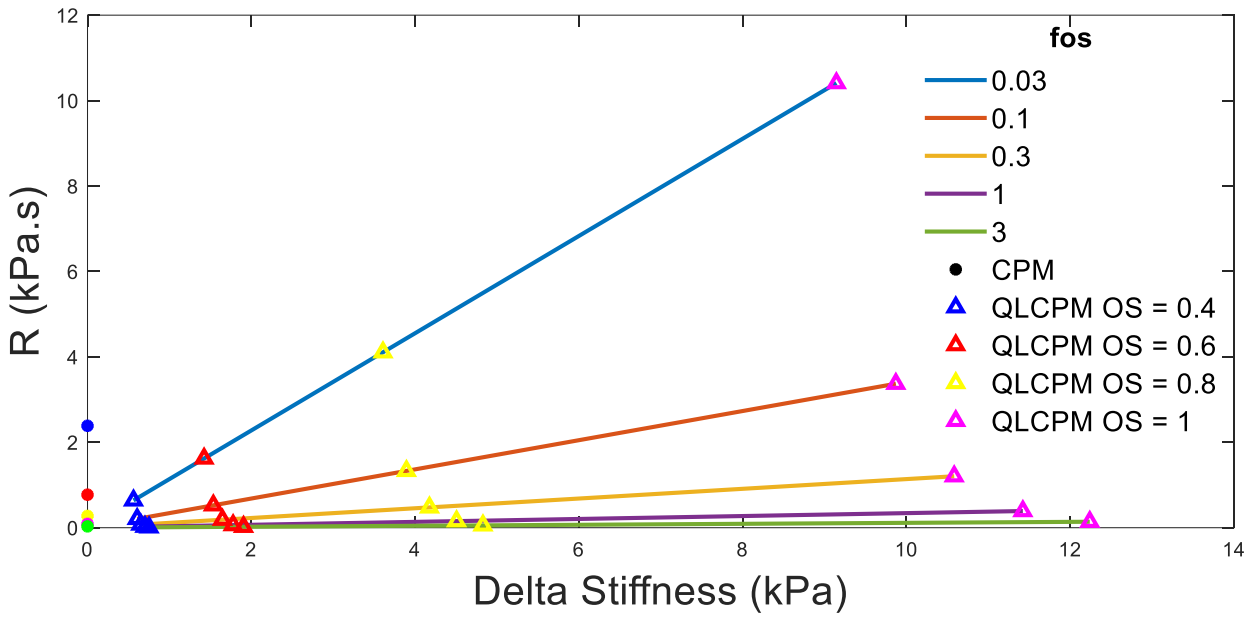

Figure 4.9: Time-varying stiffness effect of R(f) dependent on operating strains at different frequencies

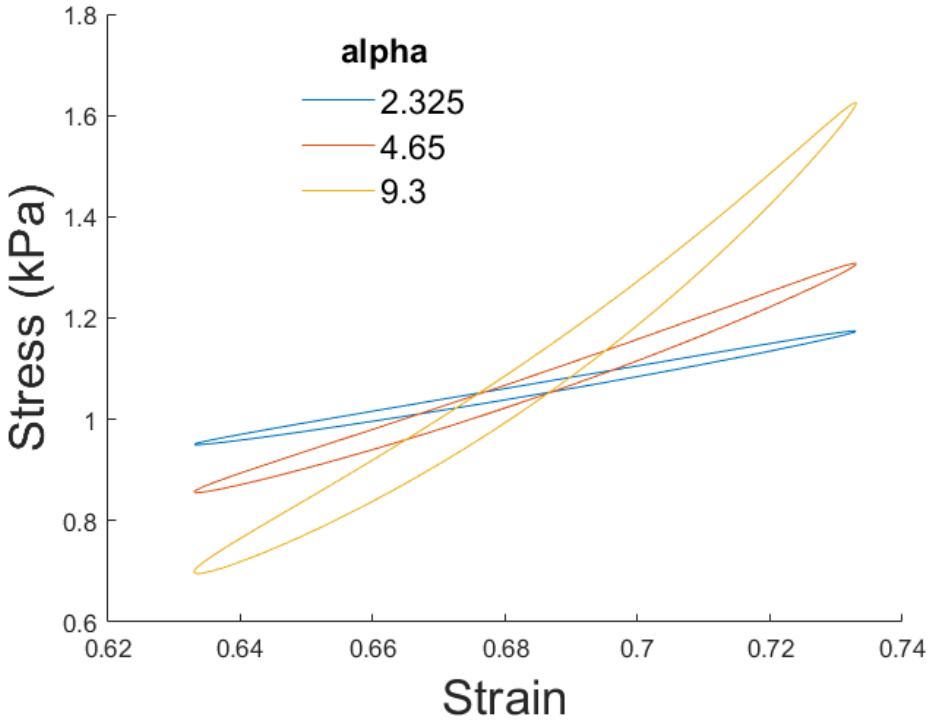

Figure 4.10: QLCPM models for a range of alphas with SA of 0.05 & OS 0.683

When we varied the degree of nonlinearity by changing the exponent α, Figure 4.10, this also results in increasing $R(f)$. with higher nonlinearity (Figure 4.11). The relationship of $R(f)$ to the time variation in stiffness quantified by delta stiffness is shown in Figure 4.12.

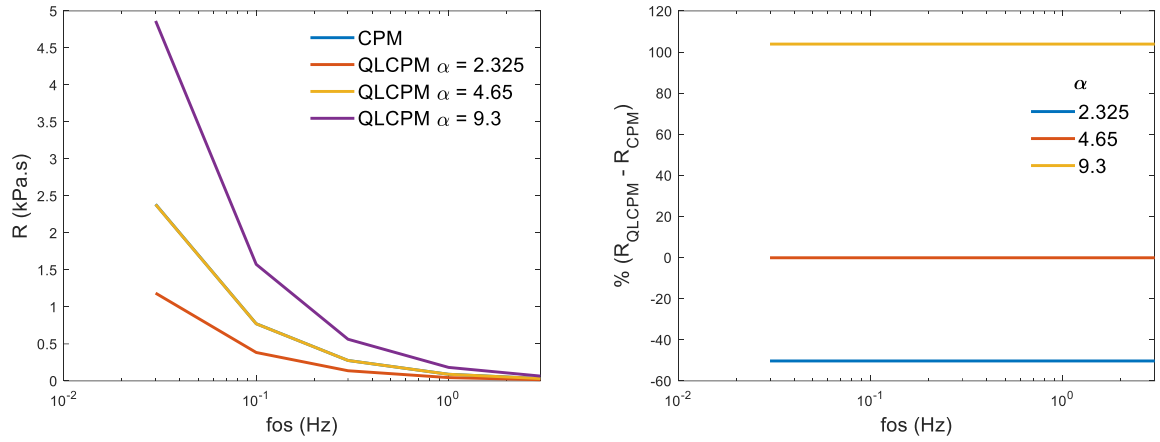

Figure 4.11: (left) R(f) for CPM & QLCPM for different operating strains and (right) percentage difference between CPM & QLCPM

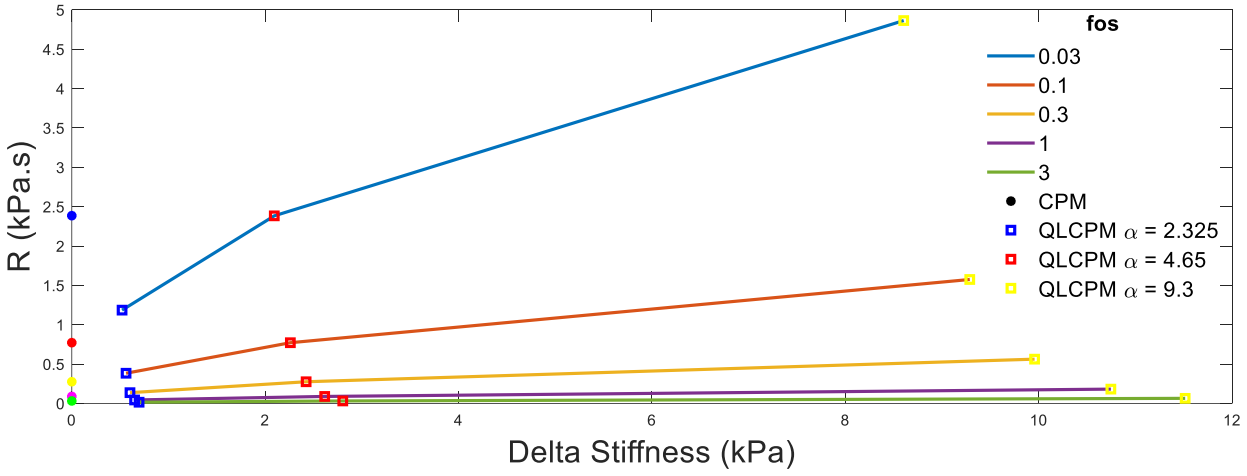

Figure 4.12: Time-varying stiffness effect on R(f) due to varying alpha at different frequencies

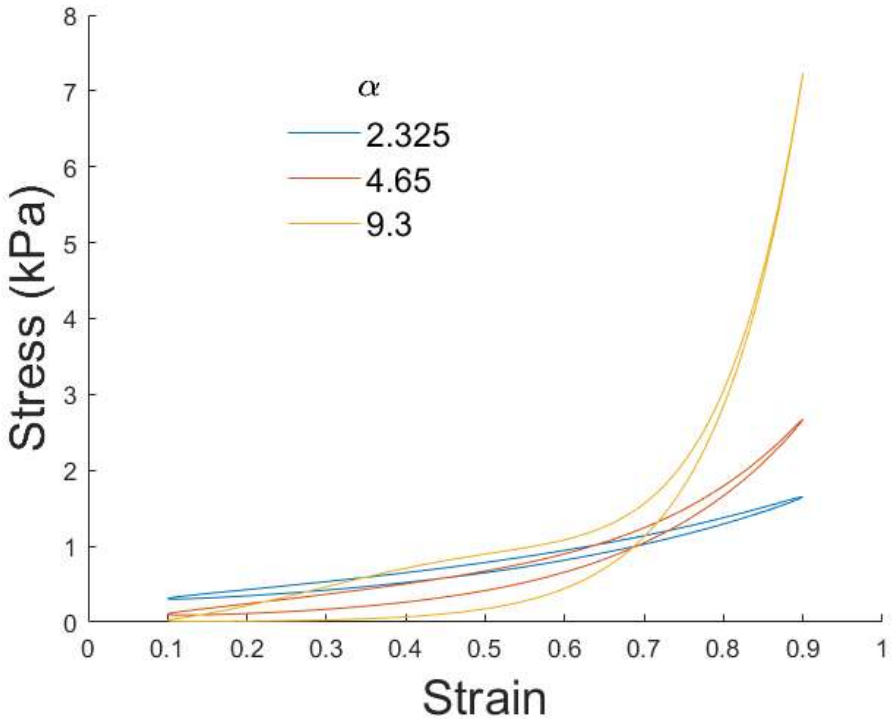

Figure 4.13: QLCPM models for a range of alphas with SA of 0.4 & OS 0.683

If SA is increased to large amplitudes such as 0.4 the effect of α is increased Figure 4.13

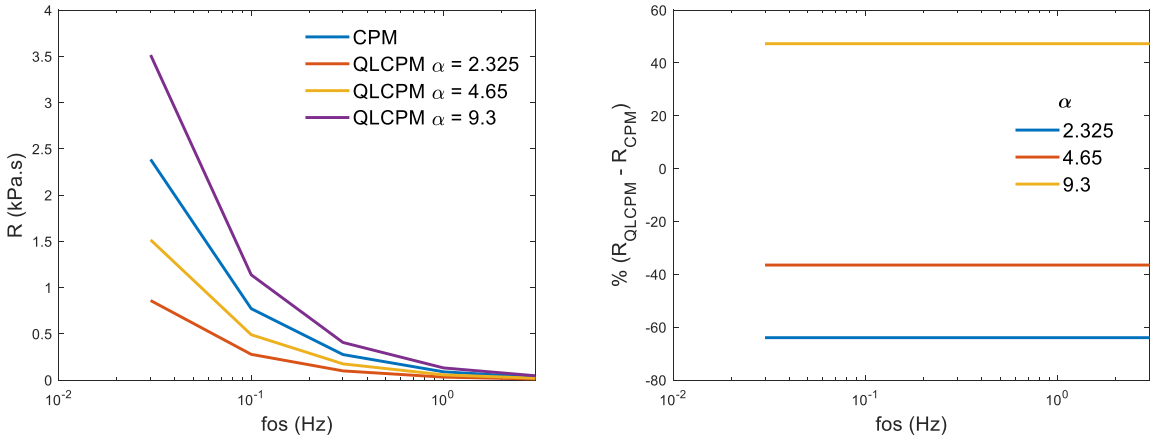

Figure 4.14: Time-varying stiffness effect over R(f) due to alpha/diseases

Interestingly, in Figure 4.14, both lower $R(f)$ ($\alpha = 2.325$ & 4.65) and higher $R(f)$ were observed ($\alpha = 9.3$) relative to CPM. This is seen again examining the behavior vs. the amplitude of the time-varying stiffness comparing curves to CPM which are the solid circles at zero delta

stiffness (Figure 4.15). Looking at 0.03 Hz, resistance increases with delta stiffness vs. alpha, but at low alpha $R(f)$ is less than CPM while at higher alpha $R(f)$ is greater than CPM. Also, $R(f)$ at higher frequencies is small.

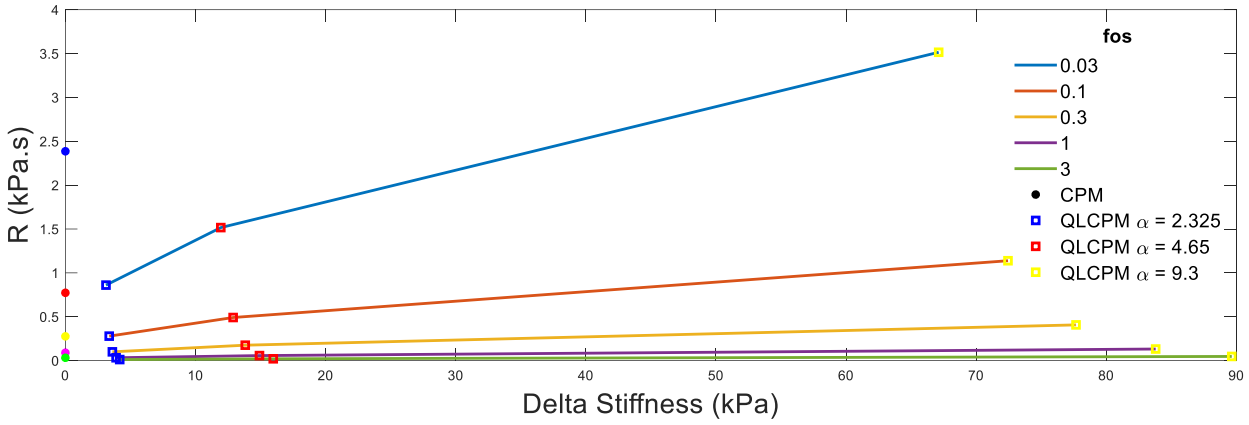

Figure 4.15: Time-varying stiffness effect on R(f) due to varying alpha at different frequencies.

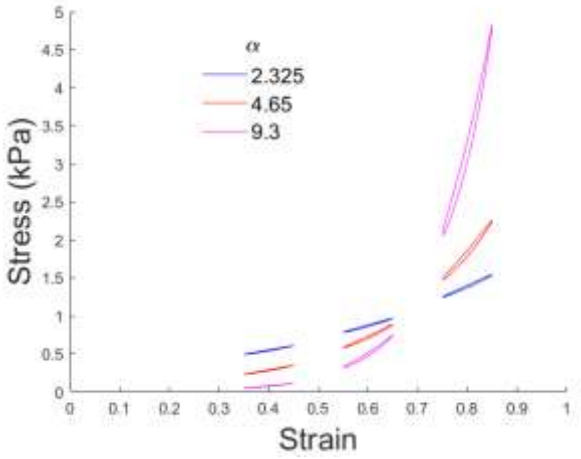

Figure 4.16: QLCPM models for a range of alphas with SA of 0.05 & range of OS

When we looked at behavior vs operating strain with different alphas (Figure 4.16) we again see the greatest $R(f)$ at the highest OS and also at the largest α (Figure 4.17) which was also when delta stiffness was largest (not shown).

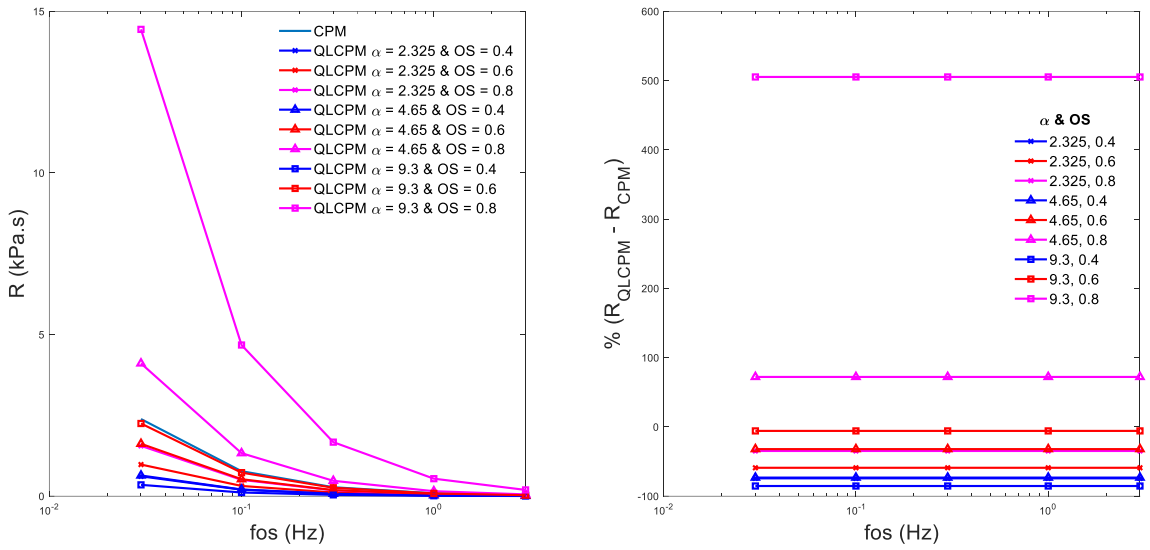

Figure 4.17: Time-varying stiffness effect over R(f) due to alpha/diseases and OS

4.3 DISCUSSION

This study shows that nonlinearity can increase $R(f)$ above what is present in the constant phase model. This is particularly strong at high strain amplitudes or operating strains. The nonlinearity leads to time variation in the stiffness, and because of the coupling of the dissipative component to the elastic behavior through the hysteresivity, η, the out-of-phase variation leads to $R(f)$. This source of frequency dependence of resistance was unrecognized previously.

The principal findings of this study are: **1)** time variation in lung parameters can be obtained if there is a nonlinearity typical of that measured in the real lung tissue mechanics, **2)** increasing the stretch amplitude results in higher nonlinear effects on time variation resulting in higher $R(f)$, **3)** higher operating strains also results in greater effects of the nonlinearity and increased time-variation resulting in higher $R(f)$, **4)** the effect of alpha which directly changes the nonlinearity causes changes in $R(f)$, **5)** when both operating strain and alpha values are increased as might occur with disease, this may mean that changes in disease that cause changes in alpha are thus likely to lead to changes in $R(f)$ affecting the interpretation of $R(f)$.

It was shown in the literature [69], [73]–[75] lung tissue has a pronounced nonlinear stress-strain relationship. Here I introduced the nonlinearity into the simple constant phase model and studied its parameters to better mimic real lung tissue. We used a more common constant phase

model for the oscillatory mechanics of the lung tissue. But other models exist. For example, this is similar to the Hildebrandt model which was developed from stress-relaxation behavior using logarithmic stress decay following a step strain. The constant phase model we used instead predicts a power law behavior [76], [77]. However, while this model has a different mathematical non-constant dependence between loss modulus and storage modulus, which is different from the constant phase model, the difference is very small. Indeed, both models do describe lung tissue deformation fairly well, and thus the differences may not be important. In any case, the constant phase model is by far the most common model used for respiratory tissue mechanics and was used here.

Our implementation investigated the role of time-varying mechanics that arises from the presence of the well-established static nonlinearity of lung tissues, and the well-established small-amplitude constant phase model, and examined its effect when combined to predict its effect on $R(f)$. Here we found that indeed, greater $R(f)$ occurred due to the presence of the nonlinearity compared to CPM, with large amplitude oscillation at low frequency.

When lung tissue is stretched in the tissue bath it should mimic these results, finding at higher operating strains that $R(f)$ should be more than at lower strain amplitudes. Navajas et al indeed did find that resistance increased with operating stress by about 250% from operating stress of 0.6 to 2.1 comparable to what we observed here for similar strain amplitudes. They developed an empirical fit to describe the behavior that was related to the nonlinearity but did not identify the mechanism attributable to the development of time variation in the mechanical properties. They did not explore changes in the nonlinearity via alpha, instead modeled the mean behavior. This would be interesting to examine since they did have different lung tissue strips with differences in nonlinearity and thus this could be examined. If the nonlinearity in lung tissue is a substantial source of $R(f)$ when measured in vivo as is possible with pressure-volume or pressure flow measurements as during mechanical ventilation or oscillometry this could be potentially useful particularly for diseases that alter the stress-strain behavior of lung tissues. This is explored in the next chapter.

It was mentioned we were planning to explore $R(f)$ in lung tissue in in-vitro models simulating altered tissue properties in disease with the use of collagenase, which would lead to increased alpha, beyond what would occur due to normal variation between samples. Here I used

3 different cases changing alpha from healthy dog lung tissue by arbitrary factors of 2 both below and above normal and studied theoretically the behavior of tissue in diseases, also at normal stretch amplitude. This produced a very large change in $R(f)$ which could be confirmed in-vitro and could also be examined using human tissue from deceased subjects, although that may be challenging. Changes in nonlinearity are known to occur due to changes in tissue from the effects of fibrosis or COPD. Rather than explore this in our tissue model, we explored the effects of altered nonlinearity in fibrosis and COPD by modeling pressure-volume relationships in whole respiratory system models in the next chapter.

Limitations to the study in this chapter are as follows: **1)** We examined only healthy canine tissue behavior using data from the literature and did not verify directly if the predicted behavior would occur in-vitro, although the behavior was similar to that reported in Navajas et al. [39] Navajas similarly found that resistance was strikingly frequency dependent. They did also explore the effect of strain amplitude and operating strain to examine the effect of the nonlinearity but unfortunately not over a range of frequencies to examine the effects on $R(f)$. However, the nonlinearity should have led to an amplitude and operating strain dependence which would be in agreement with the nonlinearity leading to increased $R(f)$. However, when Navajas et al. explored the dependance of resistance on amplitude at a single frequency of $0.3\ Hz$ they did not find an increasing dependence of resistance on strain amplitude which we had observed. However, this was only done at low operating stress and over a smaller range in amplitude than we explored, and thus the nonlinearity may not have been sufficient to lead to amplitude dependence. However, they did find a striking dependance on strain operating point also tested only at $0.3\ Hz$. Over the range of $0.6\ to\ 2\ kPa$, resistance changed 2-fold which agrees well with our findings. **2)** Another limitation is that we used arbitrary values to model changes in alpha from our canine healthy values as it seemed more reasonable to address appropriate disease models in chapter 5 when we model the pressure-volume relationship.

This study shows that frequency dependence of mechanical resistance of lung tissue can arise from static tissue nonlinearities provided it is combined with the source of the suitable viscoelastic component which is here provided by CPM. This means that nonlinearity in behavior can possibly lead to $R(f)$ observed in the whole lung which is discussed in the next chapter.

CHAPTER 5: WHOLE LUNG MODELING

Here we wanted to do a similar modeling effort as in Chapter 4 but extended to the respiratory system. This would be more meaningful since the oscillatory mechanics of the respiratory system are commonly measured in research and are increasingly being measured clinically. Indeed, $R(f)$ is commonly being attributed to small airways heterogeneity in lung diseases such as asthma and COPD, although there are other mechanisms for $R(f)$ as discussed in the introduction. In order to develop a respiratory system model including the oscillatory impedance and the pressure-volume characteristics, we repeated the approach of Chapter 4. There are several models of the respiratory system that include the very common single-compartment model to quite complex multiple branch models with $100's$ of thousands of compartments. Some of these include multiple CPM models at the termination of the branches [14], [18], [37]. Common amongst almost all of these models are that they are generally employed only for simulation of small amplitude mechanics and do not usually include the large pressure-volume nonlinearity known as the PV curve. Other models explicitly model the nonlinearity using empirical relationships [35], [78], but these are not usually coupled with small amplitude linear models. In this chapter, we use a similar approach to chapter 4 and use the CPM model of the respiratory system with a common nonlinear PV model and use this to explore where time-varying lung characteristics are expected to lead to $R(f)$.

5.1 METHODS

In this section, as in Chapter 4, I rely on the constant phase model as it has also been used to very well describe the small amplitude respiratory mechanics in vivo and I add to it the well-known pressure-volume nonlinearity known as the Salazar and Knowles equation [78] for the PV-curve. Once the model is developed using values from the literature, I explore changes in operating volumes and differences in the nonlinearity due to disease

MODEL DEVELOPMENT: In the lung/respiratory system, the mechanical relationship is not between stress and strain but between pressure and volume. This relationship is also nonlinear, and a common equation used to describe the deflation limb of the PV-curve as mentioned is known as the Salazar and Knowles equation [78] and is expressed as follows:

$$V = A - Be^{-kP}; \tag{5.1}$$

Rearranging

$$P_{QLM} = -\frac{1}{k}\ln\left(\frac{A-V}{B}\right) \tag{5.2}$$

Where V is the volume (in L), A, B and k are constants or parameters indicating the healthy and diseased cases and P is pressure obtained from the volume, which can be approximated as sinusoidal for the modeling purposes here. The CPM model with volume as input and pressure as output is found in the Kaczka et al. [72] as follows:

$$P_{CPM} = \left(\frac{G}{\omega^{\alpha}} + \frac{H}{j\omega^{\alpha}}\right) j\omega V = \left(j\eta H\omega^{\beta} + H\omega^{\beta}\right)V; \qquad where\ G = \eta H \tag{5.3}$$

Incorporating this to tissue compartment in the nonlinear version by combining P_{QLM} & P_{CPM} we get:

$$P_{QLCPM} = -\frac{1}{k}\ln\left(\frac{A-V}{B}\right)\left(j\eta\omega^{\beta} + \omega^{\beta}\right) \tag{5.4}$$

Where H is incorporated into the $\frac{1}{k}$ parameter.

To complete the CPM model used for the respiratory system we also add a linear upper airway resistance and an inertia term to account for the acceleration of the gas and any tissue accelerations as is commonly done for the standard equation of motion of the respiratory system, with the tissue compartment being the CPM model (equation 5.3) or QLCPM model (equation 5.4). The impedance is the ratio of pressure to flow for both CPM and QLCPM

$$P(t) = R\dot{V} + I\ddot{V} + P_{CPM\ or\ QLCPM}; \tag{5.5}$$

Where P is the pressure and $\dot{V}$ is the flow; P_{CPM} is the pressure of the constant phase model (5.3) obtained from the pressure-volume relationship, similarly P_{QLCPM} is quasi-linear constant phase model pressure (5.4) obtained from nonlinearity in the volume.

EXPERIMENTAL PROTOCOL: The values of the parameters were defined as follows. The values for the Salazar and Knowles equation (equation 5.4) are found in Table 5.1 from Gibson et al. [35]. The values for the CPM model were adjusted/matched to the QLCPM model in order to obtain the same impedance at specific operating volume with specific volume amplitude and a

healthy case of A, B & k constants. The matched values with mean resistance and inertance added to the equation were:

$$R_{CPM} = 2.2\ cmH_2O.s/L = R_{QLCPM};$$

$$E_{CPM} = 3.5\ cmH_2O/L = E_{QLCPM}; \qquad @H{\sim}3.38kPa \qquad 5.6)$$

In this Chapter 5, we will be looking at two different frequency ranges: first, all the experiments were done using a frequency range of 0.2 to 5 Hz. This is a frequency range used previously where ventilators delivered a selection of frequencies while providing mechanical ventilation [79]. The second group of experiments was done at the oscillometry frequency range of 5 to 37 Hz respectively. Similar to Chapter 4, we explored the effect of different operating volumes (OV), including one near a typical end-expiratory lung volume (FRC) of 2 liters and matched the CPM model to it by choosing right H value as well as two higher lung volumes of 3 and 4 liters to explore the effect of the nonlinearity on $R(f)$. We did not choose different amplitudes since this general behavior was studied in Chapter 4, and normal breathing defined by tidal volume is typically fairly constant during measurement of respiratory mechanics while operating volume can be altered when on a ventilator by adjusting the positive end-expiratory pressure or can be elevated in disease such as in COPD.

Table 5.1: Values of the nonlinear components to the QLM and QLCMPM model [35].

Diseases/Variables	$\boldsymbol{k}$ (cmH_2O^{-1})	$\boldsymbol{A}$ (l)	$\boldsymbol{B}$ (l)
Fibrosis	0.089	2.64	0.93
Normal	0.143	5.65	4.79
Emphysema	0.325	7.66	6.98

Using the values of Gibson et al. [35] for each condition altered the nonlinearity k, but also the constants A and B, but this is more representative of the physiological changes with disease. For comparison of these three cases, we also choose 3 different lung volumes, choosing volumes that worked well for each curve, that is, avoided the asymptotes as well as had the same approximate end-expiratory pressure values across conditions. These were end-expiratory volumes of $2, 3.3$ & $6.3\ L$ for each model. However, FRC often is increased in COPD associated with emphysema, so I also chose a second operating point in this model of $7.2\ L$, which while high, was

chosen to explore the effects of elevated end-expiratory pressure of approximately 11 cmH_2O. In this experiment, CPM is matched to a normal curve similar to the last experiment.

After doing the investigations of the PV curves for the low-frequency range, we also examined the oscillometry frequency range. We took the same PV curves and breathing was simulated with sinusoidal oscillation at $0.25\,Hz$. The magnitudes/amplitudes are typically inversely dependent on the frequency with specific phases to minimize peak-peak motion. The magnitudes and phases of a typical oscillometry signal used by the Tremoflo™ are indicated in table 5.2. For analysis of the impedance, the pressure and flow signals were first high pass filtered at 2 Hz using an ideal FFT domain zero phase high pass filter. The impedance was then computed using the Welch periodogram approach using windows of 1 second, applying Hanning windows also of 1 sec, with the overlap of 95% as described in Chapter 1, equation 1.9.

Table 5.2: Amplitudes and phases of the oscillometry probing signal

Frequencies	**Amplitudes (l)**	**Phase (rad)**
5	0.02504	-0.8655
11	0.01082	-2.871
13	0.009283	2.296
17	0.00616	0.9318
19	0.005471	-0.8432
23	0.004822	2.009
29	0.004048	-2.565
31	0.004551	-0.9766
37	0.004029	-2.277

Figure 5.1 shows the CPM and QLCPM pressures in the time and frequency domain for a single one-second window. The flow is the input signal, and the pressure at the oscillation frequencies is roughly the same for the CPM and QLCPM at this operating amplitude (20 mL) and volume (2 L). There appears to be some spectral, or artifactual leakage at non-input frequencies, potentially due to the windowing, but these frequencies are not part of the analysis and do not contribute to the measured impedance as they are not at the input oscillation frequencies. This was confirmed as to when a rectangular window was used (not shown here) energy was confined to the oscillation frequencies.

Figure 5.1 shows the CPM and QLCPM pressures in the time and frequency domain for a single one-second window. The flow is the input signal, and the pressure at the oscillation frequencies is roughly the same for the CPM and QLCPM at this operating amplitude ($20\ mL$) and volume ($2\ L$) for normal matched case. There appears to be some spectral, or artifactual leakage at non-input frequencies, potentially due to the windowing, but these frequencies are not part of the analysis and do not contribute to the measured impedance as they are not at the input oscillation frequencies. This was confirmed as to when a rectangular window was used (not shown here) energy was confined to the oscillation frequencies.

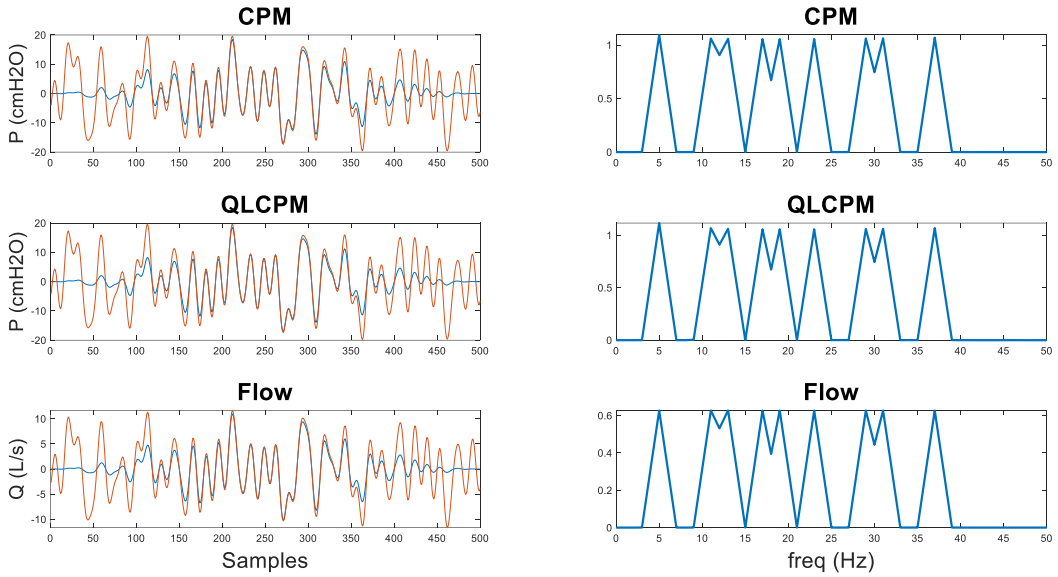

Figure 5.1: CPM & QLCPM Pressures time and frequency plot for 1-sec window with 500 samples, sampling rate of $256\ Hz$ *and high pass filtered alongside windowed flow signal, where on right orange is signal i.e. windowed using rect window and blue is signal windowed using Hanning window respectively.*

5.2 RESULTS

The pressure-volume relationships for CMP, nonlinear QLM, and constant phase QLCPM model are shown in Figure 5.2

Figure 5.3 shows the pressure-volume relationship for breathing at the different operating volumes. Similar to Figure 4.7, it is evident that for the CPM the behavior is linear each PV loop at different operating volumes with the same shape and slope, whereas, for QLCPM it can be seen that the loops change the slope and shape with nonlinearity.

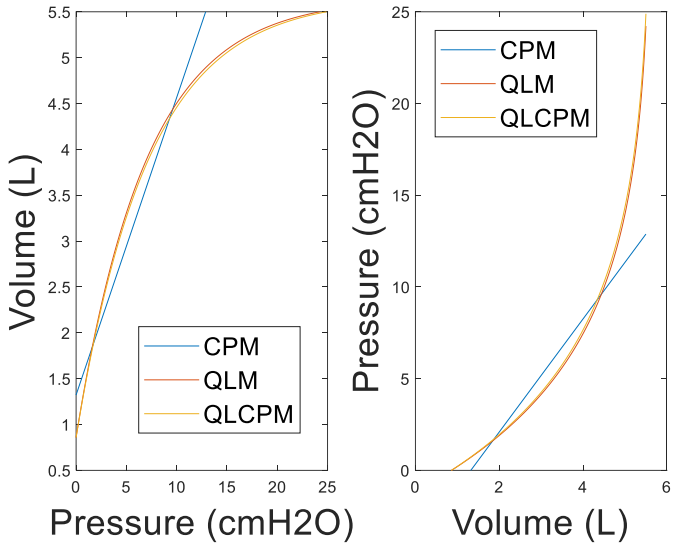

Figure 5.2: Pressure volume relationship for CPM, QLM, and QLCPM models

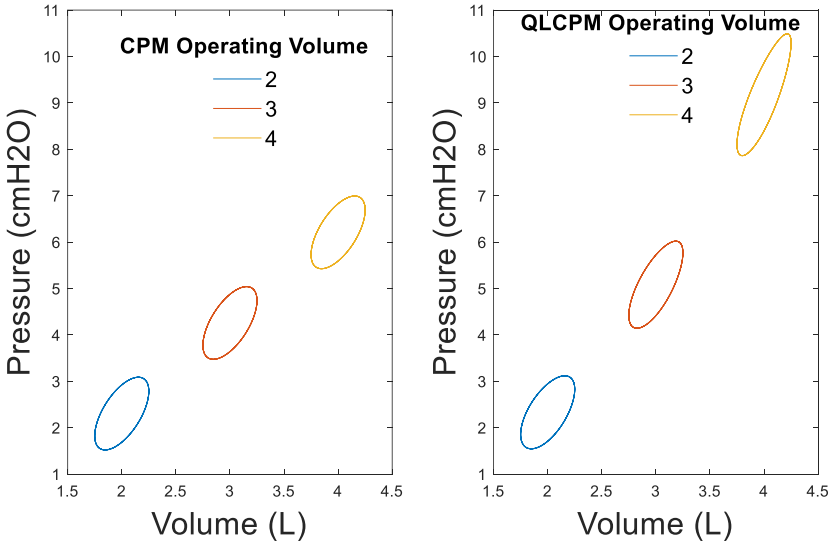

Figure 5.3: CPM & QLCPM models for a range of operating volumes

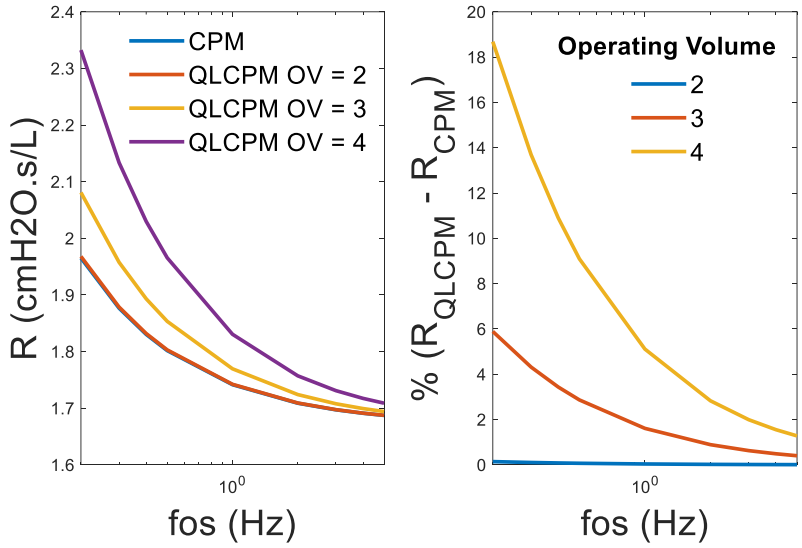

Figure 5.4 (left) R(f) for CPM & QLCPM for different operating volumes and (right) percentage difference of R(f)' of QLCPM relative to CPM

With different operating volumes, $R(f)$ does not change in CPM but increases for QLCPM in Figure 5.4.

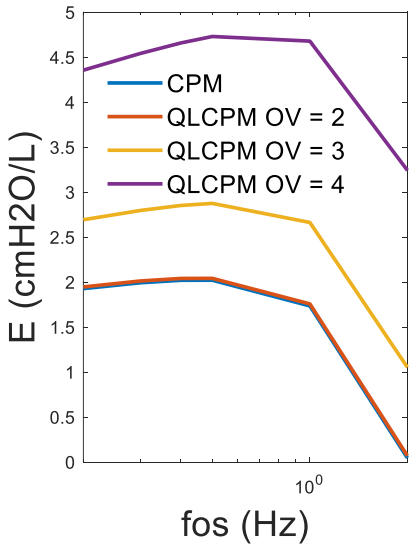

Figure 5.5 Frequency dependence of elastance (E(f)) for CPM & QLCPM for different operating volumes

Elastance estimated as in equation 5.4 is also dependent on operating volume in the QLCPM model Figure 5.5. At higher frequencies, E turns downward due to the effects of

inertance, and the approximation of equation 5.4 no longer is a good estimate of the elastic part of the impedance.

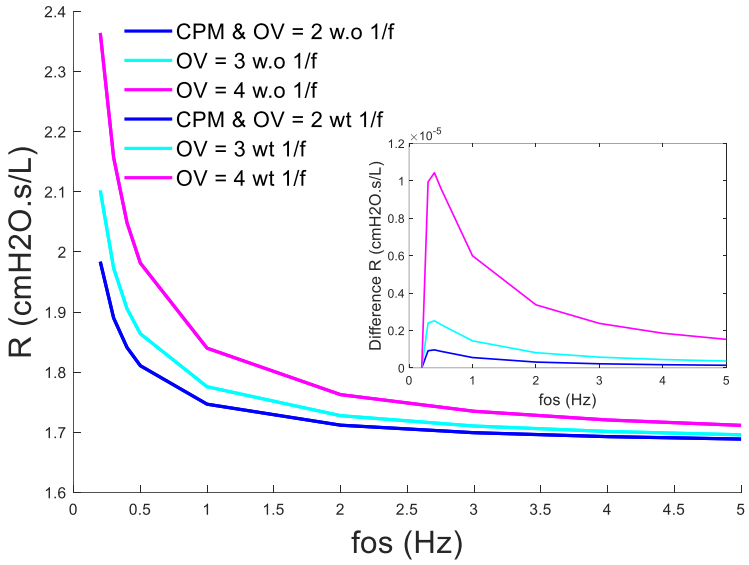

Figure 5.6: $R(f)$ for stretch amplitude changing with $\frac{1}{f}$ and without $\frac{1}{f}$ for 2-4 L Operating Volumes (OV), (inset) shows the difference of the $R(f)$ between the respective response.

Similar to Figure 4.6, here in Figure 5.7 we can see the response of fixed and $\frac{1}{f}$ amplitude input for OV of $2-4\ L$, where $OV\ =\ 2\ L$ is matched to CPM. Figure 5.7 (Inset) clearly indicates that there is no difference for constant amplitude or $\frac{1}{f}$ amplitude input volume signals on $R(f)$.

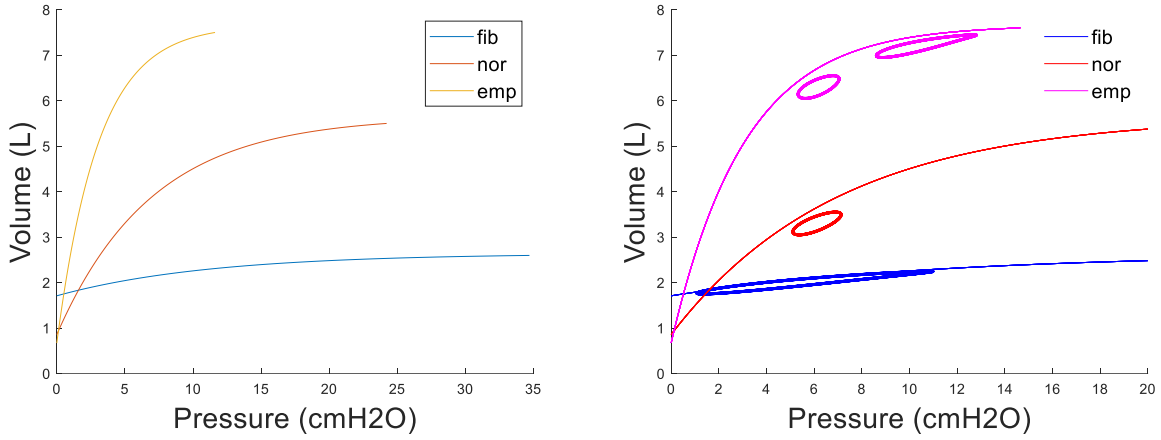

Figure 5.7: (Left) The pressure-volume relationships with different disease models from Gibson et al [35] *fib is fibrosis, nor is normal and emp is emphysema (right), with pressure-volume loops during oscillatory input at the different operating volumes*

Figure 5.7 shows pressure-volume curves that are representative of different disease cases, taken from Gibson et al. [35]. With the same operating pressure, but with the different PV curves, the slopes and shapes of the loops are very different. The fibrosis model has a larger pressure swing, likely larger than ordinarily would occur in-vivo, as likely a subject with this PV curve would move to lower lung volume and alter their breathing rate and amplitude to avoid generating larger pressures. On the emphysema model, we modeled two operating volumes, including a higher volume simulating the higher FRC typical for emphysema, which shows a shallower slope due to the higher stiffness at higher volumes and greater curvature.

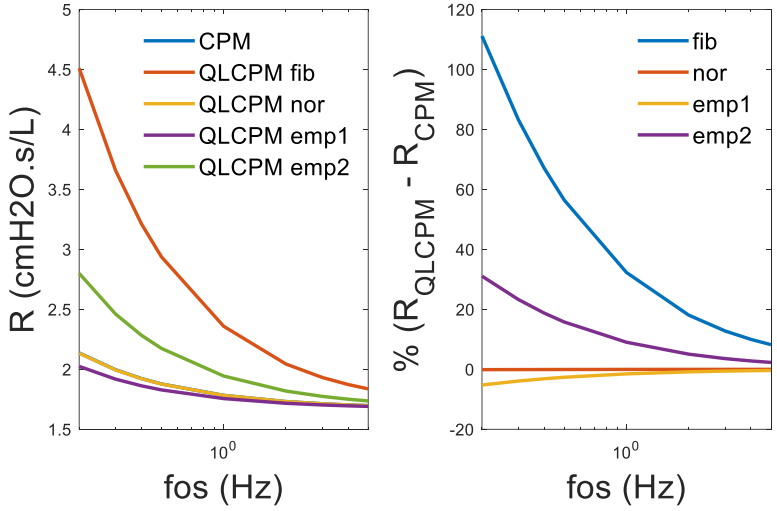

Figure 5.8: R(f) for the linear and nonlinear models including disease models.

The size of the PV loops is determined by η, the value of which was from measurements of subjects while being mechanically ventilated with the optimal ventilator waveform [79]. One can see that the loops are slightly below the PV curves, this is due to the effect of ω^{β}, the coefficient in the constant phase portion of the QLCPM model which reduces the mean pressure slightly in this frequency range.

We found $R(f)$ was present with CPM as expected due to the viscoelastic property of the CPM. But we found that nonlinearity increased the $R(f)$ in QLCPM models from the CPM which we had matched at specific operating pressure ($6\ cmH_2O$) and volume ($3.3\ L$), achieved by matching the operating point and normalizing the CPM slope to match the normal PV curve from Gibson et al [35].

The greatest $R(f)$ occurred with the fibrosis model since it had the largest PV slope at the operating pressure modeled. In the emphysema models at the lower operating pressure ($6\ cmH_2O$), the $R(f)$ was lower than the normal curve from the lower PV slope, while at higher pressure the $R(f)$ was larger than the normal curve. Thus, it can be seen that additional $R(f)$ is produced due to the nonlinearity and the $R(f)$ is dependent on the nonlinearity which agrees with clinical findings.

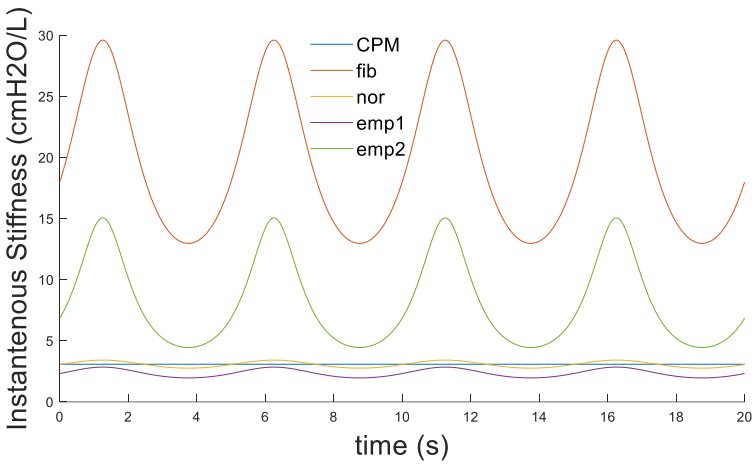

Figure 5.9: Time-varying instantaneous stiffness of CPM and QLCPM diseased models

Figure 5.9 shows the time-varying instantaneous stiffness obtained from the CPM and the QLCPM models. This illustrates that during oscillation, the mechanical properties of the model are changing due to the PV nonlinearities dependent on the local curve of the QLCPM models.

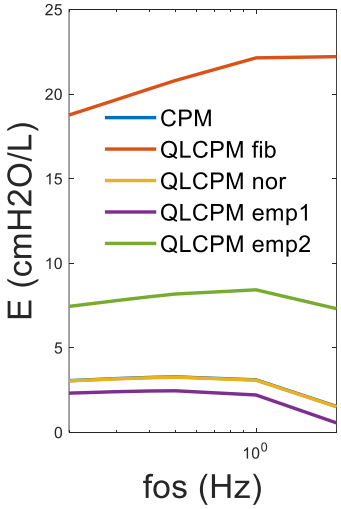

Figure 5.10: E(f) for different diseased case

We also examined $E(f)$ which as expected showed some strong dependence on the disease model due to the changes in the slope of the PV curve, but there is also some small frequency dependence in E.

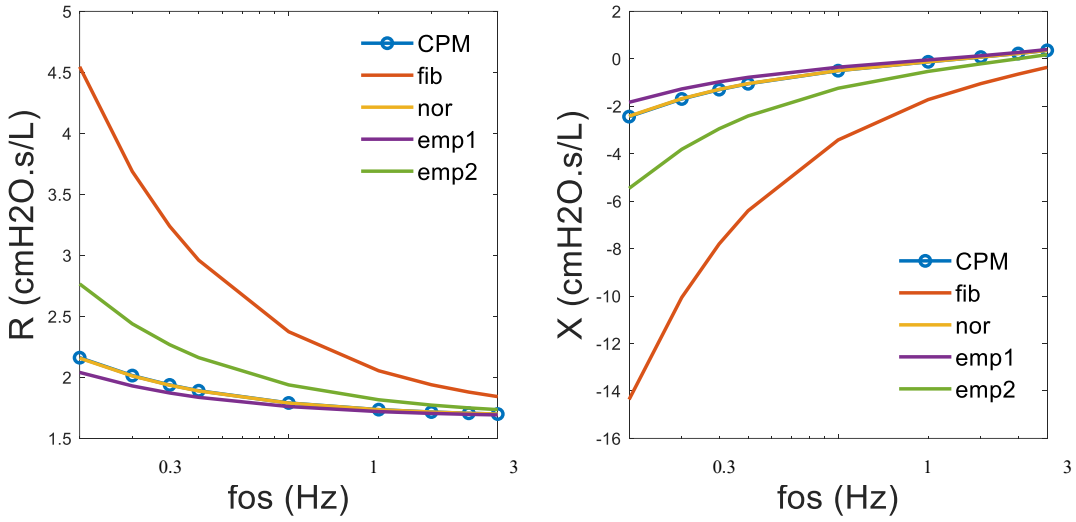

Figure 5.11: Repeat of Figure 5.8, R(f) for the CPM & QLCPM disease models as well as $X(f)$ for optimal waveform ventilation frequency range

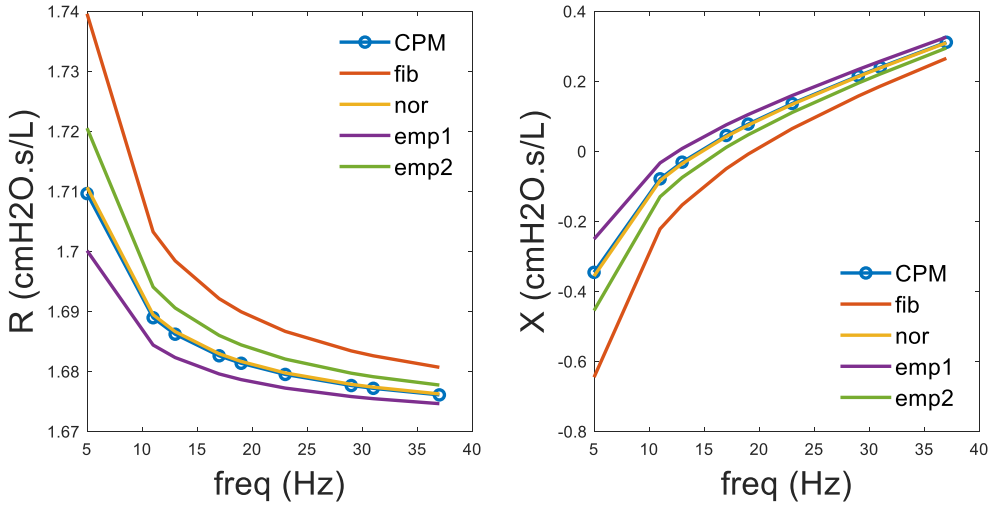

Figure 5.12 R(f) for the CPM & QLCPM disease models as well as $X(f)$ for oscillometry frequency range

Figure 5.11 shows the $R(f)$ & $X(f)$ for the CPM model matched with normal QLCPM in the optimal ventilator waveform frequency range, while Figure 5.12 shows the impedance in the oscillometry frequency range. We can see that Figure 5.12 is similar to Figure 5.11 showing the

$R(f)$ & $X(f)$, however at the oscillometry range the dependance is much smaller decreasing from approximately $0.2\ cmH_2O.s/L$ to $0.02\ cmH_2O.s/L$ for the healthy case and similar for disease cases. Therefore, while $R(f)$ is predicted to be substantially affected by the nonlinearity at low frequencies due to time-varying lung mechanics, the effect appears to be negligible for the oscillometry frequency range, from the model tested here.

5.3DISCUSSION

There have been several models to help understand the impedance and also to understand the frequency dependence of resistance. As discussed in the introduction, Otis [80], [81] showed that a parallel branch compartment model could produce frequency dependence over a limited range of frequencies if the time constants were not equal, and this is also shown over a wider frequency range in multi-branch models where airway diameters are heterogeneous [82]–[85]. Kaczka used CPM in his airway tree model, but, while complex the branching tree impedance model was linear. None of these models included the pressure-volume nonlinearity. Bates et. al. developed a recruitment model to describe the nonlinear behavior and pressure-volume relationship of the lung, but they did not explore the effect of the nonlinearity on $R(f)$. To my knowledge, no model includes the impact of time varying mechanical properties on $R(f)$ except for Alamdari et al. However, in their approach they arbitrarily assigned time variation to the elastance to show that this could be a mechanism for $R(f)$, and did not include the pressure volume nonlinearity. Here I coupled CPM with Salazar Knowles equation to investigate the influence on the nonlinearity potentially on $R(f)$ which have not been investigated before.

Principal findings of this study are **1)** higher operating volumes and alpha (A, B & k), similar to tissue model in the last section, results in higher nonlinearity and coincidentally increased time-variation resulting in higher $R(f)$; **2)** time-varying stiffness of the lung results in $R(f)$ which is substantial in diseased cases at optimal ventilator waveform frequency ranges, however, we lose this effect at oscillometry frequency range where $R(f)$ is negligible.

It is evident in the whole lung nonlinearity study we achieved similar results as in lung tissue i.e., higher operating volume results in higher nonlinearity, similarly with increase alpha values for diseases we achieved higher $R(f)$. The values of alpha in the whole lung case are taken from published pressure-volume relationships [35]. It is evident that for emphysema which had a

very pronounced nonlinear PV curve, we found stronger $R(f)$. We also saw strong $R(f)$ in the fibrosis case due to the fact that PV curve is confined to a very narrow range, and for our choice of constant volume breathing, this accentuated the effect of the nonlinearity probably more than would occur in vivo. In each case, if there is a substantial nonlinear pressure-volume relationship during breathing or mechanical ventilation this can add substantially to the $R(f)$ already present due to the viscoelastic behavior accounted for by the constant phase model. That is this modeling has identified a potentially significant source of $R(f)$ over and above any tissue property and potentially also in addition to any heterogeneity present, although this was not modeled here. This finding may be useful in helping to understand the changes in mechanics of the lung in disease. For example, if the nonlinearity is assessed it may be possible to predict the expected $R(f)$ due to this mechanism, thus additional $R(f)$ can be attributed to other sources such as heterogenetiy. The contribution of nonlinearity and heterogeneity to $R(f)$ is assessed experimentally in the next chapter, but only in the oscillometry range, which we found is not expected to have significant contribution from tissue nonlinearity.

$R(f)$ arises from time-varying elastic lung parameters if they vary in phase with the flow as Alamdari showed previously. Here we also find that because of the CPM model which includes that out of phase pressure with oscillatory volume is determined by the constant η, which causes time variation in pressure that is out of phase with volume from the PV nonlinearity. We found that the time-varying stiffness effect from the nonlinear PV curve can only be seen when the oscillations that explore the nonlinearity are the ones used for estimating the mechanical properties as with tissue strip oscillation in Chapter 3. This occurs when measuring lung mechanics using mechanical ventilation as done by the optimal ventilator waveform [79]. Thus interpreting impedance can be challenging in this case, which was recently raised by Hantos et al [86] when other mechanisms such as time-variation in mechanics may be present, and here we show may arise from nonlinear phenomena However, for oscillometry, the only signal which substantially explores the nonlinearity is breathing which occurs at frequencies below that of oscillometry, and . we found the contribution of the nonlinearity is negligible at the higher frequency range. This is likely due to two factors, the dependence diminishes with frequency, and also at the oscillometry range, the amplitude of the oscillations from oscillometry are far smaller than breathing tidal volumes. These were not sufficiently large to explore the nonlinearity of the PV curve and produce the addition $R(f)$. The breathing signal which we included is large, but it is at a much lower

frequency and thus did not affect the measurement of impedance in our model. However, we only used sinusoidal breathing and actual breathing includes higher frequencies extending beyond $5\ Hz$ although small in amplitude. These could introduce some additional $R(f)$ but this was not explored here. Nevertheless, lung disease alters the nonlinearity, and also can introduce time variation in mechanical properties that may have slightly higher effects over the $R(f)$ extending to the oscillometry frequency ranges.

Limitations to this study are: **1)** Only a single representative curve for an obstructive and a restrictive disease were studied, and compared to a representative normal PV-curve. We did not assess the variation amongst individuals in either normal or disease. **2)** We did not include simulation of real breathing waveforms which have a much wider bandwidth than the purely sinusoidal breathing that we used. This might affect frequencies at and perhaps somewhat above $5\ Hz$, since breathing noise does have frequency components in this range and adds to the noise in oscillometry measurements typically at the lower oscillometry range near $5\ Hz$, and somewhat higher frequencies in children. However, this effect will likely be small since the magnitude of pressure and flow oscillation at 5 Hz in normal breathing is also small. It is possible that in diseases such as COPD with flow limitation, leading to very non-sinusoidal waveforms and potentially harmonics in this range during breathing that the effect might become important.

This study shows that frequency dependence of mechanical resistance of lung tissue can arise from pressure-volume nonlinearity provided it is combined with the source of the suitable viscoelastic component which is here provided by CPM similar to static tissue nonlinearity explored in Chapter 4. This means that nonlinearity in behavior can possibly lead to $R(f)$ observed in the whole lung which is explored further for lung transplant patients in the next chapter along with the effect of heterogeneity over the $R(f)$.

CHAPTER 6: INVESTIGATING $R(f)$ DUE TO HETEROGENEITY OF VENTILATION IN THE LUNG

In this chapter, we took advantage of some recent measurements in my laboratory to investigate the $R(f)$ and potentially relate it to measures of heterogeneity and assessed by lung imaging (section 6.1) as well as time-varying lung mechanics (section 6.2) in data collected from post-LT patients at risk of developing CLAD as introduced in Chapter 1 section 1.6.

6.1 INVESTIGATING HETEROGENEITY IN LUNG TRANSPLANT PATIENTS

6.1.1 Methods

My lab group is conducting a study to explore measurements of heterogeneity in subjects' post-lung transplants as a potentially sensitive measure to detect CLAD. I've helped collect oscillometry data in some of the patients. In this thesis, I have included data from the 9 subjects we have recruited thus far. Their demographic data can be seen in Table 6.1. The study protocol is depicted in a flow chart in Figure 6.1. Briefly, we obtain spirometry data (with the help of S. Fulton, the respiratory technologist) and collected the oscillometry data aided by summer students C. Potter, A. Brezovan, and M. Renn using the Tremoflo™ software.

Table 6.1: Post-LT Patients demographics data

Patient	9	
Years since transplant	9.25 ± 3.99	
Sex	$7\ M\ /\ 2F$	
Age (years)	61.44 ± 8.25	
Weight (kg)	79.13 ± 14.89	
Height (cm)	171.67 ± 8.57	
	Best post-LT	**Visit 1**
FVC (% Ref)	94 ± 14.02	90.13 ± 12.85
FEV1 (% Ref)	92 ± 15.36	73.5 ± 22.99
FEV1/FVC (% Ref)	78.63 ± 11.40	64.13 ± 17.08

Table 6.1 also shows FVC, FEV1, and FEV1/FVC the measures of the Spirometry, we can see that for visit one the mean is significantly low with a substantially large standard deviation indicating the LT patients with BOS.

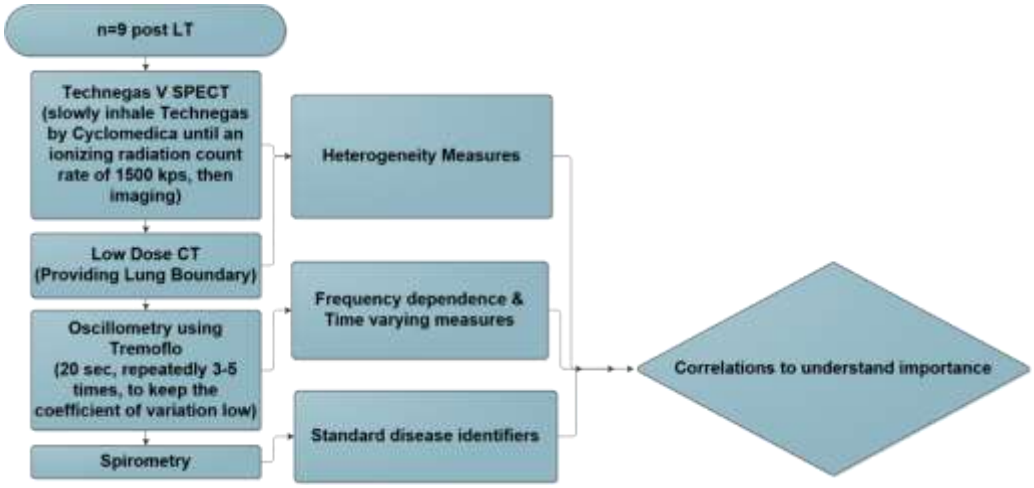

Figure 6.1: Flow Chart of CLAD Study

Figure 6.1 shows the flow chart of the study protocol. In this study for each patient, there are $3-5$ recordings of oscillometry in supine and upright followed by spirometry and then subjects inhale a bronchodilator and the measurements are repeated 20 minutes later, although for this study we only used pre-bronchodilator data. Oscillometry was performed according to ATS/ERS technical standards, with at least 3 repeated measurements with the coefficient of variation of resistance at $5\ Hz$ of less than 0.10. The study also includes SPECT/CT imaging data recorded prior to the oscillometry measurements. The summer students largely conducted the image analysis with supervision from myself and Dr. Maksym, quantifying the heterogeneity measures. The inhalation protocol for the Technegas as well as the imaging method is explained in detail later in the chapter.

From the CT images, the user chooses a threshold to segment the lungs from the chest wall (which includes the diaphragm and heart as well as larger blood vessels). The software uses thresholds from three separate slices through the lungs, central and two more slices each midway to the central surfaces and dorsal surface, and then creates a surface describing the lung chest-wall boundary. The summer students then manually removed any of the trachea and mainstem bronchi that were part of the mask in a refinement step. This mask then represents the potentially aerated

volume of the lungs for analysis. From the volume within the mask is computed the coefficient of variation of image intensity (CoV) [87] which I used as an index of ventilation heterogeneity as can be seen in equation $CoV = \frac{SD(Intensities)}{Mean(Intensities)}$ (6.1.

$$CoV = \frac{SD(Intensities)}{Mean(Intensities)} \quad (6.1)$$

I used the CoV to explore the hypothesis that heterogeneity of ventilation is related to the frequency dependence of resistance which has been thought to arise from heterogeneity of airway diameters as described in section 1.4.2. I also calculated percentage predicated R_{5-19} using the representative healthy data corresponding to individual patients from the Oostveen Database [2], which represents the comparison of disease.

As mentioned previously, the imaging is done by radiology technologists at the QEII, supervised by Dr. A. Ross, and largely the image analysis was carried out by summer students C. Potter, A. Brezovan, and M. Renn under the supervision of Dr. Ross and my supervisor G Maksym. Patients performed a ten-second breath-hold of $555Mq$ of Technetium-99m (Technegas), vaporized in a carbon vessel, inhaled through a closed spirometer system until a count rate of $1500\ kps$ or greater was reached. Briefly, patients first inhale Technegas while supine and a short SPECT scan is done to check if the inhaled dose is sufficient, if not, a second inhalation is done. Following this, CT is then obtained after exhalation and the patient is instructed to cease breathing for a few seconds. Then they can breathe normally, and Ventilation SPECT is obtained for approx. $10-15\ minutes$ of normal breathing. Details regarding the imaging methodology and image reconstruction can be found here [88], [89] but briefly. Image segmentation of the CT is used to define the chest wall boundary including the diaphragm, and some smaller regions such as mainstem bronchi, blood vessels are also excluded from the lung tissue (parenchyma) volume. This was either done using Hermes software or freely available segmentation software 3D slicer. Differences between approaches were very small (< 35 ml not shown) likely due to the clarity in the chest-wall boundary by CT. The CoV of the intensity from the VSPECT images is then calculated after applying the mask to the VSPECT.

During oscillometry we also collected 30 seconds of 10 Hz single frequency oscillometry from which the variation in impedance with time can be measured i.e., the real-time recording of $10\ Hz$ collect from lung transplant patients and tested the hypothesis the variation of X_{rs} at $10\ Hz$

as a measure of the temporal variation of lung elastance might also be related to the frequency dependence of resistance, in oscillometry measurements, even though this was not predicted to be very strong in chapter 5.

6.1.2 Results and Discussion

Two examples of coronal (frontal) plane slices showing VSPECT data using the color bar overlayed on the CT image in pale magenta are shown in Figure 6.2. Locations, where the Technegas particles have been deposited in high concentration, are indicated by the red while where little or no particles have been deposited are indicated by dark blue. These images have been scaled to the maximum intensity voxel ($value$ 1.0) over all slices of the lung volume, and thus the maximum does not necessarily appear in the slice shown. The patient on the left is a healthier patient with better deposition more thoroughly in the slice, as well as with normal spirometry and oscillometry. While the patient on the right has highly heterogeneous deposition, and we can see 'hot' spots of ventilation whereas the rest of the lung is not being ventilated indicating in the case of BOS i.e., CLAD.

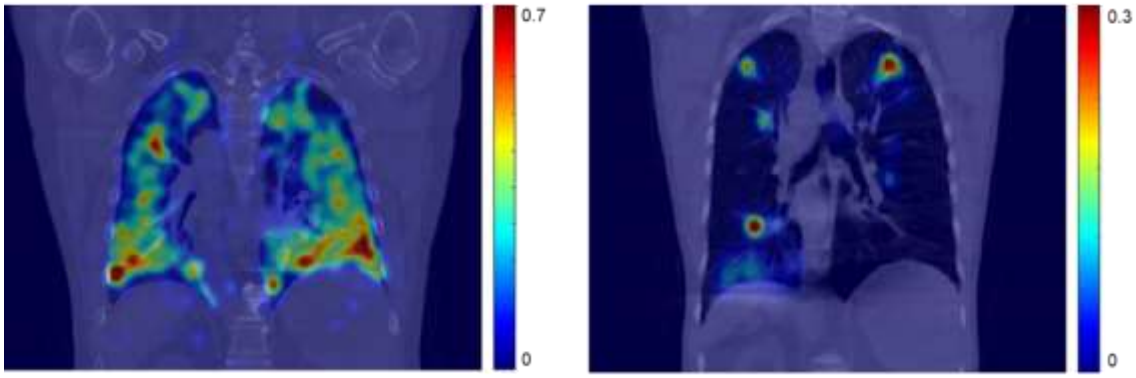

Figure 6.2: (left) Technegas deposition (red max 0.74, blue min 0) in a coronal slice of a post LT subject with normal mechanics, (right) Technegas deposition (red max 0.31) in a coronal slice of a post LT subject with Bronchiolitis Obliterans

In order to quantify the heterogeneity from the images as mentioned earlier, CoV was calculated. The imaging measure (CoV) is then correlated with R_{5-19} which is defined as $R(f)$ mentioned earlier as oscillometry measure.

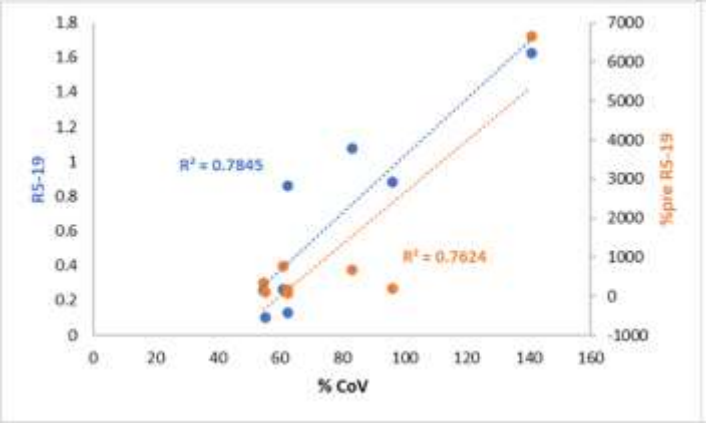

Figure 6.3: R(f) correlated with imaging variables

In Figure 6.3 we can see $R(f)$ as well as percentage predicted $R(f)$ is correlated with CoV in order to study the effect of heterogeneity over the $R(f)$. It is evident that R_{5-19} ($R(f)$) is highly correlated to CoV with $p = 0.001$ as well as it is correlation linearly increasing indicating that higher heterogeneity results in higher $R(f)$. It is also clear that there is a strong linear correlation between CoV and %predicted $R(f)$ ($p = 0.004$) indicating that the heterogeneity increases the $R(f)$ regardless of other factors like BMI etc.

We have investigated $R(f)$ in respiratory mechanics dependence on the heterogeneity of ventilation arising from diseases in lung transplant patients. This was done by exploring through VSPECT/CT imaging in post-LT subjects who develop heterogeneous lung dysfunction. Using the quantitative measures of imaging and oscillometry measurements of $R(f)$. The next section is the effect of time-varying lung mechanics in post-LT patients using the time variation in reactance at 10 Hz as an estimate of the time variation in elastance and tested by correlation with measured $R(f)$ over $5\ to\ 37\ Hz$.

6.2 INVESTIGATING TIME-VARYING CHARACTERISTICS IN LUNG TRANSPLANT PATIENTS

6.2.1 Methods

The oscillometry data collected was collected at $10\ Hz$ to obtain the time-varying lung mechanics parameters i.e., resistance and reactance. The reactance at $10\ Hz$ was used to check the

correlation with $R(f)$ using the reactance as an estimate of the time-varying elastance as Alamdari who's time variation in elastance leads to $R(f)$. The reactance at $10\ Hz$ was first cleaned using the quality control standards (Appendix B). The standard deviation of reactance at $10\ Hz$ was used to assess the variation and the correlation with $R(f)$ assessed.

6.2.2 Results and Discussions

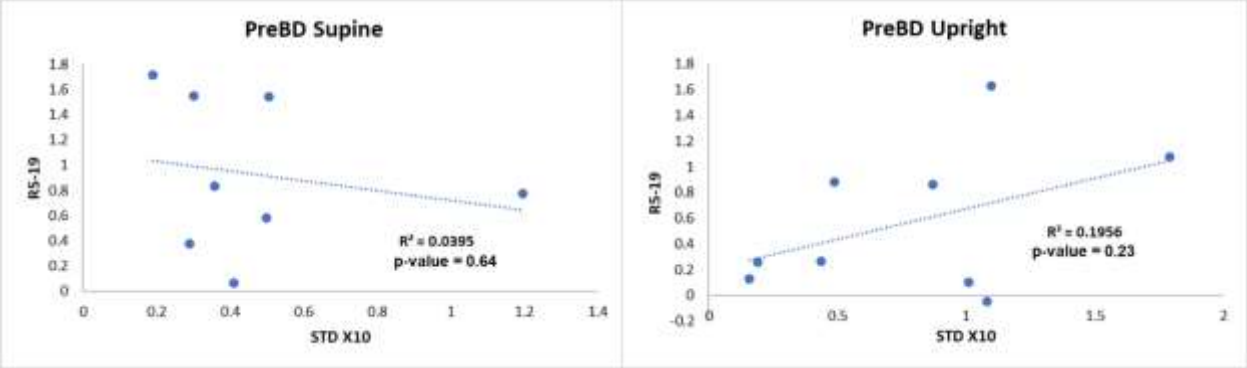

Figure 6.4: Correlations of R(f) with STD X10

In Figure 6.4, despite a wide range of both R_{5-19} and $std(X10)$ we can see that there is no correlation between $R(f)$ (R_{5-19}) with time-varying lung mechanics i.e., the standard deviation of $X10$ for either supine ($p = 0.64$) or upright ($p = 0.23$) position. This implies that for lung transplant patients time-varying lung mechanics did not affect the frequency dependence of lung resistance. However, as we showed in Figure 6.4 heterogeneity as assessed by VSPECT imaging was more related to $R(f)$ from oscillometry. However, it may be that the variation in reactance at $10\ Hz$ was not a good estimate of the elastance, since it is closer to the resonance frequency where inertance matches elastance and reactance is zero. However, more likely is that $R(f)$ was not affected by any variation in reactance. As we found in Chapter 6, time variation from nonlinearity has only negligible effects on $R(f)$ measured during oscillometry. While we did not model the effects from other sources of time variation that might induce variation in the oscillatory frequency in Chapter 5, it might be useful to assess the variation in phase with the flow in these subjects, although this is likely to be quite small. However, the correlation of $R(f)$ with heterogeneity for volume SPECT imaging leads to this being a more likely contributing mechanism to $R(f)$ in the oscillometry range.

CHAPTER 7: DISCUSSIONS & CONCLUSIONS

In Chapter 4 we found that nonlinearity can produce time-varying dependence of lung tissue mechanics that leads to $R(f)$ in the low-frequency range, which had not been demonstrated before. Thus, this thesis adds a new mechanism, nonlinear induced time variation of mechanics that can cause $R(f)$. This was found to be present at the level of the lung tissue and added to the underlying contribution by tissue viscoelasticity (η) to $R(f)$.

This was dependent on the degree of nonlinearity. Increasing the stretch amplitude resulted in higher nonlinearity and increased time-variation of mechanics that resulted in higher $R(f)$. Similarly, the contribution to $R(f)$ was increased at higher operating stains. The most interesting result we obtained was the effect of alpha which can be altered in disease increasing the tissue nonlinearity. We saw that when both operating strain and alpha values were increased that the contribution to $R(f)$ was the strongest.

In Chapter 5 we found higher operating volumes and greater nonlinearity that is associated with respiratory diseases of fibrosis and emphysema each would lead to higher $R(f)$ attributed to increased time-varying stiffness of the lung. This was true for oscillation of the lung during mechanical ventilation while measuring impedance at the frequencies of ventilation. However, we lose this effect during oscillometry, as the oscillometry is much smaller in amplitude and at higher frequencies where effects on $R(f)$ are reduced. Indeed, in chapter 6 we found no evidence of $R(f)$ being related to time variation in mechanical properties in lung transplant patients, but a strong relationship to heterogeneity as assessed by VSPECT imaging.

Thus, we show that nonlinearity in lung tissue and the PV-curve can lead to substantial $R(f)$ independent of any other mechanism and adds to any $R(f)$ due to tissue viscoelasticity in the low-frequency breathing frequency range.

These findings are potentially important for the interpretation of the number of different types of experiments currently done, where data is presented in the literature. These include measurements of mechanics for subjects on a ventilator when the waveform for ventilation is used to estimate the impedance of the respiratory system. A portion of the subject $R(f)$ will not only be due to the viscoelastic properties of the lung and chest wall tissues, but a portion of it can arise from the nonlinearity in the pressure-volume curve and the time variation that occurs in the

mechanical properties as demonstrated in Chapter 5. $R(f)$ was previously demonstrated in measurements of patients in the low-frequency range, and thus this mechanism may be responsible for some of the $R(f)$ observed including the seminal work by Suki and Kaczka [37], [79], [90], [91]. In disease there would be the possibility of additional sources of $R(f)$ arising from heterogeneity in airway resistances in the multi-branch airway tree [70], [92], this is known to be a substantial contributing mechanism as demonstrated with physical models [21], [93]–[95]. Indeed, we found using imaging that heterogeneity by VSPECT was strongly correlated to R(f) in agreement with the literature. However, these mechanisms likely overlap as tissue disease alters the PV curve, but also introduces heterogeneity, which might thus both be present adding to $R(f)$.

On the other hand, in the oscillometry range, the effect is much reduced. In Chapter 5 we showed that in the oscillometry range the effect is greatly reduced due to in theory nonlinearity being strongly excited/stimulated by large-amplitude oscillation such as breathing which we simulated at lower frequencies even though there is large amplitude breathing during oscillometry. However, it is not at the frequency of oscillations therefore as we found, it doesn't affect the measured mechanics. The only effect of the nonlinearity on $R(f)$ comes from the small amplitude of oscillation being applied due to oscillometry, which produces a small but negligible effect. Therefore, it is likely that as long as there is little contamination to the oscillatory frequencies from the breathing signal that may be affected by nonlinearity or simply varying in phase with the flow, there will be little effect on $R(f)$ from time variation in mechanical properties. It is possible that with flow limitation and very non-sinusoidal breathing patterns that contamination of the oscillometry signal could lead to some $R(f)$ but we did not examine this.

In Chapter 6 we have investigated $R(f)$ in respiratory mechanics dependence on the heterogeneity of ventilation arising from diseases in lung transplant patients. This was done by exploring through VSPECT/CT imaging in post-LT subjects who develop heterogeneous lung dysfunction. Using the quantitative measures of imaging and oscillometry measurements of $R(f)$. We observed strong correlations and significant results, where the increase in heterogeneity linearly increases $R(f)$ making it the strongest source. We also studied the effect of time-varying lung mechanics in post-LT patients using the time variation in reactance at $10\ Hz$ as an estimate of the time variation in elastance and tested by correlation with measured $R(f)$ over $5 - 37\ Hz$.

However, there was no correlation with $R(f)$ which agrees with the finding that oscillometry range time-variation is not likely to have much effect on $R(f)$

There are some limitations of this result - we only simulated breathing that was confined to a single frequency. Breathing does have noise energy that extends over many frequencies, and it is possible, particularly with flow limitation and maybe in children that the breathing oscillation noise might affect $5\,Hz$ and might introduce some $R(f)$. Flow limitation does tend to produce variation in phase with the flow during breathing, but this was not studied in this thesis.

7.2 CONTRIBUTIONS FROM THESIS

1) A. Tahir, C. Potter, P. Hernandez, A. Ross, and G. Maksym, "Ventilation Heterogeneity Assessed by VSPECT and Altered Lung Mechanics Post Lung-Transplant," *BMES 2019 Annual Meeting*, Oct 2019, presented a poster in Philadelphia, USA.
2) A. Tahir, "VSPECT/CT and FOT in Lung Transplant", *CRRN Annual General/Investigator Meeting*, Jan 2020 presented in the lightning round presentation in Ottawa, Canada.
3) A. Tahir, C. Potter, A. Brezovan, P. Hernandez, A. Ross, M. Chiasson, N. Morrison, G. Mawko, S. Fulton and G. Maksym, "Heterogeneity and Altered Lung Mechanics in Lung Allograft Dysfunction using Ventilation SPECT/CT and Oscillometry Post-Lung Transplant", *Canadian Respiratory Conference 2020*, April 2020, abstract got accepted for poster presentation in Niagara Falls, Canada.
4) A. Tahir, A. Brezovan, C. Potter, P. Hernandez, A. Ross, M. Chiasson, N. Morrison, G. Mawko, S. Fulton and G. Maksym, "Investigating Ventilation SPECT/CT and Oscillometry Post-Lung Transplant for Ventilation Heterogeneity as Marker for Chronic Lung Allograft Dysfunction", *ATS International Conference 2020*, May 2020, abstract got accepted for ORAL presentation Mini-Symposium and also got accepted for 10th Annual CTS Research Poster Competition.
5) A. Tahir, M. Renn, P. Hernandez, A. Ross, M. Chiasson, N. Morrison, and G. Maksym, "Investigating the Origin of the Frequency Dependence of Respiratory Resistance to Airflow in Post Lung Transplant Patients as a Marker for Chronic Lung Allograft Dysfunction", *ATS International Conference 2021*, May 2021, presented an online poster.

In addition to the above peer-reviewed contributions, I also presented in department seminar, October 2020 and 2 research days, June 2020, and June 2021 respectively. I also received 2nd prize in the Master presentation category in Research Day 2021.

7.3 FUTURE WORK/DIRECTIONS

To answer the question if time variation in mechanics can lead to $R(f)$ even in the oscillometry frequency range from harmonics in the breathing signal affecting $5\ Hz$ in above, this needs to be assessed experimentally. This is probably best done with subjects with flow limitation as the variation in reactance is quite large, and the waveform is a square wave not sinusoidal as can be observed in the study by Dellaca et al. [34].

Other experiments can be done to investigate this work further. I was only able to model how time variation from nonlinearity in lung tissue could lead to $R(f)$. This could be done in-vitro with lung tissue such as proposed in chapter 3. It would be useful to also model disease using enzymes to alter the nonlinearity and explore if this alters $R(f)$.

It would also be useful to explore how much additional resistance is from time variation of mechanical stiffness during mechanical ventilation, either in animals or in ventilated humans. This could be done at a single frequency or using more natural breathing waveforms from mechanical ventilation or the optimal ventilator waveform to validate the model.

The magnitude of $R(f)$ from tissue nonlinearity could also be compared to effects of shunt and heterogeneity which can be modeled using a two-compartment model or other multi-compartment models using several different exiting techniques presented in [17], [19], [20], [22], [80], [96], [97]. One could implement a model with a shunt for different patients such as children where shunt might be more important and also compare that to the effect of nonlinearity of PV curve if there is data available for pediatric PV relationships.

Optimal Ventilator Waveform can be implemented to induce heterogeneity is another idea that needs attention. There is no single ideal solution because practically all the sources' effects each other and have contribution together at the same time and you cannot separate them in order to explore individually in-vivo. For example, even in modeling, we decided to focus on nonlinearity contribution, however how big the contribution of heterogeneity over the $R(f)$, it is good to see the comparison. This can be done to quantify the magnitude of $R(f)$ in relation to heterogeneity in-vivo in comparison to nonlinearity with the disease. It is challenging because the disease can increase the effectiveness of both heterogeneity and nonlinearity.

BIBLIOGRAPHY

[1] K. Bruce and S. Bruce, *Berne & Levy Physiology - 7th Edition*. Elsevier, 2018.

[2] E. Oostveen *et al.*, "Respiratory impedance in healthy subjects: Baseline values and bronchodilator response," *Eur. Respir. J.*, vol. 42, no. 6, pp. 1513–1523, 2013.

[3] G. G. King *et al.*, "Technical standards for respiratory oscillometry," *Eur. Respir. J.*, vol. 55, no. 2, 2020.

[4] H. Schulz *et al.*, "Reference Values of Impulse Oscillometric Lung Function Indices in Adults of Advanced Age," *PLoS One*, vol. 8, no. 5, 2013.

[5] F. M. Ducharme, I. Jroundi, G. Jean, G. L. Boutin, C. Lawson, and B. Vinet, "Interdevice agreement in respiratory resistance values by oscillometry in asthmatic children," *ERJ Open Res.*, vol. 5, no. 1, 2019.

[6] J. V. Cavalcanti, A. J. Lopes, J. M. Jansen, and P. L. Melo, "Detection of changes in respiratory mechanics due to increasing degrees of airway obstruction in asthma by the forced oscillation technique," *Respir. Med.*, vol. 100, no. 12, pp. 2207–2219, 2006.

[7] C. A. Lall *et al.*, "Airway resistance variability and response to bronchodilator in children with asthma," *Eur. Respir. J.*, vol. 30, no. 2, pp. 260–268, 2007.

[8] G. N. Maksym, C. A. Lall, P. Hernandez, and P. Pianosi, "Respiratory System Reactance: a sensitive indicator of bronchodilator effect in children with asthma," in *ATS*, 2005, p. 2.

[9] D. Czövek *et al.*, "Tidal changes in respiratory resistance are sensitive indicators of airway obstruction in children," *Thorax*, vol. 71, no. 10, pp. 907–915, 2016.

[10] Z. Hantos, A. Adamicza, E. Govaerts, and B. Daroczy, "Mechanical impedances of lungs and chest wall in the cat," *J. Appl. Physiol.*, vol. 73, no. 2, pp. 427–433, 1992.

[11] Z. Hantos, B. Daroczy, B. Suki, and S. Nagy, "Low-frequency respiratory mechanical impedance in the rat," *J. Appl. Physiol.*, vol. 63, no. 1, pp. 36–43, 1987.

[12] T. Hirai, K. McKeown, R. Gomes, and J. Bates, "Effects of lung volume on lung and chest wall mechanics in rats," *J. Appl. Physiol.*, vol. 86, no. 1, pp. 16–21, 1999.

[13] S. Wagers, L. K. Lundblad, M. Ekman, C. G. Irvin, and J. H. Bates, “The allergic mouse model of asthma: normal smooth muscle in an abnormal lung?,” *J. Appl. Physiol.*, vol. 96, no. 6, pp. 2019–2027, 2004.

[14] K. R. Lutchen, D. W. Kaczka, B. Suki, G. Barnas, G. Cevenini, and P. Barbini, “Low-frequency respiratory mechanics using ventilator-driven forced oscillations,” *J. Appl. Physiol.*, vol. 75, no. 6, pp. 2549–2560, 1993.

[15] B. Suki, A. L. Barabasi, and K. R. Lutchen, “Lung tissue viscoelasticity: A mathematical framework and its molecular basis,” *J. Appl. Physiol.*, vol. 76, no. 6, pp. 2749–2759, 1994.

[16] B. Suki and J. H. T. Bates, “Lung tissue mechanics as an emergent phenomenon,” *J. Appl. Physiol.*, vol. 110, no. 4, pp. 1111–1118, 2011.

[17] J. Glapiński, J. Mroczka, and A. G. Polak, “Analysis of the method for ventilation heterogeneity assessment using the Otis model and forced oscillations,” *Comput. Methods Programs Biomed.*, vol. 122, no. 3, pp. 330–340, 2015.

[18] J. Herrmann, M. H. Tawhai, and D. W. Kaczka, “Parenchymal strain heterogeneity during oscillatory ventilation: Why two frequencies are better than one,” *J. Appl. Physiol.*, vol. 124, no. 3, pp. 653–663, 2018.

[19] J. Bates, “The Role of Airway Shunt Elastance on the Compartmentalization of Respiratory System Impedance,” *J. Eng. Sci. Med. Diagnostics Ther.*, vol. 2, no. 1, pp. 1–8, 2019.

[20] S. A. Bhatawadekar, D. Leary, and G. N. Maksym, “Modelling resistance and reactance with heterogeneous airway narrowing in mild to severe asthma,” *Can. J. Physiol. Pharmacol.*, vol. 93, no. 3, pp. 207–214, 2015.

[21] B. H. Foy *et al.*, “Lung computational models and the role of the small airways in asthma,” *Am. J. Respir. Crit. Care Med.*, vol. 200, no. 8, pp. 982–991, 2019.

[22] H. H. Alamdari, K. El-Sankary, and G. N. Maksym, “Time-Varying Respiratory Mechanics as a Novel Mechanism Behind Frequency Dependence of Impedance: A Modeling Approach,” *IEEE Trans. Biomed. Eng.*, vol. 66, no. 9, pp. 2433–2446, 2019.

[23] H. Hanafi, “Design Of Piezoelectric Oscillometry , Accuracy In Tracking Time-Varying Impedance And Implications On The Frequency Dependence Of Resistance,” 2015.

[24] S. Rutting, D. G. Chapman, C. S. Farah, and C. Thamrin, “Lung heterogeneity as a predictor for disease severity and response to therapy,” *Curr. Opin. Physiol.*, vol. 22, p. 100446, 2021, doi: 10.1016/j.cophys.2021.05.009.

[25] S. J. Dong, L. Wang, P. Chitano, H. O. Coxson, P. D. Pare, and C. Y. Seow, “Airway diameter at different transpulmonary pressures in ex vivo sheep lungs: Implications for deep inspiration-induced bronchodilation and bronchoprotection,” *Am. J. Physiol. - Lung Cell. Mol. Physiol.*, vol. 321, no. 4, pp. L663–L674, 2021, doi: 10.1152/AJPLUNG.00208.2021.

[26] Y. C. Fung, *Biomechanics — Mechanical properties of living tissue*, vol. 2. 1993.

[27] R. L. Eddy, A. Westcott, G. N. Maksym, G. Parraga, and R. J. Dandurand, “Oscillometry and pulmonary magnetic resonance imaging in asthma and COPD,” *Physiol. Rep.*, vol. 7, no. 1, pp. 1–12, 2019.

[28] M. Cauberghs and K. P. Van De Woestijne, “Effect of upper airway shunt and series properties on respiratory impedance measurements,” *J. Appl. Physiol.*, vol. 66, no. 5, pp. 2274–2279, 1989.

[29] L. A. Zadeh, “Frequency Analysis of Variable Networks,” *Proc. I.R.E. Freq.*, vol. 27, pp. 170–177, 1950.

[30] B. Min, W. Welkowitz, and S. Fich, “Frequency analysis of time-varying elastance model of the left ventricle,” *Bull Math Biol*, vol. 42, no. 2, pp. 173–80, 1980.

[31] B. Sanchez, E. Louarroudi, E. Jorge, J. Cinca, R. Bragos, and R. Pintelon, “A new measuring and identification approach for time-varying bioimpedance using multisine electrical impedance spectroscopy.,” *Physiol Meas.*, vol. 34, no. 3, pp. 339–57, 2013.

[32] K. Paliwal, K. Wójcicki, and B. Schwerin, “Single-channel speech enhancement using spectral subtraction in the short-time modulation domain,” *Speech Commun.*, vol. 23, no. 4, pp. 550–565, 2010.

[33] M. Bertha and J.-C. Golinval, “Identification of non-stationary dynamical systems using multivariate arma models,” *Mech. Syst. Signal Process.*, vol. 88, pp. 166–179, 2017.

[34] R. L. Dellacà *et al.*, “Detection of expiratory flow limitation in COPD using the forced oscillation technique,” *Eur. Respir. J.*, vol. 23, no. 2, pp. 232–240, 2004.

[35] G. J. Gibson, N. B. Pride, J. Davis, and R. C. Schroter, “Exponential description of the static pressure-volume curve of normal and diseased lungs,” *Am. Rev. Respir. Dis.*, vol. 120, no. 4, pp. 799–811, 1979.

[36] D. Navajas, S. Mijailovich, G. M. Glass, D. Stamenovic, and J. J. Fredberg, “Dynamic response of the isolated passive rat diaphragm strip,” *J. Appl. Physiol.*, vol. 73, no. 6, pp. 2681–2692, 1992.

[37] D. W. Kaczka, E. P. Ingenito, B. Suki, and K. R. Lutchen, “Partitioning airway and lung tissue resistances in humans: Effects of bronchoconstriction,” *J. Appl. Physiol.*, vol. 82, no. 5, pp. 1531–1541, 1997.

[38] H. M. Young, F. Guo, R. L. Eddy, G. Maksym, and G. Parraga, “Oscillometry and pulmonary MRI measurements of ventilation heterogeneity in obstructive lung disease: Relationship to quality of life and disease control,” *J. Appl. Physiol.*, vol. 125, no. 1, pp. 73–85, 2018.

[39] D. Navajas, G. N. Maksym, and J. Bates, “Dynamic viscoelastic nonlinearity of lung parenchymal tissue,” *J. Appl. Physiol.*, vol. 79, no. 1, pp. 348–356, 1995.

[40] E. Yi *et al.*, “Mechanical forces accelerate collagen digestion by bacterial collagenase in lung tissue strips,” *Front. Physiol.*, vol. 7, no. JUL, pp. 1–12, 2016.

[41] E. Bartolák-Suki, A. S. LaPrad, B. C. Harvey, B. Suki, and K. R. Lutchen, “Tidal stretches differently regulate the contractile and cytoskeletal elements in intact airways,” *PLoS One*, vol. 9, no. 4, p. e94828, 2014.

[42] A. O. J. Singleton, C. Dev, J. Mount, and A. O. 3rd Singleton, “Respiratory function tests and postoperative pulmonary complications.,” *Med. Times*, vol. 93, no. 10, pp. 1109–1112, Oct. 1965.

[43] A. B. Otis, “A perspective of respiratory mechanics.,” *J. Appl. Physiol.*, vol. 54, no. 5, pp. 1183–1187, May 1983.

[44] A. D. Karakaplan, M. P. Bieniek, and R. Skalak, “A mathematical model of lung parenchyma,” *J. Biomech. Eng*, vol. 102, pp. 124–136, 1980.

[45] D. Stamenovic and T. A. Wilson, “A strain energy function for lung parenchyma,” *J.*

Biomech. Eng, vol. 107, pp. 81–86, 1985.

[46] T. A. Wilson, J. J. Fredberg, J. R. Rodarte, and R. E. Hyatt, "Interdependence of regional expiratory flow," *J. Appl. Physiol*, vol. 59, pp. 1924–1928, 1985.

[47] Y. Lanir, "Constitutive equations for the lung tissue," *J. Biomech. Eng*, vol. 105, pp. 374–380, 1983.

[48] J. R. Ligas, J. F. P. Primiano, and G. M. Saidel, "Static mechanics of excised whole lung: pleural mechanics.," *Ann. Biomed. Eng*, vol. 12, pp. 437–448, 1984.

[49] E. Kimmel, R. D. Kamm, and A. H. Shapiro, "A cellular model of lung elasticity," *J. Biomech. Eng*, vol. 109, pp. 126–131, 1987.

[50] B. Budiansky and E. Kimmel, "Elastic moduli of the lungs," *J. Appl. Mech. Trans. ASME*, vol. 54, pp. 351–358, 1987.

[51] S. J. Lai-Fook, T. A. Wilson, R. E. Hyatt, and J. R. Rodarte, "Elastic constants of inflated lobes of dog lungs," *J. Appl. Physiol*, vol. 40, pp. 508–513, 1976.

[52] L. E. Mount, "The ventilation flow-resistance and compliance of rat lungs," *J. Physiol. Lond.*, vol. 127, pp. 157–167, 1955.

[53] J. Mead, T. Takishima, and D. Leith, "Stress distribution in lungs: a model of pulmonary elasticity," *J. Appl. Physiol*, vol. 28, pp. 596–608, 1970.

[54] T. A. Wilson, "A continuum analysis of a two-dimensional mechanical model of the lung parenchyma," *J. Appl. Physiol*, vol. 33, pp. 472–478, 1972.

[55] R. K. Lambert and T. A. Wilson, "A model for the elastic properties of the lung and their effect of expiratory flow," *J. Appl. Physiol*, vol. 34, pp. 34–48, 1973.

[56] D. L. Vawter, Y. C. Fung, and J. B. West, "Constitutive equation of lung tissue elasticity," *J. Biomech. Eng*, vol. 105, pp. 38–45, 1979.

[57] Y. C. Fung, "A theory of elasticity of the lung," *J. Appl. Mech. Trans. ASME*, vol. 41, pp. 8–14, 1974.

[58] D. L. Vawter, Y. C. Fung, and J. B. West, "Elasticity of excised dog lung parenchyma," *J. Appl. Physiol. Respir. Environ. Exerc. Physiol.*, vol. 45, no. 2, pp. 261–269, 1978.

[59] A. Frankus and G. C. Lee, “A theory for distortion studies of lung parenchyma based on alveolar membrane properties,” *J. Biomech*, vol. 7, pp. 101–107, 1974.

[60] G. C. Lee and A. Frankus, “Elasticity properties of lung parenchyma derived from experimental distortion data.,” *Biophys. J.*, vol. 15, pp. 481–493, 1975.

[61] G. N. Maksym, “Modelling lung tissue rheology,” 1996.

[62] Z. Hantos, B. Daroczy, B. Suki, G. Galgóczy, and T. Csendes, “Forced oscillatory impedance of the respiratory system at low frequencies,” *J. Appl. Physiol.*, vol. 60, no. 1, pp. 123–132, 1986.

[63] H. J. H. Colebatch, C. K. Y. Ng, and N. Nikov, “Use of an exponential function for elastic recoil,” *J. Appl. Physiol. Respir. Environ. Exerc. Physiol.*, vol. 46, no. 2, pp. 387–393, 1979.

[64] H. H. Alamdari *et al.*, “Tracking respiratory mechanics with oscillometry: Introduction of time-varying error,” *IEEE Sens. J.*, 2018.

[65] C. Habre *et al.*, “Radiological findings of complications after lung transplantation,” *Insights Imaging*, vol. 9, no. 5, pp. 709–719, 2018.

[66] J. M. Gauthier, R. R. Hachem, and D. Kreisel, “Update on Chronic Lung Allograft Dysfunction,” *Curr. Transplant. Reports*, vol. 3, no. 3, pp. 185–191, 2016, doi: 10.1007/s40472-016-0112-y.

[67] D. Metter, M. Tulchinsky, and L. M. Freeman, “Current status of ventilation-perfusion scintigraphy for suspected pulmonary embolism,” *Am. J. Roentgenol.*, vol. 208, no. 3, pp. 489–494, 2017.

[68] A. Voskrebenzev *et al.*, “Detection of chronic lung allograft dysfunction using ventilation-weighted Fourier decomposition MRI,” *Am. Soc. Transplant. Am. Soc. Transpl. Surg.*, vol. 18, pp. 2050–2060, 2018.

[69] G. N. Maksym, “Computer controlled oscillator for dynamic testing of biological soft tissue strips Geoff,” 1993.

[70] G. N. Maksym, R. E. Kearney, and J. H. Bates, “Nonparametric block-structured modeling of lung tissue strip mechanics,” *Ann. Biomed. Eng.*, vol. 26, no. 2, pp. 242–252, 1998.

[71] Z. Hantos, B. Suki, T. Csendes, and B. Daroczy, “Constant-phase modelling of pulmonary

tissue impedance.," *Bull. Eur. Physiopathol. Respir*, vol. 23, 1987.

[72] K. D. W. S. Jennifer L., "Constant-Phase Descriptions of Canine Lung, Chest Wall, And Total Respiratory System Viscoelasticity: Effects Of Distending Pressure," *Respir Physiol Neurobiol.*, vol. 183, no. 2, pp. 75–84, 2012.

[73] J. J. Fredberg and D. Stamenovic, "On the imperfect elasticity of lung tissue," *J. Appl. Physiol.*, vol. 67, no. 6, pp. 2408–2419, 1989.

[74] P. D. Pare *et al.*, "Exponential analysis of the lung pressure-volume curve as a predictor of pulmonary emphysema," *Am. Rev. Respir. Dis.*, vol. 126, no. 1, pp. 54–61, 1982.

[75] M. J. Thompson and H. J. H. Colebatch, "Decreased pulmonary distensibility in fibrosing alveolitis and its relation to decreased lung volume," *Thorax*, vol. 44, no. 9, pp. 725–731, 1989.

[76] T. Sugihara, C. J. Martin, and J. Hildebrandt, "Length-tension properties of alveolar wall in man.," *J. Appl. Physiol.*, vol. 30, no. 6, pp. 874–878, 1971.

[77] J. Hildebrandt, "Pressure-volume data of cat lung interpreted by a plastoelastic, linear viscoelastic model.," *J. Appl. Physiol.*, vol. 28, no. 3, pp. 365–372, 1970.

[78] E. Salazar, J. H. Knowles, and H. Knowles, "An analysis of pressure-volume characteristics of the lungs An analysis of pressure- volume characteristics of the lungs," *J Appl Physiol*, vol. c, pp. 97–104, 2013.

[79] K. R. Lutchen, K. Yang, D. W. Kaczka, and B. Suki, "Optimal ventilation waveforms for estimating low-frequency respiratory impedance," *J Appl Physiol*, vol. 75, pp. 478–88, 1993.

[80] A. B. Otis *et al.*, "Mechanical factors in distribution of pulmonary ventilation," *J. Appl. Physiol*, vol. 8, pp. 427–443, 1956.

[81] A. B. Otis, "History of respiratory mechanics," in *Handbook of physiology*, 1986, pp. 1–12.

[82] R. Harris *et al.*, "Regional Pulmonary Perfusion, Inflation, and Ventilation Defects in Bronchoconstricted Patients with Asthma.," *Amer J Resp Crit Care Med*, vol. 174, no. 3, pp. 245–253, 2006.

[83] J. Venegas *et al.*, "Self-organized patchiness in asthma as a prelude to catastrophic shifts.,"

Nature, vol. 434, no. 7034, pp. 777–782, 2005.

[84] R. Harris, H. Fujii-Rios, T. Winkler, G. Musch, M. Vidal Melo, and J. Venegas, "Ventilation defect formation in healthy and asthma subjects is determined by lung inflation.," *PLoS One*, vol. 7, no. 12, 2012.

[85] N. T. Tgavalekos *et al.*, "Relationship between airway narrowing, patchy ventilation and lung mechanics in asthmatics," *Eur. Respir. J.*, vol. 29, pp. 1174–1181, 2007.

[86] Z. Hantos, "Intra-breath oscillometry for assessing respiratory outcomes," *Curr. Opin. Physiol.*, vol. 22, pp. 1–7, 2021, doi: 10.1016/j.cophys.2021.05.004.

[87] J. K. Lui, H. Parameswaran, M. S. Albert, and K. R. Lutchen, "Linking ventilation heterogeneity quantified via hyperpolarized 3He MRI to dynamic lung mechanics and airway hyperresponsiveness," *PLoS One*, vol. 10, no. 11, pp. 1–15, 2015.

[88] G. G. King, C. E. Farrow, and D. G. Chapman, "Dismantling the pathophysiology of asthma using imaging," *Eur. Respir. Rev.*, vol. 28, no. 152, pp. 1–15, 2019.

[89] C. Farrow and G. King, "SPECT Ventilation Imaging in Asthma," *Semin. Nucl. Med.*, vol. 49, no. 1, pp. 11–15, 2019.

[90] D. W. Kaczka, E. P. Ingenito, E. Israel, and K. R. Lutchen, "Airway and lung tissue mechanics in asthma. Effects of albuterol," *Am J Respir Crit Care Med*, vol. 159, pp. 169–78, 1999.

[91] D. W. Kaczka, E. P. Ingenito, and K. R. Lutchen, "Technique to determine inspiratory impedance during mechanical ventilation: implications for flow limited patients," *Ann Biomed Eng*, vol. 27, pp. 340–55, 1999.

[92] J. H. T. Bates, G. N. Maksym, D. Navajas, and B. Suki, "Lung tissue rheology and 1/f noise," *Ann. Biomed. Eng.*, vol. 22, no. 6, pp. 674–681, 1994.

[93] S. Galant, H. Komarow, H. Shin, S. Siddiqui, and B. Lipworth, "The case for impulse oscillometry in the management of asthma in children and adults," *Ann. Allergy, Asthma Immunol.*, vol. 118, no. 6, pp. 664–671, 2017.

[94] D. Postma *et al.*, "Exploring the relevance and extent of small airways dysfunction in asthma (ATLANTIS): baseline data from a prospective cohort study," *Lancet Respir Med*,

2019.

[95] A. Bell and S. Siddiqui, “Image-based simulation and modeling: unlocking small airway function tests?,” *J. Appl. Physiol.*, vol. 129, no. 3, pp. 580–582, 2020.

[96] T. Similowski and J. H. T. Bates, “Two-compartment modelling of respiratory system mechanics at low frequencies: Gas redistribution or tissue rheology?,” *Eur. Respir. J.*, vol. 4, no. 3, pp. 353–358, 1991.

[97] J. H. T. Bates and O. B. Allen, “The estimation of lung mechanics parameters in the presence of pathology: A theoretical analysis,” *Ann. Biomed. Eng.*, vol. 34, no. 3, pp. 384–392, 2006.

APPENDIX A: DESIGN REQUIREMENTS

A.1 TISSUE BATH PERFORMANCE

1. Keeping the porcine lung tissue alive
2. The steady flow of Krebs solution with carbogen pumped into the liquid
3. High sensitivity force transducer with range for tissue force capable of submersion
4. Preconditioning and sinusoidal stretching of the lung tissue over 150% stretch and 0.03 to 3 Hz range.

A.2 TESTING AND CALIBRATION REQUIREMENTS

1. Calibration of the force transducer
    a. Use of low friction pulley with known weights: 0, 15, 25, 35, 45 grams
    b. Adjust gain and offset for input data acquisition range
2. Preconditioning
    a. Initialize software to tissue length (l_o)
    b. Tissue stretches to twice its length ($100\%\ Stretch = 2l_o$) and back to the original unstretched length with 5-10 repeated cycles, each cycle 1 min.
    c. Set appropriate velocity (VE string for the driver)
    d. Set appropriate acceleration and Deceleration for smooth turns (AC & DE strings for the driver) – e.g., setting 25 or 50
3. Triangle Wave
    a. Triangle waves with frequencies of 0.5, 1, 1.5, 2, 2.5, and 3 Hz are sent
    b. Studied the optimum characteristics of the tissue
    c. Duration – 2, 1, 0.66, 0.5, 0.4, 0.33 sec
    d. Velocity (VE), acceleration, and deceleration (AC & DE)
    e. Amplitude (position of the actuator – FP, FL, or FE string control)
4. Sinusoidal Wave
    a. Sinusoidal waves with frequencies of 0.5, 1, 1.5, 2, 2.5, and 3 Hz are sent
    b. Studied the optimum characteristics of the tissue
    c. Duration – 2, 1, 0.66, 0.5, 0.4, 0.33 sec
    d. Velocity (VE), acceleration, and deceleration (AC & DE)
    e. Amplitude (position of the actuator – FP, FL, or FE Control)

A.3 ACTUATOR REQUIREMENTS

1. 0.3 – 3 Hz Sinusoidal oscillations at full amplitude i.e., twice the length of tissue initial length.

2. For 100% amp with safety factor for 10%, actuator min, and max position 10% to min, and 10% to the max – 20% for preconditioning. The performance (i.e., VE & AC) for the PC is low.
3. For 20% amp, for 3 cm tissue with 10% safety factor, sinusoidal amplitude is $0.5 \times 3.3 \times 0.2 = 0.33\,cm$. Velocity maximums are $2\pi f \times Position\ amplitudes$. Acceleration maximums are $2\pi f \times velocity\ amplitudes$.

f_o	0.01	0.03	0.1	0.3	1	3
Position (mm)	3.3	3.3	3.3	3.3	3.3	3.3
Velocity ($\frac{mm}{s}$)	0.21	0.62	2.07	6.22	20.73	62.20
Acceleration ($\frac{mm}{s^2}$)	0.01	0.12	1.30	11.73	130.28	1172.51

A.4 PRINCIPAL DESIGN REQUIREMENTS

1. The triangle wave should achieve performance the time, position, and desired characteristic force results
2. The sinusoidal wave should achieve the time, position, and desired characteristic force results

Theoretically, we should be able to achieve the requirements, as they were in the velocity specification but practically, we were not able to, because of communication delays for sinusoidal control and switching directions.

A.5 IMPLEMENTED DESIGN LIMITATIONS OF THE SYSTEM

After several stepper motor control algorithms were tested. It was possible that the specified velocity could be achieved but only with single ramp commands. Delays for communicating multiple commands for reversing direction and for the sinusoidal motion were not possible. The stepper motor FP command could not be interrupted for adequate control. This was because this was a buffered command, not immediate and there were no immediate position control commands. Another configuration that used the encoder was also determined to be likely limited in the same way as it was also a buffered command with the same time delay. Amongst the motion commands, only the ST (Stop Command) had a short time delay for execution. Thus, it was determined that position control using this stepper motor and likely most stepper motors would be

limited. It was decided to pursue linear actuators. Below is a table of potential actuators for tissue testing that were investigated.

SR#	Speed	Stroke Length	Feedback	Power	Current	Voltage	AC/DC/Both	Price	Website
1	0.37"/sec (150 lbs); 1.14"/sec (50 lbs); 2.00"/sec (35 lbs)	2" - 40"	Built-in potentiometer feedback	N/A	5 – 1.3 A (Full Load)	12 – 48 VDC	DC	$173.74	https://www.progressiveautomations.ca/products/linear-actuator-with-potentiometer
2	3.15"/sec (33 lbs); 5.51"/sec (22 lbs); 9.05"/sec (11 lbs)	1" - 24"	No	N/A	9 - 2.3 A (Full Load)	12 – 48 VDC	DC	$181.25	https://www.progressiveautomations.ca/products/tubular-high-speed-linear-actuator
3	10m/s	5" - 50"	Linear Potentiometers	N/A	<1mA	N/A	N/A	$89.00 USD	https://www.firgelliauto.com/products/potentiometer
4	2"/sec (35 lbs);	1" - 30"	Optical Feedback	N/A	5 A	12V DC	DC	$149.99 USD	https://www.firgelliauto.com/products/optical-sensor-actuators
5	2"/sec (35 lbs);	2" - 12"	potentiometer feedback	N/A	5 A	12V DC	DC	$139.99 USD	https://www.firgelliauto.com/products/feedback-rod-actuator
6	4.5" (9" at no load) @ 22lbs	2" - 38"	No	N/A	6 A	12V DC	DC	$149.00 USD	https://www.firgelliauto.com/products/high-speed-actuator
7	No Load Speed 5000 RPM; 2mm Travel Per Revolution	6" screw extended from the motor	No	40W	Rated Current < 3A	24 V	DC	$230.00	https://www.anaheimautomation.com/products/brushless/brushless-linear-actuators-item.php?sID=842&pt=i&tID=1225&cID=562
8	No Load Speed 4200 RPM; 5mm Travel Per Revolution	12" screw extended from the motor	No	34W	Rated Current < 2.5A	24 V	DC	$271.00	https://www.anaheimautomation.com/products/brushless/brushless-linear-actuators-item.php?sID=843&pt=i&tID=1225&cID=562

Figure A.5.1: Potential linear actuators

Figure A.5.1 above shows the prospective actuators we could buy and achieve our desired requirements, however, due to COVID-19 deliveries were not being allowed due to lockdowns, and it was becoming clear with laboratory restrictions as well that it would be better to use published measurements rather than pursue measurement.

APPENDIX B: INVESTIGATING HETEROGENEITY AND TIME-VARIATION EFFECT ON $R(f)$

B.1 PUBLISHED CORRELATIONS

In addition to the work in this thesis of chapter 6, we also published some correlations from the CLAD study data which I include 3 of these below.

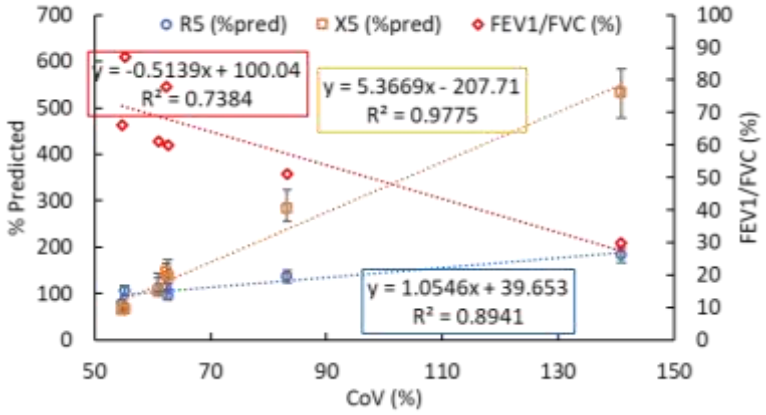

Figure B.1.1: Published figure in BMES poster

In this Figure B.1.1, there are two oscillometry variables, and one spirometry variable, each linearly correlated with the coefficient of variation i.e., a variable obtained from VSPECT imaging as described in Chapter 6. The oscillometry variables are the percent predicted values of R_5 and X_5 which are the percent of the individual patient according to their height, weight, and sex [2]. The oscillometry data are at $5\,Hz$ for resistance and reactance of the lung showing that while X_5 $(\%pred)$ was correlated with CoV, R_5 $(\%pred)$ was not. This implied that with increased heterogeneity the lung was stiffer to volume changes implying the loss of regions of the lung for ventilation which agrees with the higher levels of heterogeneity as indicated by the increased CoV%. Similarly, FEV/FVC% by spirometry decreases with CoV% indicating that there is a loss in exhaled volume in 1 second normalized to FVC, indicating some flow limitation with increased heterogeneity in the lung. Compared to spirometry which is the standard measure for bronchiolitis obliterans (BOS), the correlations appear to be better with X_5 $(\%pred)$.

B.2 QUALITY CONTROL

Here we wished to examine if our values from a single recording of 30 seconds over multiple breaths at a single frequency of 10 Hz after a quality control step were in agreement with our repeated measurements at multiple frequencies (5 to 37 Hz) examining the impedance values obtained at the closest frequency to 10 Hz out of the multi-frequency signal which was 11 Hz. The 10 Hz impedance measurements first went through quality control as follows. We visually examined all the X_{10} and R_{10} data vs time. First, a 1 Hz bandpass filter centered at 10 Hz was applied then an algorithm that separated and overlapped the breaths for visualization was used. If any breath was abnormal to the typical breath it was eliminated. We then compared the std-dev of the variable either R_{10} or X_{10} before and after this quality control step for all patients (Figure B.2.1, left). We then also compared the correlation of X_{11} to X_{10} to see if they agreed (Figure B.2.1, right)**.** The X_{10} values were then correlated with R_{5-19} to test the hypothesis presented in Chapter 6 section 6.2.2.

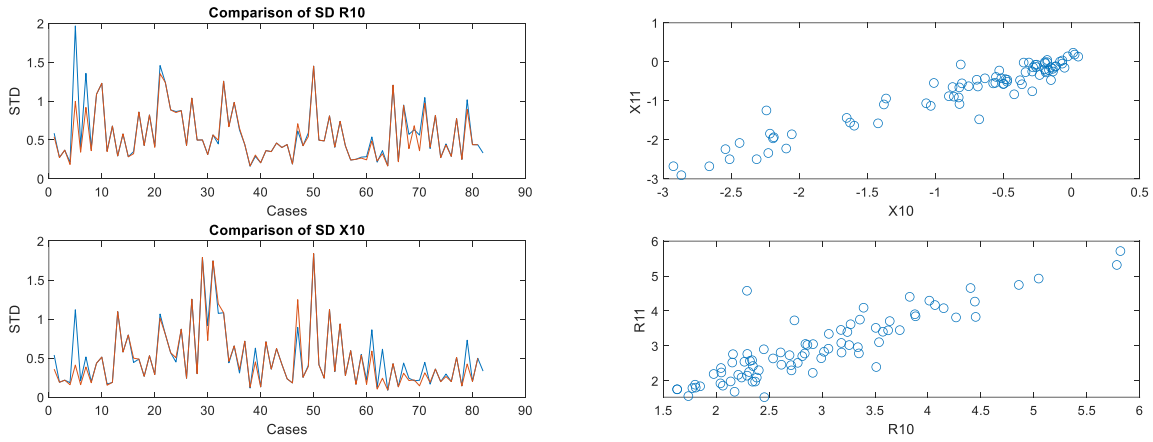

Figure B.2.1 Left: Standard deviations of R_{10} and X_{10} before (blue) and after (orange) quality control for each patient? Right: Correlations of X_{11} and R_{11} from spectral measurements vs. average X_{10} and R_{10} from single frequency-time course measurements after quality control.

In Figure B.2.1 (left), the blue line represents the older standard deviation of R_{10} and X_{10} compared with the standard deviation after quality control in orange. In a couple of subjects, the standard deviation changes, but not for most of the subjects. It is evident that the standard deviation even after the quality control has not changed significantly as it is found that a lot of data collected had noise added to it and even after removing redundant breaths the mean values do not change

significantly. In this Figure B.2.1 (right), we can see that after the quality control the impedance at 10 and 11 Hz correlate linearly, which shows that data is reliable.

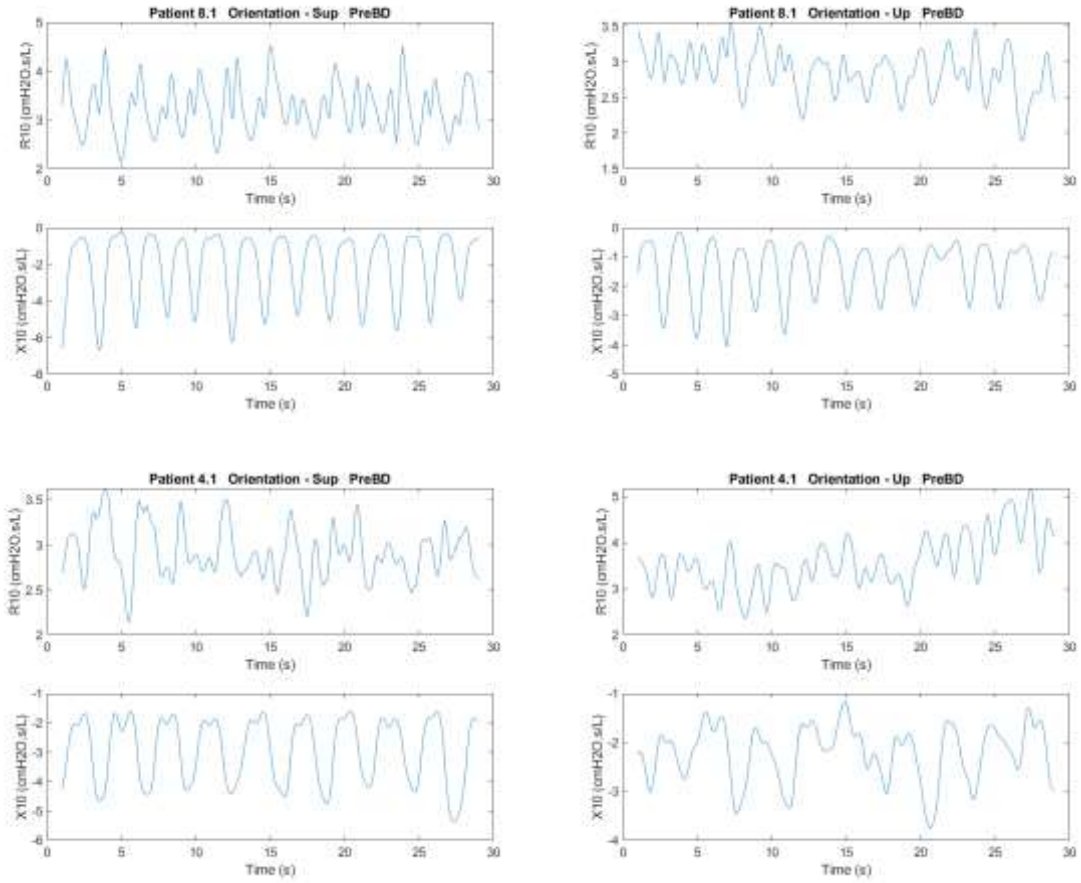

Figure B.2.2. Examples of 2 patients time domain for R_{10} and X_{10} supine (Sup) and upright (Up) pre-bronchodilator (PreBD)

In Figure B2.2, we can see the time domain plots for R_{10} and X_{10} for 2 post-lung transplant patients (4 & 8) pre-bronchodilator test for a supine and upright position in the CLAD study. We can see that is nice variability in X_{10}, however, we did not get the correlation with R_{5-19} as seen in Chapter 6, section 6.2.2. We can also see the presence of noise in the data, also the variation in the R_{10} is evident, however, that does not contribute to $R(f)$.

In conclusion, even though we employed quality control on the $std\ X_{10}$ data, however, the method was not highly effective, and we did not receive a significant correlation of $std\ X_{10}$ to $R(f)$, might be due to the low signal-to-noise ratio.

APPENDIX C: COPYRIGHT RELEASE REQUESTS

C.1 Figure 1.1 Permission

Dear ,

We hereby grant you permission to reprint the material below at no charge in your thesis subject to the following conditions:

1. If any part of the material to be used (for example, figures) has appeared in our publication with credit or acknowledgement to another source, permission must also be sought from that source. If such permission is not obtained then that material may not be included in your publication/copies.

2. Suitable acknowledgment to the source must be made, either as a footnote or in a reference list at the end of your publication, as follows:
"This article was published in Publication title, Vol number, Author(s), Title of article, Page Nos, Copyright Elsevier (or appropriate Society name) (Year)."

3. Your thesis may be submitted to your institution in either print or electronic form.

4. Reproduction of this material is confined to the purpose for which permission is hereby given

5. This permission is granted for non-exclusive world English rights only. For other languages please reapply separately for each one required. Permission excludes use in an electronic form other than submission. Should you have a

specific electronic project in mind please reapply for permission.

6. Should your thesis be published commercially, please reapply for permission.

This includes permission for the Library and Archives of Canada to supply single copies, on demand, of the complete thesis. Should your thesis be published commercially, please reapply for permission- Canada
This includes permission for UMI to supply single copies, on demand, of the complete thesis. Should your thesis be published commercially, please reapply for permission-ROW

7. Posting of the full article online is not permitted. You may post an abstract with a link to the Elsevier website www.elsevier.com, or to the article on ScienceDirect if it is available on that platform.

8. Article can used be in the University library if it is embedded in the thesis and not used commercially.

Kind regards,

Anita Mercy Vethakkan
Senior Copyrights Coordinator
ELSEVIER | HCM - Health Content Management

C.2 Figure 1.3 Permission

ELSEVIER LICENSE
TERMS AND CONDITIONS

Dec 02, 2021

This Agreement between Dalhousie University -- Anas Tahir ("You") and Elsevier ("Elsevier") consists of your license details and the terms and conditions provided by Elsevier and Copyright Clearance Center.

License Number	5200411462968
License date	Dec 01, 2021
Licensed Content Publisher	Elsevier
Licensed Content Publication	Respiratory Medicine
Licensed Content Title	Detection of changes in respiratory mechanics due to increasing degrees of airway obstruction in asthma by the forced oscillation technique
Licensed Content Author	Juliana V. Cavalcanti,Agnaldo J. Lopes,José M. Jansen,Pedro L. Melo
Licensed Content Date	Dec 1, 2006
Licensed Content Volume	100
Licensed Content Issue	12
Licensed Content Pages	13
Start Page	2207
End Page	2219
Type of Use	reuse in a thesis/dissertation

Portion	figures/tables/illustrations
Number of figures/tables/illustrations	1
Format	electronic
Are you the author of this Elsevier article?	No
Will you be translating?	No
Title	TISSUE NONLINEARITY AS A NOVEL MECHANISM FOR THE FREQUENCY DEPENDENCE OF RESPIRATORY RESISTANCE TO AIRFLOW IN DISEASE
Institution name	Dalhousie University
Expected presentation date	Dec 2021
Portions	Figure 1
Requestor Location	Dalhousie University 1881 Brunswick Street APT 415 Halifax, NS B3J3L8 Canada Attn: Dalhousie University
Publisher Tax ID	GB 494 6272 12
Total	0.00 CAD

Terms and Conditions

INTRODUCTION

1. The publisher for this copyrighted material is Elsevier. By clicking "accept" in connection with completing this licensing transaction, you agree that the following terms and conditions apply to this transaction (along with the Billing and Payment terms and conditions

established by Copyright Clearance Center, Inc. ("CCC"), at the time that you opened your Rightslink account and that are available at any time at http://myaccount.copyright.com).

GENERAL TERMS

2. Elsevier hereby grants you permission to reproduce the aforementioned material subject to the terms and conditions indicated.

3. Acknowledgement: If any part of the material to be used (for example, figures) has appeared in our publication with credit or acknowledgement to another source, permission must also be sought from that source. If such permission is not obtained then that material may not be included in your publication/copies. Suitable acknowledgement to the source must be made, either as a footnote or in a reference list at the end of your publication, as follows:

"Reprinted from Publication title, Vol /edition number, Author(s), Title of article / title of chapter, Pages No., Copyright (Year), with permission from Elsevier [OR APPLICABLE SOCIETY COPYRIGHT OWNER]." Also Lancet special credit - "Reprinted from The Lancet, Vol. number, Author(s), Title of article, Pages No., Copyright (Year), with permission from Elsevier."

4. Reproduction of this material is confined to the purpose and/or media for which permission is hereby given.

5. Altering/Modifying Material: Not Permitted. However figures and illustrations may be altered/adapted minimally to serve your work. Any other abbreviations, additions, deletions and/or any other alterations shall be made only with prior written authorization of Elsevier Ltd. (Please contact Elsevier's permissions helpdesk here). No modifications can be made to any Lancet figures/tables and they must be reproduced in full.

6. If the permission fee for the requested use of our material is waived in this instance, please be advised that your future requests for Elsevier materials may attract a fee.

7. Reservation of Rights: Publisher reserves all rights not specifically granted in the combination of (i) the license details provided by you and accepted in the course of this licensing transaction, (ii) these terms and conditions and (iii) CCC's Billing and Payment terms and conditions.

8. License Contingent Upon Payment: While you may exercise the rights licensed immediately upon issuance of the license at the end of the licensing process for the transaction, provided that you have disclosed complete and accurate details of your proposed use, no license is finally effective unless and until full payment is received from you (either by publisher or by CCC) as provided in CCC's Billing and Payment terms and conditions. If full payment is not received on a timely basis, then any license preliminarily granted shall be deemed automatically revoked and shall be void as if never granted. Further, in the event that you breach any of these terms and conditions or any of CCC's Billing and Payment terms and conditions, the license is automatically revoked and shall be void as if never granted. Use of materials as described in a revoked license, as well as any use of the materials beyond the scope of an unrevoked license, may constitute copyright infringement and publisher reserves the right to take any and all action to protect its copyright in the materials.

9. Warranties: Publisher makes no representations or warranties with respect to the licensed material.

10. Indemnity: You hereby indemnify and agree to hold harmless publisher and CCC, and their respective officers, directors, employees and agents, from and against any and all claims arising out of your use of the licensed material other than as specifically authorized pursuant to this license.

11. No Transfer of License: This license is personal to you and may not be sublicensed, assigned, or transferred by you to any other person without publisher's written permission.

12. No Amendment Except in Writing: This license may not be amended except in a writing signed by both parties (or, in the case of publisher, by CCC on publisher's behalf).

13. Objection to Contrary Terms: Publisher hereby objects to any terms contained in any purchase order, acknowledgment, check endorsement or other writing prepared by you, which terms are inconsistent with these terms and conditions or CCC's Billing and Payment terms and conditions. These terms and conditions, together with CCC's Billing and Payment terms and conditions (which are incorporated herein), comprise the entire agreement between you and publisher (and CCC) concerning this licensing transaction. In the event of any conflict between your obligations established by these terms and conditions and those established by CCC's Billing and Payment terms and conditions, these terms and conditions shall control.

14. Revocation: Elsevier or Copyright Clearance Center may deny the permissions described in this License at their sole discretion, for any reason or no reason, with a full refund payable to you. Notice of such denial will be made using the contact information provided by you. Failure to receive such notice will not alter or invalidate the denial. In no event will Elsevier or Copyright Clearance Center be responsible or liable for any costs, expenses or damage incurred by you as a result of a denial of your permission request, other than a refund of the amount(s) paid by you to Elsevier and/or Copyright Clearance Center for denied permissions.

LIMITED LICENSE

The following terms and conditions apply only to specific license types:

15. **Translation**: This permission is granted for non-exclusive world **English** rights only unless your license was granted for translation rights. If you licensed translation rights you may only translate this content into the languages you requested. A professional translator must perform all translations and reproduce the content word for word preserving the integrity of the article.

16. **Posting licensed content on any Website**: The following terms and conditions apply as follows: Licensing material from an Elsevier journal: All content posted to the web site must maintain the copyright information line on the bottom of each image; A hyper-text must be included to the Homepage of the journal from which you are licensing at http://www.sciencedirect.com/science/journal/xxxxx or the Elsevier homepage for books at http://www.elsevier.com; Central Storage: This license does not include permission for a scanned version of the material to be stored in a central repository such as that provided by Heron/XanEdu.

Licensing material from an Elsevier book: A hyper-text link must be included to the Elsevier homepage at http://www.elsevier.com . All content posted to the web site must maintain the copyright information line on the bottom of each image.

Posting licensed content on Electronic reserve: In addition to the above the following clauses are applicable: The web site must be password-protected and made available only to bona fide students registered on a relevant course. This permission is granted for 1 year only. You may obtain a new license for future website posting.

17. **For journal authors:** the following clauses are applicable in addition to the above:

Preprints:

A preprint is an author's own write-up of research results and analysis, it has not been peer-reviewed, nor has it had any other value added to it by a publisher (such as formatting, copyright, technical enhancement etc.).

Authors can share their preprints anywhere at any time. Preprints should not be added to or enhanced in any way in order to appear more like, or to substitute for, the final versions of articles however authors can update their preprints on arXiv or RePEc with their Accepted Author Manuscript (see below).

If accepted for publication, we encourage authors to link from the preprint to their formal publication via its DOI. Millions of researchers have access to the formal publications on ScienceDirect, and so links will help users to find, access, cite and use the best available version. Please note that Cell Press, The Lancet and some society-owned have different preprint policies. Information on these policies is available on the journal homepage.

Accepted Author Manuscripts: An accepted author manuscript is the manuscript of an article that has been accepted for publication and which typically includes author-incorporated changes suggested during submission, peer review and editor-author communications.

Authors can share their accepted author manuscript:

- immediately
  - via their non-commercial person homepage or blog
  - by updating a preprint in arXiv or RePEc with the accepted manuscript
  - via their research institute or institutional repository for internal institutional uses or as part of an invitation-only research collaboration work-group
  - directly by providing copies to their students or to research collaborators for their personal use
  - for private scholarly sharing as part of an invitation-only work group on commercial sites with which Elsevier has an agreement
- After the embargo period
  - via non-commercial hosting platforms such as their institutional repository
  - via commercial sites with which Elsevier has an agreement

In all cases accepted manuscripts should:

- link to the formal publication via its DOI
- bear a CC-BY-NC-ND license - this is easy to do
- if aggregated with other manuscripts, for example in a repository or other site, be shared in alignment with our hosting policy not be added to or enhanced in any way to appear more like, or to substitute for, the published journal article.

Published journal article (JPA): A published journal article (PJA) is the definitive final record of published research that appears or will appear in the journal and embodies all value-adding publishing activities including peer review co-ordination, copy-editing, formatting, (if relevant) pagination and online enrichment.

Policies for sharing publishing journal articles differ for subscription and gold open access articles:

Subscription Articles: If you are an author, please share a link to your article rather than the full-text. Millions of researchers have access to the formal publications on ScienceDirect, and so links will help your users to find, access, cite, and use the best available version.

Theses and dissertations which contain embedded PJAs as part of the formal submission can be posted publicly by the awarding institution with DOI links back to the formal publications on ScienceDirect.

If you are affiliated with a library that subscribes to ScienceDirect you have additional private sharing rights for others' research accessed under that agreement. This includes use for classroom teaching and internal training at the institution (including use in course packs and courseware programs), and inclusion of the article for grant funding purposes.

Gold Open Access Articles: May be shared according to the author-selected end-user license and should contain a CrossMark logo, the end user license, and a DOI link to the formal publication on ScienceDirect.

Please refer to Elsevier's posting policy for further information.

18. **For book authors** the following clauses are applicable in addition to the above: Authors are permitted to place a brief summary of their work online only. You are not allowed to download and post the published electronic version of your chapter, nor may you scan the printed edition to create an electronic version. **Posting to a repository:** Authors are permitted to post a summary of their chapter only in their institution's repository.

19. **Thesis/Dissertation**: If your license is for use in a thesis/dissertation your thesis may be submitted to your institution in either print or electronic form. Should your thesis be published commercially, please reapply for permission. These requirements include permission for the Library and Archives of Canada to supply single copies, on demand, of the complete thesis and include permission for Proquest/UMI to supply single copies, on demand, of the complete thesis. Should your thesis be published commercially, please reapply for permission. Theses and dissertations which contain embedded PJAs as part of the formal submission can be posted publicly by the awarding institution with DOI links back to the formal publications on ScienceDirect.

Elsevier Open Access Terms and Conditions

You can publish open access with Elsevier in hundreds of open access journals or in nearly 2000 established subscription journals that support open access publishing. Permitted third party re-use of these open access articles is defined by the author's choice of Creative Commons user license. See our open access license policy for more information.

Terms & Conditions applicable to all Open Access articles published with Elsevier:

Any reuse of the article must not represent the author as endorsing the adaptation of the article nor should the article be modified in such a way as to damage the author's honour or reputation. If any changes have been made, such changes must be clearly indicated.

The author(s) must be appropriately credited and we ask that you include the end user license and a DOI link to the formal publication on ScienceDirect.

If any part of the material to be used (for example, figures) has appeared in our publication with credit or acknowledgement to another source it is the responsibility of the user to ensure their reuse complies with the terms and conditions determined by the rights holder.

Additional Terms & Conditions applicable to each Creative Commons user license:

CC BY: The CC-BY license allows users to copy, to create extracts, abstracts and new works from the Article, to alter and revise the Article and to make commercial use of the Article (including reuse and/or resale of the Article by commercial entities), provided the user gives appropriate credit (with a link to the formal publication through the relevant DOI), provides a link to the license, indicates if changes were made and the licensor is not represented as endorsing the use made of the work. The full details of the license are available at http://creativecommons.org/licenses/by/4.0.

CC BY NC SA: The CC BY-NC-SA license allows users to copy, to create extracts, abstracts and new works from the Article, to alter and revise the Article, provided this is not done for commercial purposes, and that the user gives appropriate credit (with a link to the formal publication through the relevant DOI), provides a link to the license, indicates if changes were made and the licensor is not represented as endorsing the use made of the work. Further, any new works must be made available on the same conditions. The full details of the license are available at http://creativecommons.org/licenses/by-nc-sa/4.0.

CC BY NC ND: The CC BY-NC-ND license allows users to copy and distribute the Article, provided this is not done for commercial purposes and further does not permit distribution of the Article if it is changed or edited in any way, and provided the user gives appropriate credit (with a link to the formal publication through the relevant DOI), provides a link to the license, and that the licensor is not represented as endorsing the use made of the work. The full details of the license are available at http://creativecommons.org/licenses/by-nc-nd/4.0. Any commercial reuse of Open Access articles published with a CC BY NC SA or CC BY NC ND license requires permission from Elsevier and will be subject to a fee.

Commercial reuse includes:

- Associating advertising with the full text of the Article
- Charging fees for document delivery or access
- Article aggregation
- Systematic distribution via e-mail lists or share buttons

Posting or linking by commercial companies for use by customers of those companies.

20. **Other Conditions**:

v1.10

Questions? customercare@copyright.com or +1-855-239-3415 (toll free in the US) or +1-978-646-2777.

C.3 Figure 1.4 Permission

THE AMERICAN PHYSIOLOGICAL SOCIETY LICENSE
TERMS AND CONDITIONS

Dec 02, 2021

This Agreement between Dalhousie University -- Anas Tahir ("You") and The American Physiological Society ("The American Physiological Society") consists of your license details and the terms and conditions provided by The American Physiological Society and Copyright Clearance Center.

The publisher has provided special terms related to this request that can be found at the end of the Publisher's Terms and Conditions.

License Number	5200810577014
License date	Dec 02, 2021
Licensed Content Publisher	The American Physiological Society
Licensed Content Publication	Journal of Applied Physiology
Licensed Content Title	Lung tissue viscoelasticity: a mathematical framework and its molecular basis
Licensed Content Author	B. Suki, A. L. Barabasi, K. R. Lutchen
Licensed Content Date	Jun 1, 1994
Licensed Content Volume	76
Licensed Content Issue	6
Type of Use	Thesis/Dissertation

Requestor type	non-profit academic/educational
Readers being charged a fee for this work	No
Format	electronic
Portion	figures/tables/images
Number of figures/tables/images	2
Will you be translating?	no
World Rights	no
Title	TISSUE NONLINEARITY AS A NOVEL MECHANISM FOR THE FREQUENCY DEPENDENCE OF RESPIRATORY RESISTANCE TO AIRFLOW IN DISEASE
Institution name	Dalhousie University
Expected presentation date	Dec 2021
Portions	Figure 4 & 7
Requestor Location	Dalhousie University 1881 Brunswick Street APT 415 Halifax, NS B3J3L8 Canada Attn: Dalhousie University
Billing Type	Invoice
Billing Address	Dalhousie University 1881 Brunswick Street APT 415 Halifax, NS B3J3L8

Canada
Attn: Dalhousie University

Total 0.00 USD

Terms and Conditions

Terms and Conditions:

Original Authors of Published Works: To see a full list of original authors rights concerning their own published work http://www.the-aps.org/publications/authorinfo/copyright.htm

Content reuse rights awarded by the APS may be exercised immediately upon issuance of this license, provided full disclosure and complete and accurate details of the proposed reuse have been made; no license is finally granted unless and until full payment is received either by the publisher or by CCC as provided in CCC's Billing and Payment Terms and Conditions. If full payment is not received on a timely basis, then any license preliminarily granted shall be deemed automatically revoked and shall be void as if never granted. Further, in the event that you breach any of these Terms and Conditions or any of CCC's Billing and Payment Terms and Conditions, the license is automatically revoked and shall be void as if never granted. Use of materials as described in a revoked license, as well as any use of the materials beyond the scope of the license, may constitute copyright infringement and the Publisher reserves the right to take action to protect its copyright of its materials.

The APS makes no representations or warranties with respect to the licensed material. You hereby indemnify and agree to hold harmless the publisher and CCC, and their respective officers, directors, employees and agents, from and against any and all claims arising out of your use of the licensed material other than as specifically authorized pursuant to this license.

This license is personal to you /your organization and may not be sublicensed, assigned, or transferred by you /your organization to another person /organization without the publisher's permission.This license may not be amended except in writing signed by both parties, or in the case of the publisher, by CCC on the publisher's behalf.

The APS reserves all rights not specifically granted in the combination of (i) the license details provided by you and accepted in the course of this licensing transaction, (ii) these Terms and Conditions and (iii) CCC's Billing and Payment Terms and Conditions.

v1.0

Questions? customercare@copyright.com or +1-855-239-3415 (toll free in the US) or +1-978-646-2777.

C.4 Figure 1.7 Permission

THE AMERICAN PHYSIOLOGICAL SOCIETY LICENSE
TERMS AND CONDITIONS

Dec 02, 2021

This Agreement between Dalhousie University -- Anas Tahir ("You") and The American Physiological Society ("The American Physiological Society") consists of your license details and the terms and conditions provided by The American Physiological Society and Copyright Clearance Center.

The publisher has provided special terms related to this request that can be found at the end of the Publisher's Terms and Conditions.

License Number	5200810637936
License date	Dec 02, 2021
Licensed Content Publisher	The American Physiological Society
Licensed Content Publication	Journal of Applied Physiology
Licensed Content Title	Effect of upper airway shunt and series properties on respiratory impedance measurements
Licensed Content Author	M. Cauberghs, K. P. Van de Woestijne
Licensed Content Date	May 1, 1989
Licensed Content Volume	66
Licensed Content Issue	5
Type of Use	Thesis/Dissertation

Requestor type	non-profit academic/educational
Readers being charged a fee for this work	No
Format	electronic
Portion	figures/tables/images
Number of figures/tables/images	2
Will you be translating?	no
World Rights	no
Title	TISSUE NONLINEARITY AS A NOVEL MECHANISM FOR THE FREQUENCY DEPENDENCE OF RESPIRATORY RESISTANCE TO AIRFLOW IN DISEASE
Institution name	Dalhousie University
Expected presentation date	Dec 2021
Portions	Figure 1 & 5
Requestor Location	Dalhousie University 1881 Brunswick Street APT 415 Halifax, NS B3J3L8 Canada Attn: Dalhousie University
Billing Type	Invoice
Billing Address	Dalhousie University 1881 Brunswick Street APT 415 Halifax, NS B3J3L8

Canada
Attn: Dalhousie University

Total 0.00 USD

Terms and Conditions

Terms and Conditions:

Original Authors of Published Works: To see a full list of original authors rights concerning their own published work http://www.the-aps.org/publications/authorinfo/copyright.htm

Content reuse rights awarded by the APS may be exercised immediately upon issuance of this license, provided full disclosure and complete and accurate details of the proposed reuse have been made; no license is finally granted unless and until full payment is received either by the publisher or by CCC as provided in CCC's Billing and Payment Terms and Conditions. If full payment is not received on a timely basis, then any license preliminarily granted shall be deemed automatically revoked and shall be void as if never granted. Further, in the event that you breach any of these Terms and Conditions or any of CCC's Billing and Payment Terms and Conditions, the license is automatically revoked and shall be void as if never granted. Use of materials as described in a revoked license, as well as any use of the materials beyond the scope of the license, may constitute copyright infringement and the Publisher reserves the right to take action to protect its copyright of its materials.

The APS makes no representations or warranties with respect to the licensed material. You hereby indemnify and agree to hold harmless the publisher and CCC, and their respective officers, directors, employees and agents, from and against any and all claims arising out of your use of the licensed material other than as specifically authorized pursuant to this license.

This license is personal to you /your organization and may not be sublicensed, assigned, or transferred by you /your organization to another person /organization without the publisher's permission.This license may not be amended except in writing signed by both parties, or in the case of the publisher, by CCC on the publisher's behalf.

The APS reserves all rights not specifically granted in the combination of (i) the license details provided by you and accepted in the course of this licensing transaction, (ii) these Terms and Conditions and (iii) CCC's Billing and Payment Terms and Conditions.

v1.0

Questions? customercare@copyright.com or +1-855-239-3415 (toll free in the US) or +1-978-646-2777.

C.5 Figure 1.10 Permission

THE AMERICAN PHYSIOLOGICAL SOCIETY LICENSE
TERMS AND CONDITIONS

Dec 02, 2021

This Agreement between Dalhousie University -- Anas Tahir ("You") and The American Physiological Society ("The American Physiological Society") consists of your license details and the terms and conditions provided by The American Physiological Society and Copyright Clearance Center.

The publisher has provided special terms related to this request that can be found at the end of the Publisher's Terms and Conditions.

License Number	5200810760177
License date	Dec 02, 2021
Licensed Content Publisher	The American Physiological Society
Licensed Content Publication	Journal of Applied Physiology
Licensed Content Title	Dynamic viscoelastic nonlinearity of lung parenchymal tissue
Licensed Content Author	D. Navajas, G. N. Maksym, J. H. Bates
Licensed Content Date	Jul 1, 1995
Licensed Content Volume	79
Licensed Content Issue	1
Type of Use	Thesis/Dissertation

Requestor type	non-profit academic/educational
Readers being charged a fee for this work	No
Format	electronic
Portion	figures/tables/images
Number of figures/tables/images	1
Will you be translating?	no
World Rights	no
Title	TISSUE NONLINEARITY AS A NOVEL MECHANISM FOR THE FREQUENCY DEPENDENCE OF RESPIRATORY RESISTANCE TO AIRFLOW IN DISEASE
Institution name	Dalhousie University
Expected presentation date	Dec 2021
Portions	Figure 1
Requestor Location	Dalhousie University 1881 Brunswick Street APT 415 Halifax, NS B3J3L8 Canada Attn: Dalhousie University
Billing Type	Invoice
Billing Address	Dalhousie University 1881 Brunswick Street APT 415 Halifax, NS B3J3L8

Canada
Attn: Dalhousie University

Total 0.00 USD

Terms and Conditions

Terms and Conditions:

Original Authors of Published Works: To see a full list of original authors rights concerning their own published work http://www.the-aps.org/publications/authorinfo/copyright.htm

Content reuse rights awarded by the APS may be exercised immediately upon issuance of this license, provided full disclosure and complete and accurate details of the proposed reuse have been made; no license is finally granted unless and until full payment is received either by the publisher or by CCC as provided in CCC's Billing and Payment Terms and Conditions. If full payment is not received on a timely basis, then any license preliminarily granted shall be deemed automatically revoked and shall be void as if never granted. Further, in the event that you breach any of these Terms and Conditions or any of CCC's Billing and Payment Terms and Conditions, the license is automatically revoked and shall be void as if never granted. Use of materials as described in a revoked license, as well as any use of the materials beyond the scope of the license, may constitute copyright infringement and the Publisher reserves the right to take action to protect its copyright of its materials.

The APS makes no representations or warranties with respect to the licensed material. You hereby indemnify and agree to hold harmless the publisher and CCC, and their respective officers, directors, employees and agents, from and against any and all claims arising out of your use of the licensed material other than as specifically authorized pursuant to this license.

This license is personal to you /your organization and may not be sublicensed, assigned, or transferred by you /your organization to another person /organization without the publisher's permission.This license may not be amended except in writing signed by both parties, or in the case of the publisher, by CCC on the publisher's behalf.

The APS reserves all rights not specifically granted in the combination of (i) the license details provided by you and accepted in the course of this licensing transaction, (ii) these Terms and Conditions and (iii) CCC's Billing and Payment Terms and Conditions.

v1.0

Questions? customercare@copyright.com or +1-855-239-3415 (toll free in the US) or +1-978-646-2777.

C.6 Figure 1.2 Permission

RE: URGENT: Thorasys Permission for thesis

GD Guy Drapeau [THORASYS] <guy.drapeau@thorasys.com>
To Anas Tahir
Cc Geoffrey Maksym

CAUTION: The Sender of this email is not from within Dalhousie

Hi Anas,

Yes it is ok.

Kind regards,

Guy

Guy Drapeau, Eng. | Vice President of Research and Development
THORASYS Thoracic Medical Systems Inc. | www.thorasys.com
p +1 514-418-0854 | tf 1-855-THORASYS ext. 1260

C.7 Figure 1.5 Permission

Creative Commons License for:

R. L. Eddy, A. Westcott, G. N. Maksym, G. Parraga, and R. J. Dandurand, "Oscillometry and pulmonary magnetic resonance imaging in asthma and COPD," *Physiol. Rep.*, vol. 7, no. 1, pp. 1–12, 2019.

C.8 Figure 1.8 Permission

Creative Commons License for both:

S. A. Bhatawadekar, D. Leary, and G. N. Maksym, "Modelling resistance and reactance with heterogeneous airway narrowing in mild to severe asthma," *Can. J. Physiol. Pharmacol.*, vol. 93, no. 3, pp. 207–214, 2015.

B. H. Foy *et al.*, "Lung computational models and the role of the small airways in asthma," *Am. J. Respir. Crit. Care Med.*, vol. 200, no. 8, pp. 982–991, 2019.

C.9 Figure 1.9 Permission

Creative Commons License for:

R. L. Dellacà *et al.*, "Detection of expiratory flow limitation in COPD using the forced oscillation technique," *Eur. Respir. J.*, vol. 23, no. 2, pp. 232–240, 2004.